

i

MODELING THE SHEAR STRENGTH IMPROVEMENT  
AT THE INTERFACE OF  
LIME-STABILIZED SOIL AND CONCRETE

by

Burak BATUKAN

B.S. in C.E., Istanbul Technical University, 1995

Submitted to the Institute for Graduate Studies in

Science and Engineering in partial fulfillment of

the requirements for the degree of

Master of Science

in

Civil Engineering

Bogazici University Library



39001100053621

14

Boğaziçi University

1997

## ACKNOWLEDGMENTS

I would hereby express my sincere gratitude to Prof. Dr. Gökhan BAYKAL for the aid he supplied in every stage of my thesis study.

Special thanks also to the finite element application engineers namely Halil BILAL and Ali ÖGE as well as to Mr. Tarık ÖĞÜT, general manager of FIGES which is the distributor company of the ANSYS software in Turkey.

I would also declare my gratefulness to Kemal BEYEN due to the advices he made during the numerical simulation stage of this study.

Also appreciation to Sinan ERİŞEN due to his invaluable contributions on model development.

High regards also to my family who had not only encouraged me but also provided emotional support every time I got confused and became pessimistic about completing this challenging research.

## ABSTRACT

Drilling operations remold the shaft soil, leading to significant shear strength losses. Lime stabilization has been proposed to increase the shaft resistance capacity of friction piles installed into clayey soils. For verifying this hypothesis lime slurries can be prepared in boreholes prior to subsequent concreting. The infiltration of lime is provided by this means through the cracks and fissures that are exposed during the augering process. The beneficial effects of the enabled lime-clay interaction are likely to enhance the shear resistance of the remolded interface zone. Provided that the soil characteristics of the interface have been improved, the required load bearing capacity of piles can thus be obtained without increasing its dimensions. Besides its ease and convenience, the economical aspect of this method makes this proposal even more attractive for field applications.

Using the finite element method, the numerical simulations have been performed in order to distinguish the effect of lime as well as the contribution of treatment duration. A simplified finite element model has been developed under the *ANSYS 5.2* computer software in order to analyze the response behavior of lime treated and untreated natural soil with concrete under identical shearing conditions. The models have been primarily founded on the mechanical parameters (*Young modulus, Poisson ratio and yield stresses*) of the interface soil and its surrounding semi-finite soil domain.

Supporting the corresponding laboratory test results obtained formerly by *Metehan C.T.* (1994), figures have revealed an approximately doubled shear strength at the interface consequent to lime treatment. However, the varied interface thickness accounting for the intensity of lime infiltration, which is in turn dependent upon the duration of treatment, revealed no significant impact onto the results obtained.

*Keywords* : Cast-in-situ concrete piles, skin friction, lime stabilization, diffusion-advection, finite element modeling, interface, thin-layer element.

## ÖZET

Şaft zemini kazı işlemleri sonucu bozularak önemli ölçüde kesme dayanımı kaybına uğramaktadır. Killi zeminlere yerleştirilen kazıkların yanal sürtünme dayanım kapasitesinin kireç stabilizasyonu ile artırılması önerilmiştir. Yapılan bu öneriyi doğrulamak amacıyla beton dökümünden önce hafriyat çukuru kireç bulamacı ile doldurulabilir. Böylece kirecin kazı işlemleri sonucu ortaya çıkan çatlak ve fisürlerden nüfuz etmesi sağlanır. Mümkün kılınan yararlı kireç-kil etkileşimi sonucu bozulmuş olan arayüzey bölgesinin kesme dayanımı artırılmış olur. Nitekim arayüzeye ait zemin karakteristiklerinin iyileştirilmesi sonucu kazık boyutlarını artırmadan kazığın gerekli taşıma kapasitesi elde edilebilir. Metodun kolaylığı ve rahatlığı yanı sıra ekonomik oluşu öneriyi saha uygulamaları için daha da çekici kılmaktadır.

Sonlu elemanlar yöntemi kullanılarak kirecin etkisi ile uygulama süresinin katkısını belirlemek amacı ile nümerik simülasyonlar gerçekleştirilmiştir. Basitleştirilmiş bir sonlu elemanlar modeli *ANSYS 5.2* bilgisayar programı altında geliştirilerek, kireç bulamacı uygulanmış ve uygulanmamış doğal zeminin beton ile tamamen aynı kesme koşulları altında davranışı analiz edilmiştir. Modeller temelde arayüzey zemini ile onu çevreleyen yarı sonlu zemin ortamının mekanik parametreleri (*Young* modülü, *Poisson* oranı, akma gerilmeleri) üzerine kurulmuştur.

*Metehan C.T.* (1994) tarafından önceden gerçekleştirilen ilgili laboratuvar deneylerinden elde edilen değerleri destekleyen sonuçlar, kireç bulamacı uygulanmış duruma ait arayüzey kesme dayanımının yaklaşık iki kat civarında olduğunu ortaya koymuştur. Ancak, nüfuz etme derecesine karşılık gelen ve esasında etkime süresine bağlı olan arayüzey kalınlığının elde edilen sonuçlar üzerinde önemli bir etkisinin olmadığı ortaya çıkmıştır.

*Anahtar kelimeler* : Yerinde dökme beton kazıklar, yanal sürtünme, kireç stabilizasyonu, difüzyon-adveksiyon, sonlu elemanlar ile modelleme, arayüzey, ince kalınlıklı eleman.

## TABLE OF CONTENTS

	Page
ACKNOWLEDGMENTS .....	iii
ABSTRACT .....	iv
ÖZET .....	v
LIST OF FIGURES .....	viii
LIST OF TABLES .....	xi
LIST OF SYMBOLS AND ABBREVIATIONS .....	xii
1. INTRODUCTION .....	1
2. LITERATURE REVIEW .....	3
2.1. Approach to the Interface Model of Concrete Surface and Soil.....	5
2.2. Behavior and Deformation Modes at the Interface .....	8
2.3. Review of Proposed Interface Elements .....	12
2.3.1. The Joint Element ( Zero - Thickness ) .....	14
2.3.2. The Thin – Layer Element ( Finite Thickness ) .....	17
2.4. Fundamental Aspects of the Pile-Soil Assembly .....	23
2.4.1. Influence of Soil Type on Static Pile Capacity .....	23
2.4.2. Soil - Pile Interaction : Mechanism of Load Transmission .....	25
2.4.3. Components of Pile Resistance.....	28
2.4.4. Criterion and Computation of the Ultimate-Load .....	31
2.4.5. Construction Methods of Cast-In-Situ Concrete Piles.....	33
2.5. Stabilization Effect of Lime on Clayey Soils .....	37
2.5.1. Lime Release due to Mechanism of Cement Hydration .....	38
2.5.2. Alteration of Soil Parameters by Stabilization with Lime .....	40
2.5.3. Theory and Mechanism of Lime-Soil Interaction .....	43
2.5.4. Effect of Curing Conditions on Strength Development.....	49
2.6. Mechanism of Mass Transport into Clayey Soils .....	51
2.6.1. Background of Mass Transport into Soil .....	52
2.6.2. Diffusion of Lime into Clayey Soils .....	56
2.7. Review of Interface Testing Apparatus.....	58
2.8. Principles of the Finite Element Method .....	60

3. PRESENT STUDY .....	63
3.1. Description and Scope of the Problem .....	63
3.2. Fundamental Assumptions Regarding the Physical Problem .....	67
3.3. Material Properties .....	70
3.4. Application of the Finite Element Method to the Physical Problem .....	76
3.5. Employed Technique for Nonlinear Analysis .....	85
4. RESULTS AND DISCUSSION.....	88
5. CONCLUSIONS .....	98
APPENDIX .....	101
REFERENCES.....	110

## LIST OF FIGURES

		Page.
FIGURE 2.1.	Identification index [6].....	7
FIGURE 2.2.	Direction angle with normal force and tangential force [6].....	7
FIGURE 2.3	Idealization of the interface [9].....	9
FIGURE 2.4.	Schematic illustration of deformation modes at interface [12]..	11
FIGURE 2.5.-a,b	Curves of shearing versus deformation [11].....	11
FIGURE 2.6.	Representative geometry of the joint element [14].....	15
FIGURE 2.7.	The thin-layer interface element [12].....	17
FIGURE 2.8.-a,b	Behavior at the interface with "thin-layer" element [12].....	20
FIGURE 2.9.	Load transmission mechanism for piles [40].....	27
FIGURE 2.10.	Load-settlement relationship for axially loaded piles [41].....	29
FIGURE 2.11.	Dry method of cast-in-situ construction [30].....	34
FIGURE 2.12.	Casing in method of cast-in-situ construction [30].....	35
FIGURE 2.13.	Slurry method of cast-in-situ construction [30].....	36
FIGURE 2.14.-a,b	Time respective effect of lime on parameters of clayey soils [56].....	42
FIGURE 2.15.	Illustration of mechanism of lime stabilization for clayey soil [68].....	48

FIGURE 2.16.	Mechanical conceptual model of shear strength development with time for high water content and low water content varying-lime stabilized soils ( p refers to the model of Perrat ) [59].....	50
FIGURE 2.17.	Effective length concept in transport through porous medium [74].....	54
FIGURE 2.18.	Diffusion of calcium into cores of lime stabilized [15 per cent] clayey lumps [75].....	57
FIGURE 2.19.	Subdivision into finite elements of arbitrary continuum [3].....	60
FIGURE 3.1.	Schematic illustration of the physical problem [12].....	69
FIGURE 3.2.	Adopted elasto-perfectly plastic stress-strain relationship.....	75
FIGURE 3.3.	Plane-42, two dimensional structural solid element.....	78
FIGURE 3.4.	Resultant meshed finite element model with assigned appropriate element attributes and material properties.....	78
FIGURE 3.5.	Overburden pressure, DOF constraints, coupled node sets and relative displacements applied on pre-meshed model.....	81
FIGURE 3.6.	Diagram of applied load step history.....	82
FIGURE 3.7.	Deformed shape of a typical analyzed model .....	84
FIGURE 3.8.	Comparison between the pure incremental approach and the <i>Newton- Raphson</i> approach.....	86
FIGURE 3.9.	Errors are imminent when relied only on displacement convergence checking.....	87

FIGURE 4.1.	Average shear strength vs displacement behavior of pure bentonite samples with 2mm interface thickness (a) Without lime treatment (b) Treated with 7 % lime.....	92
FIGURE 4.2.	Average shear strength vs displacement behavior of pure bentonite samples with 4mm interface thickness (a) Without lime treatment (b) Treated with 7 % lime.....	93
FIGURE 4.3.	Average shear strength vs displacement behavior of pure bentonite samples with 6mm interface thickness (a) Without lime treatment (b) Treated with 7 % lime.....	94
FIGURE 4.4.	Average shear strength vs displacement behavior of pure bentonite samples with 8mm interface thickness (a) Without lime treatment (b) Treated with 7 % lime.....	95
FIGURE 4.5.	Interface respective failure envelopes for pure bentonite specimens (a) Without lime treatment (b) Treated with 7 % lime.....	96
FIGURE 4.6.	Effect of interface thickness onto maximum acquired shear stresses (a) Without lime treatment (b) Treated with 7 % lime.....	97
FIGURE A.1.	Time respective evolution of shear stress patterns (Pa) for the untreated case with 4 mm interface thickness and 150 kPa overburden pressure.....	102
FIGURE A.2.	Time respective evolution of shear stress patterns (Pa) for the lime treated case with 4 mm interface thickness and 150 kPa overburden pressure.....	104
FIGURE A.3.	Time respective evolution of shear stress patterns (Pa) for the untreated case with 8 mm interface thickness and 150 kPa overburden pressure.....	106

FIGURE A.4. Time respective evolution of shear stress patterns (Pa) for the lime treated case with 8 mm interface thickness and 150 kPa overburden pressure..... 108

## LIST OF TABLES

	Page
TABLE 2.1. Comparison of interface testing apparatus .....	59
TABLE 3.1. Properties of commercially available limes.....	72
TABLE 3.2. Assigned values for the <i>Young</i> modulus and <i>Poisson</i> ratio.....	73
TABLE 3.3. Yield stresses derived from laboratory direct shear tests conducted on pure bentonite specimens [after <i>Metehan, C. T.</i> ]...	75

## LIST OF SYMBOLS AND ABBREVIATIONS

$A$	Area of the concrete surface
$a$	A mineralogical parameter including mineralogy, specific surface, Grain size and cation exchange capacity
$A_a$	Appearant contact area
$A_c$	Area on interface plane covered with asperities
$A_f$	Total area of flat regions on interface plane
$A_i$	Contact area of individual microasperity
$A_s$	Bearing area of the pile shaft
$A_p$	Area of the pile tip
$A_w$	Initial pore-water parameter
$a$	Empirical constant related to testing conditions
$b$	Pile diameter
$[C]_i$	Constitutive matrix for the interface or joint element
$c$	Concentration of additive
$c$	Soil cohesion value
$c_p$	Shape factor of the plowing asperity
$d$	Embedded length of pile into soil
$D_0$	"free solution" Diffusion coefficient
$e$	<i>Young</i> modulus
$f$	Resultant contact friction force at the interface
$F_p$	Friction force resulting from plowing
$F_s$	Friction force utilized due to adhesion

$f_s$	Skin resistance of piles
$f_z$	Distribution of skin resistance per unit area along the pile shaft
$j$	Mass flux
$i$	Resistance due to interlocking of roughness.
$K_o$	Coefficient of lateral earth pressure at rest
$K_a$	Coefficient of active lateral earth pressure
$K_p$	Coefficient of passive lateral earth pressure
$K_s$	Coefficient of skin pressure
$k_n$	Normal stiffness
$k_s$	Shear stiffness
$n$	Normal force for two bodies in contact
$n$	Statistical average spt blow count
$N_c^*$	Bearing capacity factor at the pile tip related to cohesion
$N_q^*$	Bearing capacity factor at the pile tip related to surcharge
$n$	Total soil porosity
$P_m$	Mean pressure on contact area
$p$	Perimeter of the pile shaft
$q$	Vertical central load applied onto the top of the pile shaft
$Q_p$	Load carried by the pile point
$Q_s$	Load carried along the pile shaft by skin friction
$Q_u$	Ultimate pile load
$q$	Sorbed concentration of solute per mass of soil
$q_p$	Unit bearing capacity value of the pile tip

$q_s$	Normal stress on the pile shaft
$q_c$	Cone-penetration resistance
$q_u$	Unconfined compressive strength of soil
$q'$	Sorbed concentration of the chemical species
$q_v$	Effective vertical stress in the soil at the foundation level
$\bar{q}$	Effective vertical stress on element $\Delta L$ of soil stratum
$R_n^{cri}$	Critical interface roughness
$S_m$	Mean shear strength on the contact area
$S_r$	Degree of soil saturation
$s_u$	Undrained shear strength of soil
$t$	Interface thickness
$u_r$	Shear component of relative displacement
$\nu$	<i>Poisson</i> ratio
$\nu_r$	Normal component of relative displacement
$x$	Direction of transport
$\alpha$	Fluidity factor
$\alpha$	Empirical adhesion factor
$\alpha$	Fraction of real contact area where plowing takes place
$\alpha$	Shear strength reduction factor
$\mu_c$	Coefficient of friction between a soil grain and a concrete asperity
$\mu_0$	Coefficient of <i>coulomb</i> friction
$\gamma$	Anion exclusion factor
$\gamma'$	Effective unit weight of soil

$\delta$	Angle of friction between soil and pile
$\phi$	Angle internal friction of soil
$\theta$	Volumetric water content
$\tau$	Tortuosity factor
$\tau$	Shear stress
$\sigma_n$	Normal stress
$\Delta L$	Embedded increment of the pile shaft

## 1. INTRODUCTION

When the upper soil layers are highly compressible and too weak to support the load transmitted by the superstructure, piles are used to transmit the load to underlying bedrock or a stronger soil layer. However, if bedrock is not located within a reasonable depth below the ground surface, piles are used to transfer the structural load to the soil gradually. The resistance to the applied structural load is derived mainly from the frictional resistance developed at the pile-soil interface. Drilling operations remold the soil, causing a major decrease in shear strength properties. Improving the shear strength properties in this remolded zone will improve the frictional resistance of the pile installed. Lime stabilization is widely used for the stabilization of clayey soils; however, its use for the improvement of pile frictional resistance will be the first time.

Contrary to many applications of lime stabilization where lime is mixed with soil prior to compaction, the diffusion-advection mechanisms can be utilized for lime stabilization of clay based soils surrounding the pile shaft. Free lime expelled from fresh concrete can be recognized as a source for this stabilization provided that cast-in-situ concrete piles are used. Nevertheless, previous studies pointed out that the free lime content in fresh concrete hardly ever exceeds 1-2 per cent [1]. Relying on this fact, more lime is required in order to achieve desired stabilization effects. For verifying this proposal lime slurries can be prepared in boreholes before subsequent concreting such that lime diffusion-advection is enabled through the cracks and fissures that are created in the shaft soil during the augering process.

Except the introduction made by *Metehan C. T.* (1994), no related work has been encountered that attempts to apply lime treatment of the bearing shaft soil before pile installment. *Metehan C. T.* (1994) conducted in his previous study the laboratory direct shear tests in order to observe the increase in shear strength at the interface between lime stabilized compacted clayey soil and concrete. An increase of a great extend up to 100 per cent in the shear strength at the soil-concrete interface has been among his findings. Supplementary to *Metehan's* work, this study constitutes the numerical analyses, namely the finite element modeling of the effect of lime stabilization on clayey soil and concrete interaction.

The computer software *ANSYS* has been utilized throughout the analyses to model the physical problem that is actually in close resemblance with the direct shear box. Respecting the interface thickness, the interaction behavior of natural (nontreated) soil with concrete has been compared with the corresponding lime treated case.

The results obtained revealed that the shear strength considerably increased through the beneficial effects of lime on the interface soil whereby the observed shear stresses remained somewhat intact as the interface thickness has been changed.

The proposed interface elements, the deformation modes and behavior of the interface under shearing, the mechanism of lime-soil interaction, the diffusion-advection characteristics of lime into porous mediums, the skin resistance characteristics and other fundamentals of the pile-soil assembly have been mentioned in the succeeding sections.

## 2. LITERATURE REVIEW

Both the existence and behavior of interfaces or junctions between structure and foundation soils considerably affect the response of structure-foundation systems subjected to static or dynamic loading [2]. Although complete bonding at the interfaces is often assumed during the design procedure, such an assumption can lead to erroneous results in the prediction of stresses and deformations. This can be attributed to the fact that the inclusions of relative motions and resulting mechanism(s) of load transfer between contacting mediums can introduce strong nonlinearities [2]. Hence, closed-form solutions become difficult, and recourse has to be made to numerical techniques. Numerical methods being more comprehensive and powerful are applicable to problems involving complex material properties and boundary conditions in order to obtain approximate, but still acceptable solutions.

The finite element method provides a powerful technique for analysis of stresses and displacements in soil masses, and has already been applied to a number of practical problems in geotechnical engineering such as embankment dams, open excavations, braced excavations, and a variety of soil-structure interaction problems. In particular, the accommodation of complex and difficult problems such as nonhomogeneous materials, nonlinear stress-strain behavior and complicated boundary conditions can be overcome with the finite element method. It is applicable to a wide range of boundary value problems in engineering. In a typical boundary value problem as the one examined herein, a solution is sought in the region of the body, while on the boundaries of the region the values of the dependent variables are prescribed [3].

Additionally, if the results of soil deformation analysis are to be realistic and meaningful, it is important that the stress-strain characteristics of the soil are represented in the analysis in a reasonable way. This is often difficult to accomplish since the stress-strain characteristics of soil are extremely complex, and the behavior of soil is highly nonlinear, inelastic and much dependent on the magnitudes of the initial stresses in the soil [3].

Understanding and being able to assess the mechanical behavior of interfaces between structural elements and soil is quite important and received therefore much attention in foundation engineering. Typically in stronger soil masses, this behavior is highly nonlinear and involves significant coupling between the shear and dilational modes of behavior. Relative or shear displacement of the two sides of the interface is very often accompanied by some normal separation of the interface (dilation) [4].

In the past, many models have been developed to describe and predict the mechanical behavior of perfectly mated and perhaps rough, naturally formed interfaces in rock. In most cases no actual bonding or cementation across the interface has been assumed. In these cases the shear strength of the interface is derived from the combined effects of friction, interlocking and the tendency for the rough interface to dilate [4].

In contrast to natural joints, the man-made interfaces usually involve a degree of bonding between the two surfaces. A concrete pile foundation cast into a soil medium can be regarded as an example for this case. In this case the cementation or bonding may be a significant contribution to the shear strength of the interface. Cementation will combine usually in some complex way, with other factors like surface roughness, friction and dilation to determine the complete shear behavior of the interface [4].

Interface laws have been used for a long time in rock mechanics but much more recently in soil mechanics due to their obvious advantages in problems of contact between solids. In the case of piles, anchorings or nailings, strain localization visualized by *Davis and Plumelle, Habib*, leads to include in design calculations an interface behavior as a rheological model. The thin transition layer between the structure and the soil is represented by an equivalent continuum [5]. Directional dependence or the coupling between tangential and normal phenomena is a fundamental characteristic and is still ignored in commonly used interface laws [5]. This is due to its small influence for normal stresses of medium intensity and for grain crushing resistant granular materials [5].

## 2.1. Approach to the Interface Model of Concrete Surface and Soil

Granular materials are often involved in the frictional interaction of soil with a concrete surface [6]. The effect of the granular material to the behavior is examined in previous studies either by the continuum approach or by the particle approach. However, since the latter is based directly on the description of the material structure, it provides better insight into the behavior phenomena. The actual model of the concrete surface consists of a flat concrete plane with geometrically varying caps protruding from it [6]. This approach represents basically the roughness or asperities of the concrete surface. However, the distribution of the cap sizes which can be defined by their protrusion heights and other geometric characteristics have to be determined or estimated. Since they are actually randomly distributed over the flat surface with varying density per unit area, their actual influence to the interface behavior is unambiguously difficult to express in numerical methods and thus to model [7]. In addition to the uncertainties introduced by the concrete asperities, the soil particles in contact with the concrete interface may also differ in number, particle size and distribution as well. From the macroscopic point of view, such a modeling approach permits only for a single contact between a soil grain and a concrete surface asperity [6-8].

Besides, when a load is applied to the soil medium, the normal contact force developed at the contact point between a soil grain and an asperity will have an oblique direction relative to the interface plane [6]. This obliquity will provide the normal force to be a function of the state of stress of the loaded soil rather than just a function of the component of stress normal to the interface [6]. At each contact point the contact pressure deforms the bodies forming a common contact area between the soil grain and concrete asperity. This contact area, if assumed not spherical, will permit the presence of microasperities which are further assumed to lie in a plane perpendicular to the normal contact force. The complex friction phenomenon during the sliding of soil grains relative to the concrete surface results from the interaction of these microasperities [6-8].

Intimate contact is provided at various points whenever two solid bodies are pressed together. Nevertheless, adhesion is limited and takes place only at the individual microasperities' contact area  $A_i$  which is clearly much less than the apparent contact area  $A_a$ . Obviously, the sum  $A$  of all contact areas  $A_i$  equals to the real area of contact. The junctions begin to shear as the tangential force during sliding increases. Hence, the friction force  $F_s$  utilized due to adhesion at a definite contact point between two relative sliding bodies can be expressed as;

$$F_s = A \cdot S_m \quad (2.1)$$

where  $S_m$  is designated as the mean shear strength on the contact area. Since microasperities are in abundance on the concrete surface the average value of  $S_m$  can be assumed as constant without much loss in accuracy for a specific soil-concrete combination. If such a structurally hard surface (micro)-asperity is forced against a softer material (e.g. soil) on the other body, two main mechanisms are initialized. The first one being a function of  $S_m$  is the shearing of the softer material. Plowing out the softer material by the asperities of the harder material and the interlocking of the surface irregularities constitute the second mechanism. The latter one can also be characterized as the work done against the pressure around the asperity and can be regarded as a function of the mean pressure  $P_m$  [6,7]. Finally, the resultant contact friction force at the interface equals to;

$$F = F_s + F_p + I = AS_m + \alpha A c_p P_m + I \quad (2.2)$$

where  $F_p$ ,  $\alpha$  and  $c_p$  correspond to the friction force resulting from plowing, the fraction of real contact area where plowing takes place and the shape factor of the plowing asperity, respectively.  $I$ , being usually negligible, denotes the resistance due to interlocking of roughness [6,7]. If  $\mu_c$  expresses the coefficient of friction between a soil grain and a concrete asperity at a definite contact point, it follows that;

$$\mu_c = \frac{F}{N} = \frac{A(S_m + \alpha c_p P_m)}{AP_m} = \frac{S_m}{P_m} + \alpha c_p \quad (2.3)$$

yielding;

$$F = \mu_0 N + CN^\lambda \quad 0 < \lambda < 1 \quad (2.4)$$

The coefficient  $\mu_0$  defined by Equation 2.4 is known as the *Coulomb* friction coefficient. If a nonzero positive value is assigned to  $C$ , the additional component of friction force will increase with respect to the normal force  $N$  [6,7].

When concrete asperities are designated with index  $j$  and each soil grain in contact with index  $i$ , the double index  $ij$  can identify a soil grain  $i$  in contact with asperity  $j$  as shown in Figure 2.1. If this formulation is then applied to the forces  $F$  and  $N$ , they will imply them as contact forces on the asperity  $j$  due to the contact with grain  $i$  as plotted in Figure 2.2.

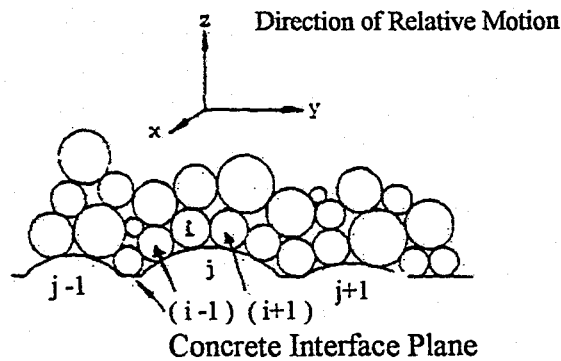


**FIGURE 2.1. : Identification index [6]**

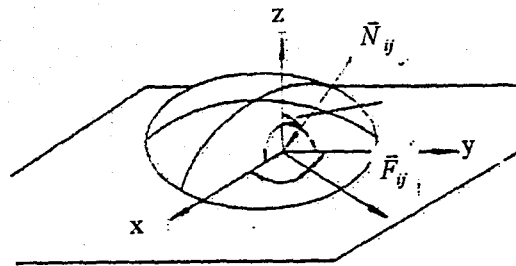


**FIGURE 2.2. : Direction angle with normal force and tangential force [6]**

$$F_{ij} = -\mu_0 N_{ij} + C |N_{ij}|^\lambda \quad 0 < \lambda < 1 \quad (2.5)$$

The resultant vector implying the resultant contact force on the asperity equals to;

$$\vec{D}_{ij} = \vec{N}_{ij} + \vec{F}_{ij} \quad (2.6)$$

where  $\vec{N}_{ij}$  and  $\vec{F}_{ij}$  define the normal and frictional force on the asperity, respectively.

The average interface friction force  $T_y$  and corresponding average normal stress  $P_z$  are equal to;

$$\vec{T}_y = T_y \vec{j} = (A_c + A_f) \tau_{ay} \vec{j} \quad (2.7)$$

$$\vec{P}_z = P_z \vec{k} = (A_c + A_f) \tau_{az} \vec{k} \quad (2.8)$$

where  $A_c$  is the area on the interface plane covered with asperities.  $A_f$  equals to the total area of flat regions.  $\tau_{ay}$  and  $\tau_{az}$  denote the average shear and normal stress, respectively. The magnitudes of  $T_y$  and  $P_z$  depend on the number of asperities  $j$  per unit area of  $A_c$ , the number of soil grains ( $m_j$ ) making contact with asperity  $j$ , the number of separate flat spots ( $m_f$ ), the number of soil grains making contact with flat spots and the direction of the forces  $\vec{N}_{ij}$  and  $\vec{F}_{ij}$  [6].

The parameters  $\mu_0$ ,  $C$  and  $\lambda$  have to be determined experimentally and are dependent only on the materials involved. The geometric parameters of the concrete interface, on the other hand, can perhaps be measured. The parameters  $m_j$ ,  $m_f$ , the radius of soil grain and direction angles request statistical treatment. Known or estimated particle size distributions for the soil and measured or estimated particle size distributions for the concrete surface may constitute the input data for such calculations [6].

## 2.2. Behavior and Deformation Modes at the Interface

The interface between two contacting bodies  $A$  and  $B$  can be idealized as shown in Figure 2.3. During the stress transfer between these two bodies presented, very often relative slip takes place along the interface plane. This tendency of relative slip develops forces both in the tangential ( $T$ , shear) and normal ( $N$ , compression) directions to the interface plane to occur. As a consequence of these forces, corresponding displacements  $u$  and  $v$  in the tangential and normal directions to the interface plane are generated, respectively. Additional complexities also occur when relative slip is accompanied by damage that results in degradation and strain-softening [9].

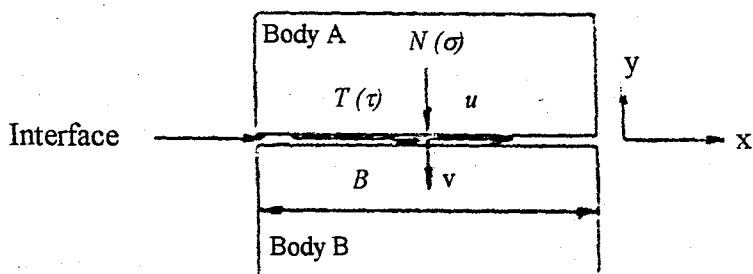


FIGURE 2.3. : Idealization of the interface [9]

Behavior at junctions or interfaces between structural and geological materials involve relative translational and rotational motions under static and dynamic loading as depicted schematically in Figure 2.4 [12]. During the no-slip or stick mode where the normal stress  $\sigma_n$  is compressive, the shear stress  $\tau$  has not reached the failure or its ultimate state. However,  $\sigma_n$  being still compressive; slip occurs when deformations increase further such that the shear stress exceeds a failure stress defined by criteria such as the *Mohr-Coulomb* yield criteria [2,9,10].

The interface is initially under compression in its in-situ state. During loading, the compressive stress  $\sigma_n$  may diminish gradually, may become zero or even transit to the tensile regime. Depending upon the tensile strength of the interface  $\sigma_t$ , debonding or separation during the no-slip or slip modes can therefore be experienced [9]. During subsequent loading,  $\sigma_n$  may become compressive again, and a rebonded state is established allowing for reloading to occur [9]. Another important mode, although not shown, is the interpenetration of one material into its neighbor. For the soil-structure problems it is often necessary to control this so as to satisfy physical conditions between the two materials [2,9,10].

Tests performed on interfaces under monotonic loading conditions revealed that until the shear stress reaches the peak value  $\tau_f$ , negligibly small relative motions occur at the interface [9]. However, the soil mass deformed uniformly throughout its height. Furthermore, both the frictional resistance ( $\tau/\sigma$ ) and volumetric behavior are predominantly governed by the interface roughness [9]. Interface sliding is initialized whenever the interface is smoother than the existing critical interface roughness  $R_n^{cri}$ .

Contrary, on condition that the interface is rougher than  $R_n^{cri}$ , shear failure occurs in the soil mass instead of sliding along the interface. Observations also pointed out that smooth interfaces exhibit very small volume changes, whereas higher dilatational behavior is valid for a rough interface [9].

Soils do experience shear deformation under applied relative displacements. The curve representing shearing versus deformation is determined by the structural arrangement of the cohesive soil regardless whether drained or undrained conditions exist or whether the soil is normally consolidated or overconsolidated [11]. If the structure is characteristic of a flocculated soil, similarly to the condition acquired after treatment with lime, the sheared specimen exhibits an unstable curve with a marked peak as shown in Figure 2.5.-(a). The peak indicates the maximum level of shearing required to rupture a majority of the interparticle contacts such that the sliding of some particles over each other is provided. When the contacts have been disrupted, failure continues to occur at much lower levels of shearing stress since the structure of the soil is changed by the shearing deformation to a more parallel orientation [11].

Clays with dispersed or remolded structures and few contacts demonstrate a resistance to shear which increases with deformation until as shown in Figure 2.5.-(b) a constant shearing resistance is manifested at a particular shear rate. Unlike the previous one, this curve is stable. The required increase in shear stress orientates the particles in the shearing zone parallel to the direction of shearing stress [11].

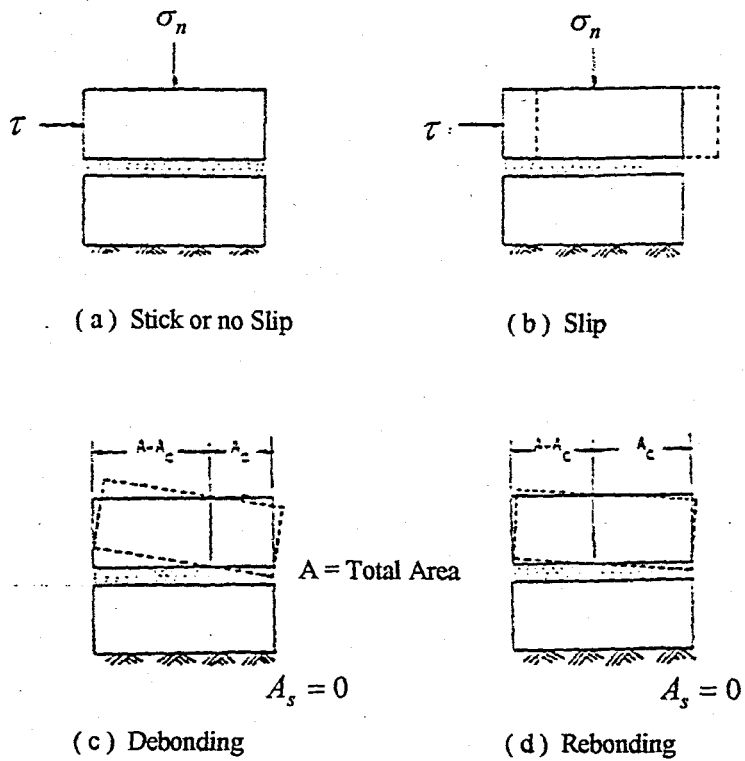


FIGURE 2.4. : Schematic illustration of deformation modes at interface [12]

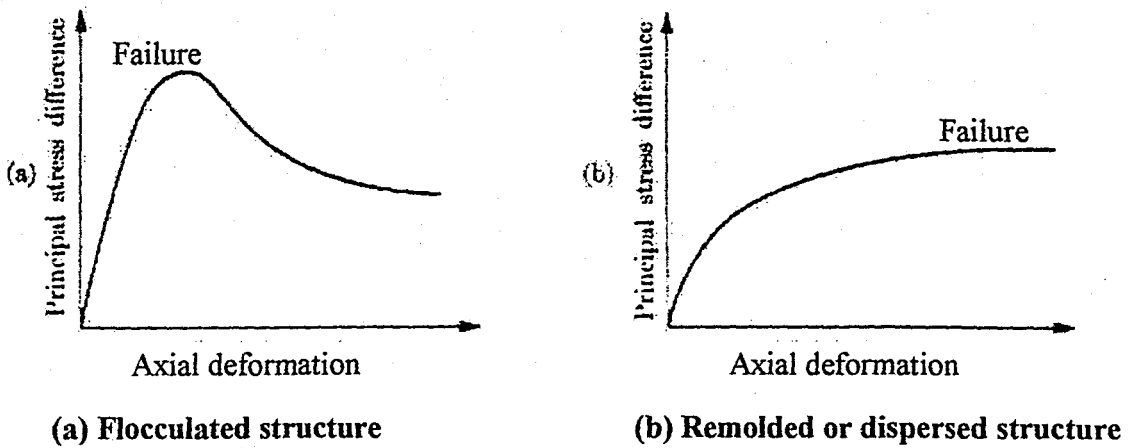


FIGURE 2.5. : Curves of shearing versus deformation [11]

### 2.3. Review of Proposed Interface Elements

Many geotechnical problems involve interaction between structure and soil or rock. If numerical methods are applied to obtain solutions to this type of problems, proper modeling of the interaction zone generated between structure and soil becomes important. Because of the importance of proper modeling of interfaces extensive research in this subject has led to various formulations capable of modeling the interaction phenomena. Many formulations of joint and interface elements have been proposed by a number of researchers. However an easy to handle, robust element for routine analyses has not yet been presented. Some successful applications have been reported using conventional solid elements, but in general these elements can not be used because of numerical problems due to very high aspect ratios. Additionally meaningful stresses - especially shear stresses - in the contact zone are difficult to obtain.

A commonly used interface element is the one proposed by *Goodman, Taylor and Brekke* with relative displacements being the nodal unknowns. The thickness is often assumed to be zero and to avoid overlapping and penetrating, a very high normal stiffness is assigned to the interface, which does not coincide with the actual behavior [12,13].

*Ghaboussi, Wilson and Isenberg* introduced a description for the interface element which is derived by considering relative motions between surrounding soil elements as independent degrees-of-freedom [12,14].

*Zienkiewicz et al.* took advantage of an isoparametric finite element formulation for an interface element that is treated essentially like a solid element. They advocate the use of continuous isoparametric elements with a simple nonlinear material property for shear and normal stresses, assuming uniform strain in the thickness direction. Numerical difficulties may arise from ill conditioning of the stiffness matrix due to very large off-diagonal terms or very small diagonal terms which are generated by these elements in certain cases [12,15].

A similar element to that proposed by *Ghaboussi, Wilson and Isenberg*, based on an isoparametric, "shell-type" - formulation has been proposed by *Beer* for two- and three-dimensional applications [12,16].

Modified spring elements have also been used and although the desired effect may be obtained, data preparation, mesh generation and interpretation of results turn out to be very involved [12,17].

*Desai* proposed a thin-layer element based on an isoparametric formulation. The main features are the introduction of an independent shear modulus in the elastic range and the possibility of taking into account stick, slip, debonding and rebonding modes [12]. Although some applications have been reported the performance of this element is not fully investigated. The main advantage of this element is that it can be easier implemented into existing finite element codes [12,18].

*Isenberg* and *Vaughan* made use of a thin element in dynamic analysis [19].

*Pande* and *Sharma* made performance comparisons of thin and zero thickness elements and studied the aspect of ill-conditioning occurring in computations with reference to the element thickness [20].

*Katona et al.* derived an interface model from the virtual work principle modified by appropriate constraint conditions. His proposed formulation incorporates various deformation modes at the interface [21,22].

*Herrman* presented an algorithm for an interface element which is similar to an element of *Goodman et al.*, with certain improvements through introduction of constraint conditions. Various modes of interface behavior such as sliding and debonding were among his major concerns [23].

The beforehand mentioned elements have been incorporated into soil-structure interaction problems by various investigators. In most of these studies, the shear behavior of soil is often simulated as either nonlinear elastic or plastic while the shear stiffness is evaluated as a tangent modulus from laboratory stress-strain behavior in triaxial or direct shear tests.

### 2.3.1. The Joint Element ( Zero - Thickness )

Previous attempts have been made to develop discrete elements to represent the joint behavior. One of the commonly used interface elements in soil-structure interaction is the joint element. This simple four noded two-dimensional rectangular element with eight degrees-of-freedom was proposed by *Goodman, Taylor and Brekke* [13]. The element supports reciprocal penetration of continuous elements from adjacent blocks. Provided that the joint element uses relative displacements as the independent degrees of freedom, its formulation is derived on the basis of relative nodal displacements of the solid elements surrounding the interface element as shown in Figure 2.6. The displacement degrees-of-freedom of one side of the slip surface are transformed into the relative displacements between the two sides of the slip surface. The transformation relations are often formulated as follows;

$$u_{xi}^T = u_{xi}^B + \Delta u_{xi} \quad u_{yi}^T = u_{yi}^B + \Delta u_{yi} \quad (2.9)$$

$$u_{xj}^T = u_{xj}^B + \Delta u_{xj} \quad u_{yj}^T = u_{yj}^B + \Delta u_{yj} \quad (2.10)$$

With respect to the slip surface, the superscripts *T* and *B* refer to the top and bottom elements. Those degrees of freedom of the upper element, which are on the slip surface, are transformed while the degrees of freedom of the lower element remain as the original displacement quantities [14].

The material properties that can be assigned to the joint element consist merely of the shearing and normal stiffness values [13]. They correspond physically to the stiffness and strength of the interface, to the roughness of the interface and to the angles of slip surfaces relative to the principle plane of the interface. They can be classified either as dilatant if shearing produces interface expansion or contraction; or nondilatant if shearing and normal displacement are uncoupled [13,14,16].

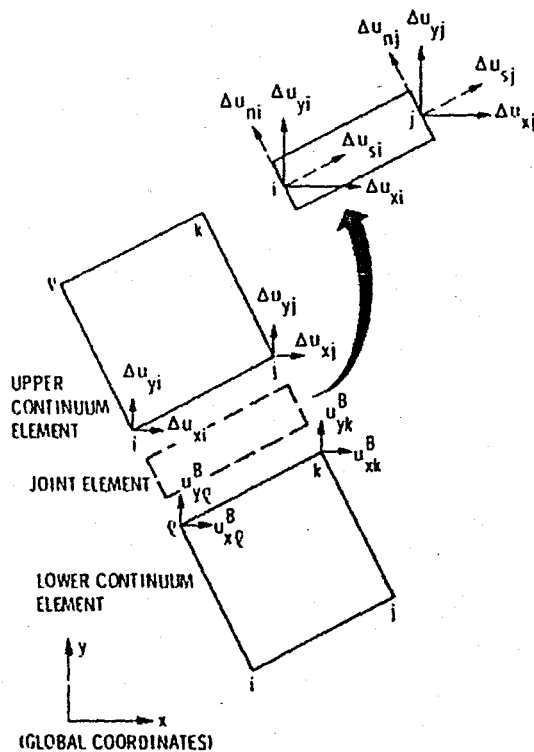


FIGURE 2.6. : Representative geometry of the joint element [14]

Simplifying with the assumption that the joint element is nondilatant, interfaces are simple to model mathematically since there is no volume change due to shear strains [13]. Therefore, the shear and normal components of deformation are uncoupled. Thus, for two-dimensional analysis (nondilatant), the constitutive or stress-relative displacement relation is expressed as follows [12-14,16];

$$\begin{Bmatrix} \sigma_n \\ \tau \end{Bmatrix} = \begin{bmatrix} k_n & 0 \\ 0 & k_s \end{bmatrix} \begin{Bmatrix} v_r \\ u_r \end{Bmatrix} = [C]_i \begin{Bmatrix} v_r \\ u_r \end{Bmatrix} \quad (2.11)$$

where  $\sigma_n$ ,  $\tau$  account for the normal and shear stress;  $k_n$ ,  $k_s$  denote the normal and shear stiffness;  $v_r$ ,  $u_r$  express the relative normal and shear displacements, respectively.  $[C]_i$  is the constitutive matrix for the interface or joint element. However, both  $k_n$  and  $k_s$  are nonlinear functions [14]. The thickness of the element is often assumed to be zero when utilized for soil-structure interaction problems [12].

When the joint element is used to simulate the interfaces between two different mediums, two values can be assigned to  $k_n$  - zero (debonding) or infinity (contact) [14]. The element permits to slip under these circumstances. In case of debonding the joint element is physically non-existent and disappears from the assembly of the global stiffness matrix [14]. In case of contact, the relative displacements in the direction of normal to the joint plane are zero. Thus, the relative displacements can be transformed into the joint element's local directions, so that a zero displacement boundary condition can be imposed on  $\Delta u_{ni}$  and  $\Delta u_{nj}$ . Another possible alternative procedure is to assign a large value to  $k_n$ .

Based on the assumption that the structural and geological media do not overlap at the interface, a high value of the magnitude of  $10^8 - 10^{12}$  units is assigned to the normal stiffness  $k_n$  [12]. There exists no logical basis for adoption of such values, which need to be determined for the problem on hand by performing parametric studies. Furthermore, in most problems, the formulation can provide satisfactory solutions for the stick (bonded) and slip modes for which the normal stress remains compressive. Unreliable solutions are often pronounced for other modes such as debonding [12].

Development and use of a thin solid element to simulate interface behavior is proposed herein. It is referred as a "thin-layer" element since the proposed element essentially represents a solid element of small finite thickness and since it can represent a thin layer of material between two bodies [12]. In recent works conducted, a number of investigators have considered and analyzed the performance of this "thin" element. The authors and their coworkers have been involved in research and implementation of the concept for static and dynamic problems for the last several years.

The distinguishing features of the investigations herein lie in the special treatment of the constitutive laws for the thin layer element, choice of its thickness, incorporation of various modes of deformation and implementation for a number of problems with displacement, mixed and hybrid finite element procedures [12].

### 2.3.2. The Thin - Layer Element ( Finite Thickness )

In many soil-structure interaction problems it is appropriate to assume a thin soil zone in the vicinity of the structure to participate in the interaction action [24]. Schematic diagrams of the thin-layer element for two- and three-dimensional idealizations are shown in Figure 2.7. Modeling the interface behavior using this type of element can be founded on both nonlinear elastic or elastic-plastic concepts [24]. The element is capable to incorporate loading, unloading and reloading behavior. It also allows for various modes of deformation such as no-slip, slip, debonding or separation, and rebonding, and can control interpenetration at the interface [12,24]. The element is treated essentially like any other solid (soil, rock or structural) element so that the contact or interface can be replaced by an equivalent continuum element with a finite thickness,  $t$  [12,24] . This assumption is consistent with actual behavior of many practical problems in which the response and failure are concentrated in a small neighboring zone and not exactly at the soil-structure interface.

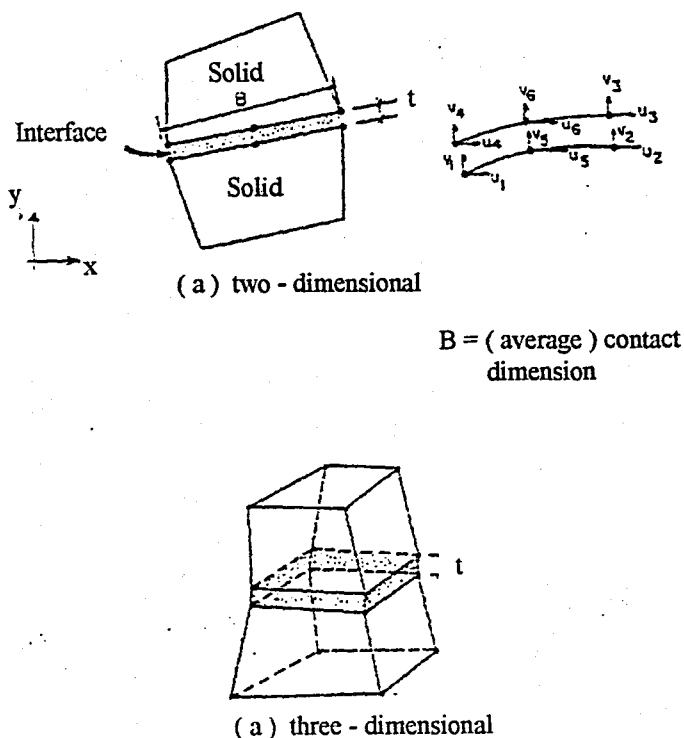


FIGURE 2.7. : The thin-layer interface element [12]

Among various possibilities, the followings represent some practical situations for this element : First, a different material with finite (small) thickness  $t$  develops between two solid mediums (or elements) as in the case of a filled rock joint with inclusion of a thin soil layer [10]. Second, interface occurs between two bodies having different properties such as soil and concrete. Thus, enabling the interface elements to represent a thin zone in the softer material, in which the action is mainly concentrated. It has been found from field and laboratory tests that a thin layer of clay participates in the interface action and stress transfer between a cohesive soil and a concrete pile [10]. Third, contact occurs directly between two bodies, in which case the thin element represents a “smeared” zone that has properties different from those of the two bodies [10].

If appropriate laboratory tests can be performed on the equivalent solid specimens that can simulate the material in the thin layer, the elastic or elasto-plastic incremental constitutive matrix is obtained just like the case of surrounding solid elements [10].

Thus, its constitutive matrix  $[C]_i$ , is expressed through incremental stress-strain relation as;

$$\{d\sigma\} = [C]_i \{d\varepsilon\} \quad (2.12)$$

where all components of stress and strain are included in the equation above.  $\{d\sigma\}$  denotes the vector of increments of stresses;  $\{d\varepsilon\}$  expresses the vector of increments of strains whereas the constitutive matrix  $[C]_i$  is given by;

$$[C]_i = \begin{bmatrix} [C_{nn}]_i & [C_{ns}]_i \\ [C_{sn}]_i & [C_{ss}]_i \end{bmatrix} \quad (2.13)$$

where  $[C_{nn}]$  and  $[C_{ss}]$  express the normal and shear components respectively.  $[C_{ns}]$   $[C_{sn}]$  represents the coupling effects. The coupling terms are usually excluded since they are difficult to determine from laboratory tests [10].

If it is not possible to find properties of the thin layer from testing with solid specimens that simulate the material at the interface, which is more often the case, one can use an approximation. In this case, the properties are often found from shear tests on interfaces between two bodies. The laboratory results are obtained in terms of shear stress,  $\tau$ , versus relative shear displacement,  $u_r$ ; and normal stress,  $\sigma_n$ , versus relative normal displacement,  $v_r$ , which leads to;

$$k_s = \frac{d\tau}{du_r} \quad (2.14)$$

$$k_n = \frac{d\sigma_n}{dv_r} \quad (2.15)$$

where  $k_s$  and  $k_n$  are the (tangent) shear and normal stiffnesses of the interface, respectively.

Unlike the assumption of zero thickness in previous other formulations, a basic assumption made is that the behavior near the interface involves a finite thin zone. As mentioned formerly, the assignment of arbitrarily high values for the normal stiffness may cause erroneous results. Provided that the interface is encircled by the structural and geological materials, its normal characteristics during the deformation process must be dependent upon the characteristics of the thin interface zone as well as the state of stress and characteristics of the surrounding elements. This approach, as stated previously, prevents one to assign an inappropriate arbitrarily high value for the normal stiffness. Relying on these considerations, it was proposed to express the normal stiffness as a function of such influencing factors [25];

$$[C_n]_i = [C_n(\alpha_m^i, \beta_m^g, \gamma_m^{st})] \quad (2.16)$$

where  $\alpha_m^i, \beta_m^g, \gamma_m^{st}$  ( $m = 1, 2, \dots$ ) express the nature of the interface, geological and structural elements, respectively. Equation 2.16 can be re-written as;

$$[C_n]_i = \lambda_1[\bar{C}_n]_i + \lambda_2[C_n^g] + \lambda_3[C_n^{st}] \quad (2.17)$$

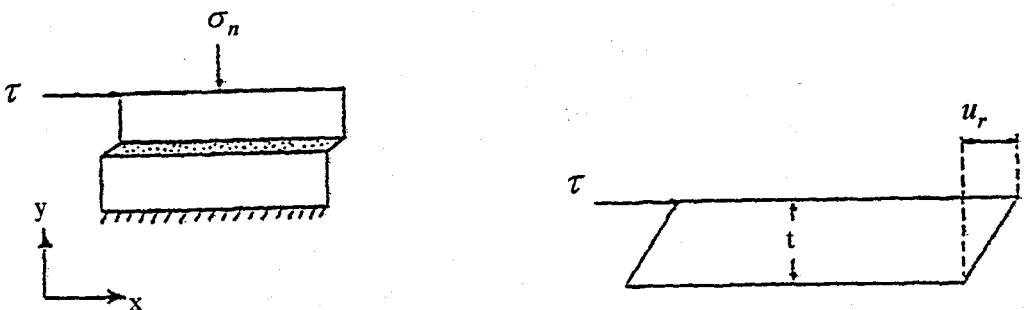
where  $[\bar{C}_n]_i$  indicates the normal behavior of the thin interface element.

Depending on the degree of influence, the participation factors  $\lambda_1$ ,  $\lambda_2$  and  $\lambda_3$  are varying from 0 to 1. Equation 2.17 is expressed as an addition of various components. One simplification of assigning  $\lambda_1 = 1$  and  $\lambda_2 = \lambda_3 = 0$  would imply that the normal component is based on the normal behavior of the thin-layer element evaluated just as the adjacent soil element [12]. Furthermore, studies pointed out that satisfactory results are acquired when the interface normal component is attributed with equivalent properties as the geological media [26,27]. This assumption provides satisfactory results as long as the significant deformation is the stick mode. The contribution of the participation factors becomes especially essential when opening or debonding is initiated [12].

The shear component  $[\bar{C}_s]_i$  is obtained from direct shear or other interface shear testing devices shown in Figure 2.8. Assumptions are made that  $[\bar{C}_s]_i$  is composed of a shear modulus  $G_i$  for the interface. The widecommon expression used for tangent  $G_i$  is given by;

$$G_i(\sigma_n, \tau, u_r) = \frac{\partial[\tau(\sigma_r, u_r)]}{\partial u_r} t \Big|_{\sigma_n} \quad (2.18)$$

where  $t$  defines the thickness of the element and  $u_r$  stays for the amount of exercised relative displacement.



(a) Schematic of direct shear test

(b) Deformation at the interface

FIGURE 2.8. : Behavior at the interface with "thin-layer" element [12]

The thin-layer element can be formulated either by assuming it to be linear elastic, nonlinear elastic or elastio-plastic. The evolution of its stiffness properties traces essentially the same procedure as solid elements. That is its stiffness matrix  $[k]_i$  is written as;

$$[k]_i = \int_V [B]^T [C^{ep}]_i [B] dV \quad (2.19)$$

where  $[B]$  stays for the transformation matrix;  $V$  for volume and  $[C^{ep}]_i$  for the constitutive matrix. So that the corresponding element equations are formulated as;

$$[K]_i \{q\} = \{Q\} \quad (2.20)$$

where  $\{q\}$  is the vector of nodal displacements and  $\{Q\}$  is the vector of nodal forces. For linear elastic behavior,  $[C^e]_i$  can be expressed as [12];

$$[C^e]_i = \begin{bmatrix} C_1 & C_2 & C_2 & 0 & 0 & 0 \\ C_2 & C_1 & C_2 & 0 & 0 & 0 \\ C_2 & C_2 & C_1 & 0 & 0 & 0 \\ 0 & 0 & 0 & G_{i1} & 0 & 0 \\ 0 & 0 & 0 & 0 & G_{i2} & 0 \\ 0 & 0 & 0 & 0 & 0 & G_{i3} \end{bmatrix} = \begin{bmatrix} [C_n]_i & 0 \\ 0 & [C_s]_i \end{bmatrix} \quad (2.21)$$

where;

$$C_1 = \frac{E(1-\nu)}{(1+\nu)(1-2\nu)} \quad (2.22)$$

$$C_2 = \frac{E\nu}{(1+\nu)(1-2\nu)} \quad (2.23)$$

Here,  $E$  is the elastic modulus (*Young modulus*),  $\nu$  is the *Poisson ratio* and  $G_{ii}$  ( $i = 1,2,3$ ) are the shear moduli defined formerly in Equation 2.18. If the material's shear behavior is assumed to be isotropic; it follows that  $G_{i1} = G_{i2} = G_{i3}$ . By this formulation it has been assumed that the shear response is uncoupled from the normal response represented by  $[C_n]$ .

For two-dimensional plane strain idealization, the special form of  $[C^e]_i$ , and its inverse form  $[D^e]_i$ , are given as [12];

$$[C^e]_i = \begin{bmatrix} C_1 & C_2 & 0 \\ C_2 & C_1 & 0 \\ 0 & 0 & G_i \end{bmatrix} \quad (2.24)$$

$$[D^e]_i = \begin{bmatrix} \frac{1-\nu^2}{E} & \frac{-\nu(1+\nu)}{E} & 0 \\ \frac{-\nu(1+\nu)}{E} & \frac{1-\nu^2}{E} & 0 \\ 0 & 0 & \frac{1}{G_i} \end{bmatrix} \quad (2.25)$$

The latter expression is used in mixed finite element procedures.

On behalf of nonlinear elastic behavior,  $E$ ,  $\nu$  and  $G$  can be defined as variable moduli founded on either triaxial or direct shear tests [28,29]. One way of expressing  $G_i$  is;

$$G_i = K\gamma_w \left( \frac{\sigma_n}{p_a} \right)^n \left( 1 - \frac{R_{fr}}{c_a + \sigma_n \tan \phi} \right)^2 \quad (2.26)$$

where  $K$ ,  $n$  and  $R_{fr}$  are material parameters;  $\gamma_w$  is the unit weight of water;  $p_a$  stays for atmospheric pressure;  $c_a$  and  $\phi$  are cohesion and the angle of friction, respectively.

In addition to the foregoing linear and nonlinear elastic models, when required to account for elastic-plastic behavior, the formulation of the resultant constitutive matrix for the interface is expressed as;

$$[C]_i^{ep} = [C^e(k_s, k_n)]_i - [C^p(k_s, k_n, \{du_r^p\})]_i \quad (2.27)$$

where  $\{du_r^p\}$  is the vector of incremental relative displacements. Equation 2.27 is founded on the basis of the yield and flow criteria of the theory of plasticity. Conventional criteria such as *Mohr-Coulomb* can be used with yield function,  $f$ ; and plastic potential function,  $Q$ . It follows for associated plasticity that  $f = Q$  [12]. To allow for dilatancy in the case of rock joints different  $f$  and  $Q$  can be used in the context of non-associative plasticity [12].

## 2.4. Fundamental Aspects of the Pile-Soil Assembly

### 2.4.1. Influence of Soil Type on Static Pile Capacity

Internal friction  $\phi$  and cohesion  $c$  are the soil parameters required for static bearing capacity analyses of piles. These soil parameters may be derived from laboratory direct shear or triaxial tests conducted on “undisturbed” samples. Although such an approach is quite satisfactory for piles in predrilled holes, the resulting parameters are not conveniently accountable for driven piles since the soil in immediate vicinity of the pile experiences both extensive remolding and a change in water content that is very often accompanied with an increase in density [30]. Alternatively, there is also a tendency to refer to CPM or PMT to obtain such in situ parameters. However, most pile design parameters still rely heavily on SPT  $N$  values in sands and unconfined compression strength tests for unconfined compression strength  $q_u$  in cohesive soil mediums [30].

Driven piles always produce due to the advancing process significant remolding of the soil in the immediate vicinity of the pile. At this instant, provided that the degree of saturation  $S_r$  is low, undrained soil-strength parameters are produced which may approach remolded drained values [30]. In general, considerable time has to be elapsed ( several months to years ) before the full design loads are applied. During this interval the excess pore pressures dissipate such that drained, remolded, soil parameters account for the soil behavior [30].

When placed into soft clays, the pile capacity increases with time, with most strength regain occurring in from 1 to 3 months [30-32]. This is partially explicable by the high pore pressures and the displaced volume effect producing a rapid drainage and consolidation of the soil very close to the pile shaft. Actually, the soil zone of 50 ~ 200 mm close to the pile is likely to consolidate to such a high extent that the effective diameter of the pile is increased by 5 to 7 per cent beyond its actual value. The reduced water content resulting from consolidation in this zone has been observed for some time [30,33]. The increase is likely to be marginal in very stiff and/or overconsolidated clays; in fact the capacity may decrease slightly with time as high lateral pressure dissipates via creep over a period of time [30].

The existing soil state remains almost nearly the drained condition, where piles are placed in predrilled holes. Possible deterioration of the cohesion at the interface due to the fresh concrete paste and liquified soil may occur but this may be partially offset by the slight increase in pile diameter as grains in the surrounding soil become part of the pile shaft as a consequence of cement hydration [30]. The loss of  $K_0$  from expansion into the cavity may be partially overcome by the lateral pressure produced from the fresh concrete paste which has a higher density when compared with that of the soil [30].

Additionally, to prevent an imminent undesired decline of the friction angle at the pile-soil interface, concreting should subsequently follow the boring process with least possible delay. Initially, the friction angle is relatively higher than the internal angle of the soil due to the surface roughness of concrete. Even a one day delay in concreting would be sufficient to lower the friction angle value below the internal friction angle value. It has been observed that shearing, in this case, occurs within the pile-soil interface that is smoother in texture when compared with that of the surrounding soil medium [34].

It has been confirmed by *Skempton* that adhesion along the pile shaft is directly related to the water content of the clay adjacent to the pile shaft [35]. An increase in water content around the pile shaft can be declared by any of the succeeding factors : (1) out-flow of water from the clay medium during the boring process. (2) water migration from clay surrounding the pile to the bore-hole through the less highly stressed zone. (3) water poured into the boring to facilitate the advancing process. (4) water expelled from the fresh concrete mortar. Thus, an increase in water content inevitably softens the clay and consequently leads to a reduction in adhesion. *Skempton* claimed further that even in the case where perfect contact generated between clay and concrete with no change in water content, the ratio of adhesion to the original strength is limited to 0.8 [35]. Furthermore, a deviation of even one per cent from the initial water content can account for a 20 per cent change in the adhesion factor  $\alpha$  [35].

## 2.4.2. Soil - Pile Interaction : Mechanism of Load Transmission

Analysis of the bearing capacity of a pile contains the assumption that both the pile tip and all points of the pile shaft have moved sufficiently with respect to adjacent soil to develop simultaneously the ultimate point and skin resistance of the pile [36]. Investigations made in the field on bored-cast in-situ piles as well as microfabric studies conducted on laboratory specimens revealed the fact that upon loading, shearing occurs within a thin zone in the clay adjacent to the pile shaft [36-38]. It was *Meyerhof* who pointed out that the dimensions (i.e., pile length and shaft diameter) of a pile have by far no impact on shaft adhesion of bored piles [39]. Since the soil is subjected to shearing while it is being augered prior casting the concrete, small settlements are sufficient to mobilize complete shaft adhesion afterwards. Modern research on pile behavior has established that full mobilization of skin resistance requires that slip to develop maximum skin resistance is on the order of 5 to 10 mm, regardless of pile size and length [30,36]. The amount of slip required is relatively independent of shaft diameter and embedment length, but may depend upon soil parameters [30,36]. However, sufficient slip at any point along the shaft to mobilize the limiting shear resistance is not the same as the tip movement measured in a pile-load test but is larger than the slip to produce maximum resistance [30].

Contrary, the displacement needed to mobilize point resistance for very large piles may be relatively large. Mobilization of the ultimate point resistance requires a point displacement in the order of 10 per cent of the tip diameter  $B$  for driven piles and up to 30 per cent of the base diameter for bored piles. This is a total point displacement and in material other than rock it may include point displacement caused by skin resistance stresses transferred through the soil to produce settlement of the soil beneath the pile tip. With the exception in very soft soils it is highly probable that skin resistance can be regarded as the principal load-carrying mechanism in the usual range of working loads [30,36].

Relying on the fact that the pile unloads to the surrounding soil through skin resistance, the pile load will diminish from top to point. The elastic shortening (and relative slip) will be larger in the upper shaft length from the larger axial load being carried. Examination of a large number of load-transfer curves suggested that the load transfer is approximately parabolic and decreasing with depth for cohesive soils [36].

The mechanics of load transfer between pile and the adjacent soil represent a relatively complex phenomenon. It is affected mainly by stress-strain-time and failure characteristics of all elements of the pile-soil system [36]. Imperceptible features resulting from the procedures used in placing the pile into its particular location play also a role in this mechanism [36]. However, some parameters affecting this load transfer are often difficult to express in numerical terms. The numerical assessment of load transfer characteristics of a pile-soil system is essential both for settlement computations and for rational design of pile foundations. The followings may illustrate the essential elements of analytical approaches currently used for that purpose.

The ultimate load  $Q_u$  that a pile can safely bear without suffering excessive deformation and stresses can be expressed mathematically as the addition of the point resistance and the skin friction, yielding in;

$$Q_u = Q_p + Q_s \quad (2.28)$$

where  $Q_p$  represents the load carried by the pile point and  $Q_s$  expresses the load taken by skin friction of the pile shaft. The mechanism of transfer of these components will depend upon the properties of soils and interfaces and on other factors introduced by construction and geological characteristics of the site.

The case where a single pile of diameter  $B$  is placed in soil to depth  $D$  and loaded by a vertical central load  $Q$  is shown in Figure 2.9.-(a). If the axial load applied on the pile at the ground surface level ( $z = 0$ ) is gradually increased the measured axial force in the pile against depth  $z$  can be plotted as curve 1, plotted in Figure 2.9.-(b). The function  $Q(z)$  represents the nature of the load transfer along the pile shaft. The ordinate of this curve at  $z = D$  represents the pile point load  $Q_p$ , whereas the difference  $Q - Q_p = Q_s$  equals to the pile skin load. The slope of the function  $Q(z)$  divided by the pile perimeter length  $p$  yields the distribution of skin resistance per unit area ( $f_z$ ) along the shaft as shown in Figure 2.9.-(c) [30,36]. Accordingly;

$$(f_z) = \frac{1}{p} \frac{dQ(z)}{dz} \quad (2.29)$$

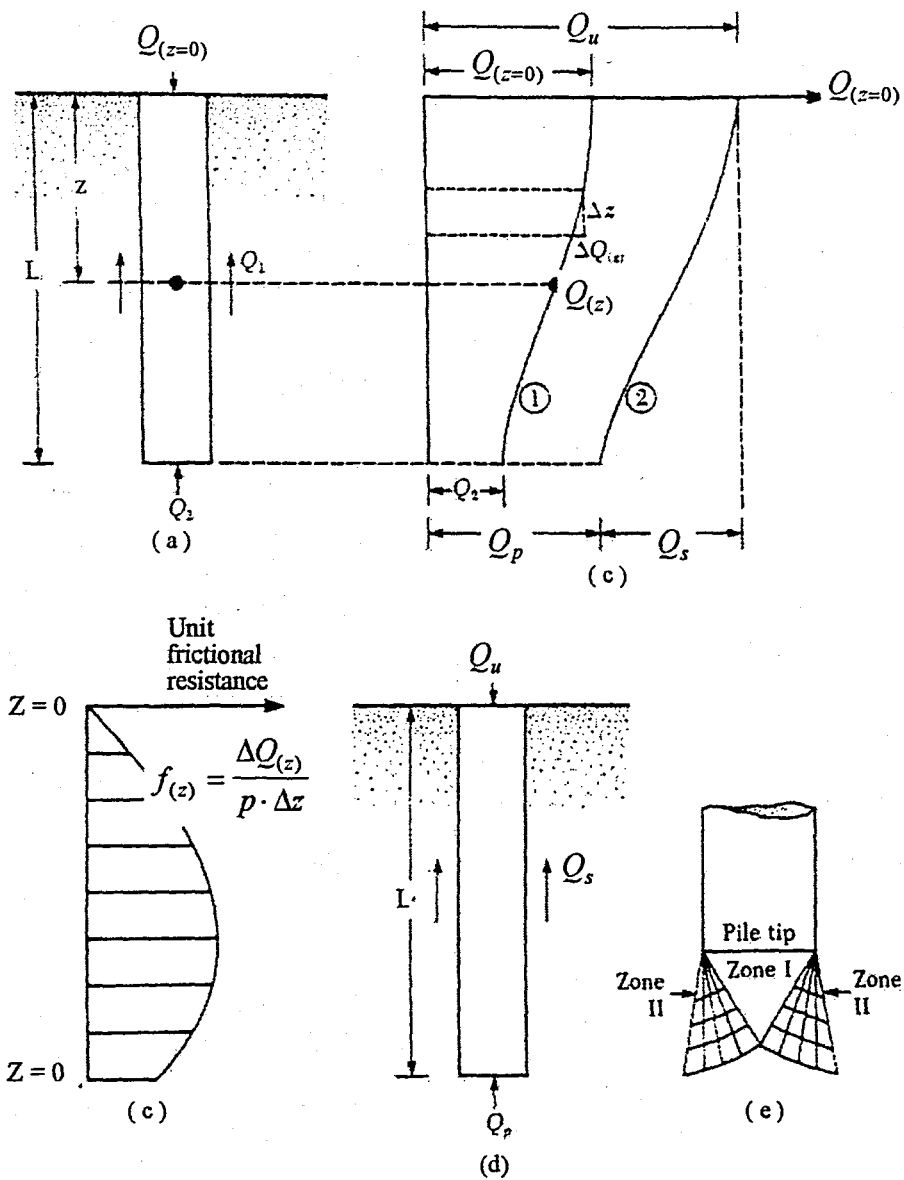


**FIGURE 2.9. : Load transmission mechanism for piles [40]**

When the load applied to the pile reaches its ultimate value like that in curve 2 of Figure 2.9, it follows that  $Q_{z=0} = Q_u$ ,  $Q_1 = Q_s$  and  $Q_2 = Q_p$ . However, as mentioned before, skin friction  $Q_s$  is developed significantly prior to the point resistance,  $Q_p$ .

Finally, according to the observations experienced on models and full-size piles, a highly compressed conical wedge as it is illustrated in Figure 2.9.-(e) is always available under the pile tip. In relatively loose soil, this wedge forces its way through the mass without producing other visible slip surfaces [30,36].

### 2.4.3. Components of Pile Resistance

For design purposes the ultimate load capacity of a pile, superimposed as in Equation 2.28, is composed of the point or tip resistance  $Q_p$  and the shaft or skin resistance  $Q_s$ .

The way how the ultimate bearing capacity of shallow foundations is calculated resembles the calculation of the unit point resistance of a pile differing in the way that the dimensionless bearing capacity factors are related to both shape and depth [36].

Conventional theories present the solutions for the unit bearing capacity  $q_p$  of the pile tip in the well-known form as;

$$q_p = cN_c^* + q_v N_q^* \quad (2.30)$$

in which  $c$  represents the strength intercept (cohesion) of the assumed straight-line *Mohr* envelope of the soil supporting the pile tip whereby  $q_v$  accounts for the effective vertical stress in the ground at the foundation level.  $N_c^*$  and  $N_q^*$  are dimensionless bearing capacity factors.

Thus, the point bearing capacity  $Q_p$  of piles can be expressed as follows where  $A_p$  equals to the area of the pile tip;

$$Q_p = A_p q_p = A_p (cN_c^* + q_v N_q^*) \quad (2.31)$$

Since the pile diameter  $D$  is relatively small, the term arising from friction can be neglected without loss in accuracy.

The *skin resistance* being the other main component of the ultimate load capacity of a pile is positively affected by the introduction of lime into the surrounding soil and constitutes the main concern in this study. Skin resistance is generated whenever small value of relative slip is provided between the pile and soil. Slip is recognized through the accumulated differences in shaft strain from axial load and the soil strain caused by the load transferred to it via skin resistance [30].

The slip progresses down the pile shaft as the applied vertical load increases. Where limiting shear resistance is developed due to large slips in the upper zones, part of the load is transferred back into the pile shaft. This leads to generation of larger relative slips at progressively greater depths. Figure 2.10 depicts ultimate and limiting shear with respect to relative slip. The skin resistance approaches a limiting value all along the pile shaft with possible exception close to the tip as the pile is further loaded axially [30,36].

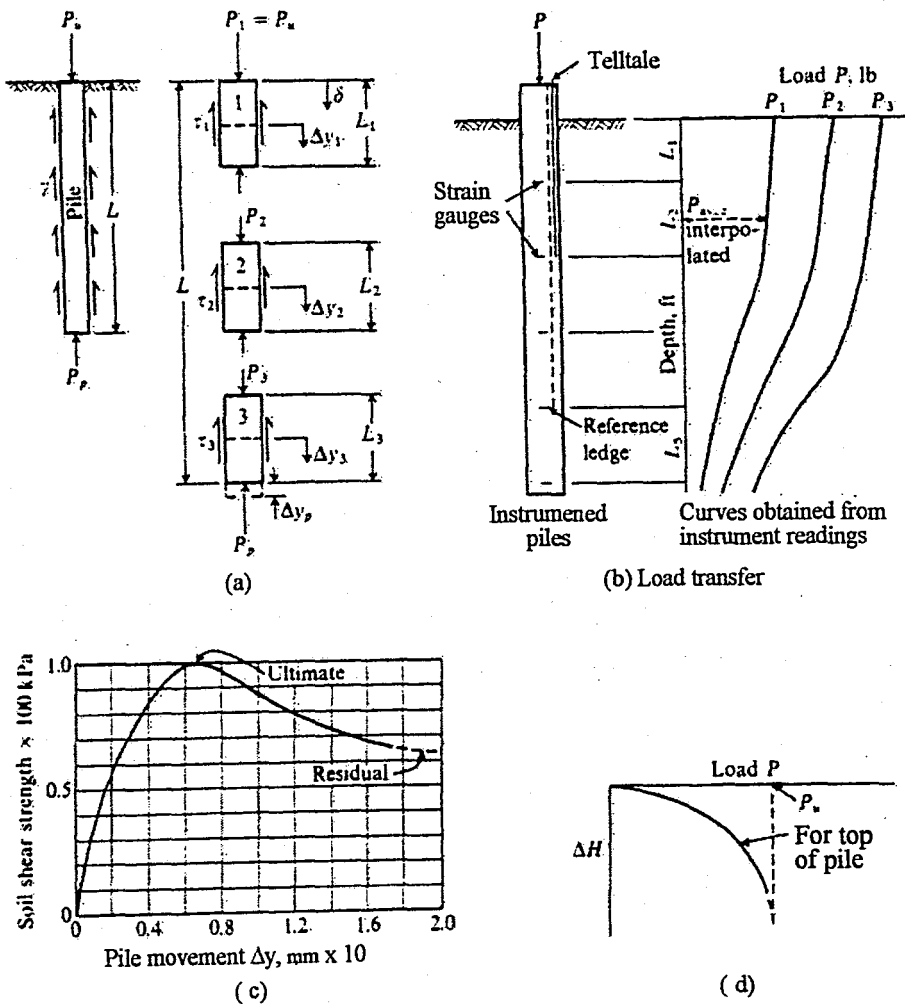


FIGURE 2.10. : Load-settlement relationship for axially loaded piles [41]

Similarly to the analysis of resistance to sliding of a rigid body in contact with soil, the theoretical approach for evaluation of unit skin resistance  $f_s$  for cohesive soils consists of two main parts : (1) *adhesion*  $c_a$ , which should be considered independent of normal stress  $q_s$  acting on foundation shaft. (2) *friction*, which should be proportional to that normal stress. Thus, the unit skin resistance between any particular soil medium and the foundation shaft equals to;

$$f_s = c_a + q_s \tan \delta \quad (2.32)$$

In this equation,  $\tan \delta$  accounts for the coefficient of friction between the soil and the shaft. Experiences with piles of normal roughness proved that it can be taken equal to  $\tan \phi'$ , the coefficient of friction of the remolded soil in terms of effective stresses. The pile-soil adhesion  $c_a$  is normally small and can be neglected for design purposes. The normal stress on the shaft  $q_s$  is usually related to the effective vertical stress at the corresponding level by a coefficient of skin pressure  $K_s$ . Since  $K_s$  is defined as  $q_s/q_v$ , the prescribed equation can be rewritten as;

$$f_s = K_s \tan \phi q_v \quad (2.33)$$

The coefficient  $K_s$  is governed mainly by the initial ground-stress conditions and the method of placement of the pile as well as by the pile shape (particularly taper) and length.  $K_s$  is equal to or smaller than the coefficient of earth pressure at rest  $K_0$  in bored or jetted piles. Although it is somewhat larger, it hardly exceeds 1.5 for low displacement driven piles.  $K_s$  can be as high as the coefficient of passive earth pressure  $K_p$  for short, driven, high-displacement piles operating in sand. However, its magnitude seems to decrease with increasing penetration depth. This reflects the fact that the effective stresses beneath the tips of such piles can be remarkably lower than the initial ground stresses at the same level [36,42-44].

For the case where piles are driven into normally consolidated soft-to-firm clays,  $K_s$  roughly equals to  $K_0$ . Low initial skin resistance can be attributed to the presence of pore pressures produced due to pile driving and corresponding reduction in effective overburden stress  $q_v$ .

As the pore pressures dissipate and  $q_v$  approaches its initial value, the skin resistance of many clays may become approximately equal to their undrained shear strength  $s_u$ . This fact is actually provided over a considerable time span and has established a basis to make comparison between the skin resistance and the undrained shear strength for all clays [36,45].

$$f_s = \alpha s_u \quad (2.34)$$

where  $\alpha$  is known as the shear strength ( reduction ) factor that can vary between 0.2–1.5 for different pile types and soil conditions. It has been suggested that for soft-to-firm clays,  $\alpha$  should be equal to 1. For cast-in-situ bored piles in London clay  $\alpha$  varies between 0.3 for very short piles to 0.6 for long piles, with an average value of 0.45 [36,46].

Recall that with the addition of lime,  $f_s$  is unambiguously improved, whereby the skin or frictional resistance component of the ultimate load capacity of a pile can be estimated as follows;

$$Q_s = A_s f_s = \sum p \Delta L f_s \quad (2.35)$$

where  $A_s$  expresses the bearing area of the shaft,  $p$  equals to the perimeter of the pile shaft,  $\Delta L$  is the embedded increment,  $f_s$  accounts for the unit skin resistance and  $\sum$  sums the contributions from possible strata or pile segments.

#### 2.4.4. Criterion and Computation of the Ultimate-Load

The mode of shear failure that the soil under a shallow foundation will experience varies with the soil type, rate of loading and other factors. Contrary, experience shows that soil under a deep foundation fails essentially in the same manner [47]. Failure is reached through punching shear below the foundation point that is accompanied or preceded by direct-shear failure of the soil along the foundation shaft [47]. The ultimate load is hardly well defined in many instances while the foundation neither exhibits a visible collapse nor a clearly defined peak load [30,36,40,47].

The various empirical ultimate-load criteria proposed by many different researchers are often based on considerations of plastic or total settlements of the pile under the test load. A comparison of ultimate loads obtained by applying these criteria to results of actual load tests shows relatively little difference ( $\pm 10$  per cent). However, substantial differences between ultimate loads obtained by various criteria can be found from results of load tests of large-diameter or very long piles [36,48].

Based on knowledge of basic load-settlement relationships of loaded areas demonstrates that (0.8 mm/metric ton) of deformation may be indicative of failure stage for a small pile and still represent a normal deformation rate of a large pile in the safe-load range [36]. The most acceptable ultimate load criterion for general engineering practice states; "Unless the load-settlement curve of a pile shows a definite peak load, the ultimate load is defined as the load causing total pile settlement equal to 10 per cent of the point diameter for driven piles and 25 per cent of the point diameter for bored piles." [36].

There exists an obvious similarity between the basic problem of the ultimate load computation of a deep foundation and the analogous problem for a shallow foundation. Despite this similarity there are some distinct differences present. The bearing soil under the foundation base of a shallow foundation is normally not disturbed. Cases where changes in effective ground stresses caused by excavation, placing of the footing or backfilling occur, are regarded as exceptions. Contrary, the bearing soil along a deep foundation is normally almost always disturbed. The soil type and method of placement of the foundation determine the degree of disturbance. In the case of bored piles most of the change occurs around the foundation shaft [36].

A relatively narrow zone of soil surrounding the pile inevitably undergoes some remolding because of soil removal by augering. Simultaneously, with respect to the construction procedure, some lateral-stress is provided prior the installation of the foundation. When piles are driven, substantial soil remolding both above and below the foundation base is unavoidable. If the bearing soil is clayey based, a zone extending about one pile diameter around the pile may experience significant changes in structure. Depending on clay sensitivity, the soil may lose considerable shear strength, which is partially or totally regained over an extended period of time [36,40]. In the cases where piles are driven into saturated stiff clay, serious changes in secondary structure such as closing of fissures is exhibited [40].

This change extends to a distance of several diameters around the pile, with remolding and complete loss of effects of previous stress history in the immediate vicinity of the pile [36]. If the surrounding soil is cohesionless silt, sand, or partially saturated clay, pile driving may cause soil densification. It is more noticeable in the immediate proximity of the pile shaft and extends in gradually diminishing intensity over a region that encircles the pile shaft between one to two pile diameters [36]. The driving process is also accompanied by increases in horizontal ground stress and changes in vertical stress at the pile vicinity [36]. In dense and cohesionless soils, loosening may take place in some zones accompanied by substantial grain crushing and densification in the immediate vicinity of the pile [36]. In such soils there are highly noticeable permanent changes in both horizontal and vertical ground stress. Hard driving can leave large residual stresses in both the pile and the soil, consideration of which may be essential for understanding the behavior of the soil-pile system [36]. In applications, piles are often designed in groups such that the situation is further complicated by the complex and not always well-understood effect of placing of adjacent piles. For these and other reasons the problem under consideration poses difficulties. A general solution to the problem is not yet available and will be difficult to formulate.

#### 2.4.5. Construction Methods of Cast-In-Situ Concrete Piles

Cast-in-situ piles are constructed by one of the below described methods :

Dry Method : The shaft is drilled to the desired depth and is partially filled with concrete afterwards. The rebar cage is placed allowing the shaft to be completed. Although there exists no limitation on the length of the rebar cage, it should not extend to the bottom level of the shaft where a minimum concrete cover is required. The demanded site conditions for the utilization of this method are such that the shaft can be drilled and concreted before it is filled with sufficient water to adversely affect the concrete strength. Cohesive soil with low permeability characteristics as well as a water table below the base can thus be regarded as ideal conditions [30].

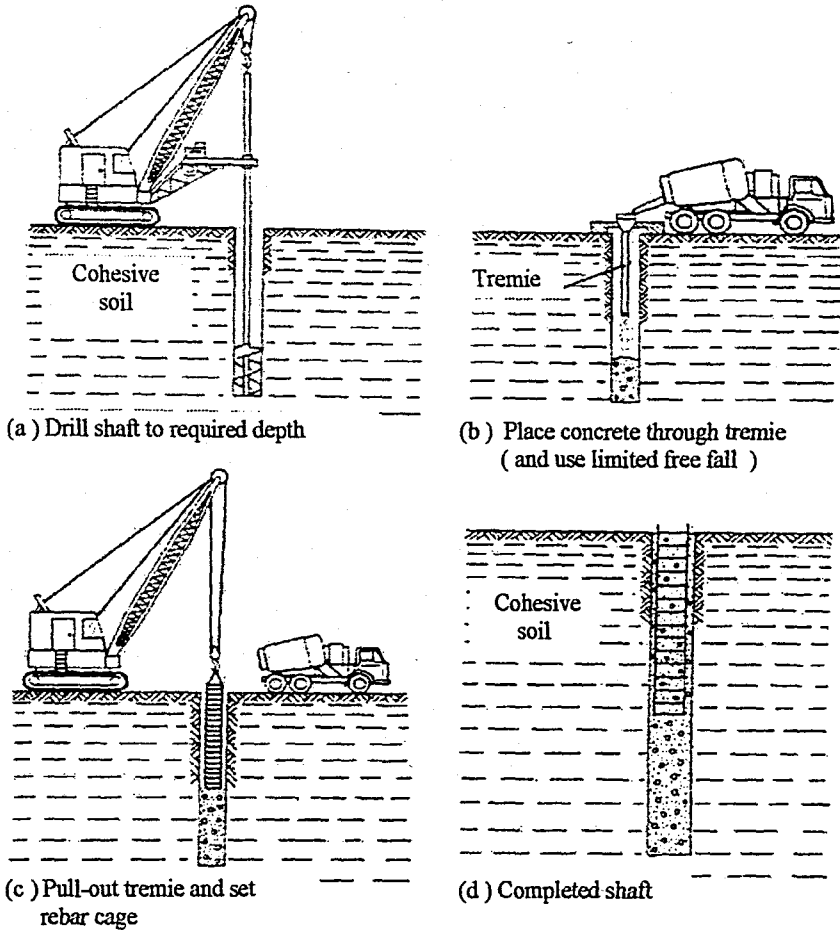


**FIGURE 2.11. : Dry method of cast-in-situ construction [30]**

**Casing Method :** The procedure sequence is outlined in Figure 2.11. This method is essentially required at sites where excessive lateral deformations toward the pile cavity are unavoidable. Sealing the hole against groundwater entry is another application reason despite the need of an impermeable stratum below the casing zone into which the casing can be socketed. The slurry injected serves to stabilize the hole and is bailed out after the casing is seated such that the shaft can be extended to the required depth in the dry [30].

The casing may be either left in place or removed. When it is decided to leave the casing in place, pressure-injected grout is applied to the base of the slurry providing to displace the slurry over the top and filling the void with grout. Alternatively, the casing can be removed with care on condition that the concrete inside the casing is still in its fluid state and the concrete “head” is maintained above the slurry head such that the concrete displaces the slurry and not vice versa [30].

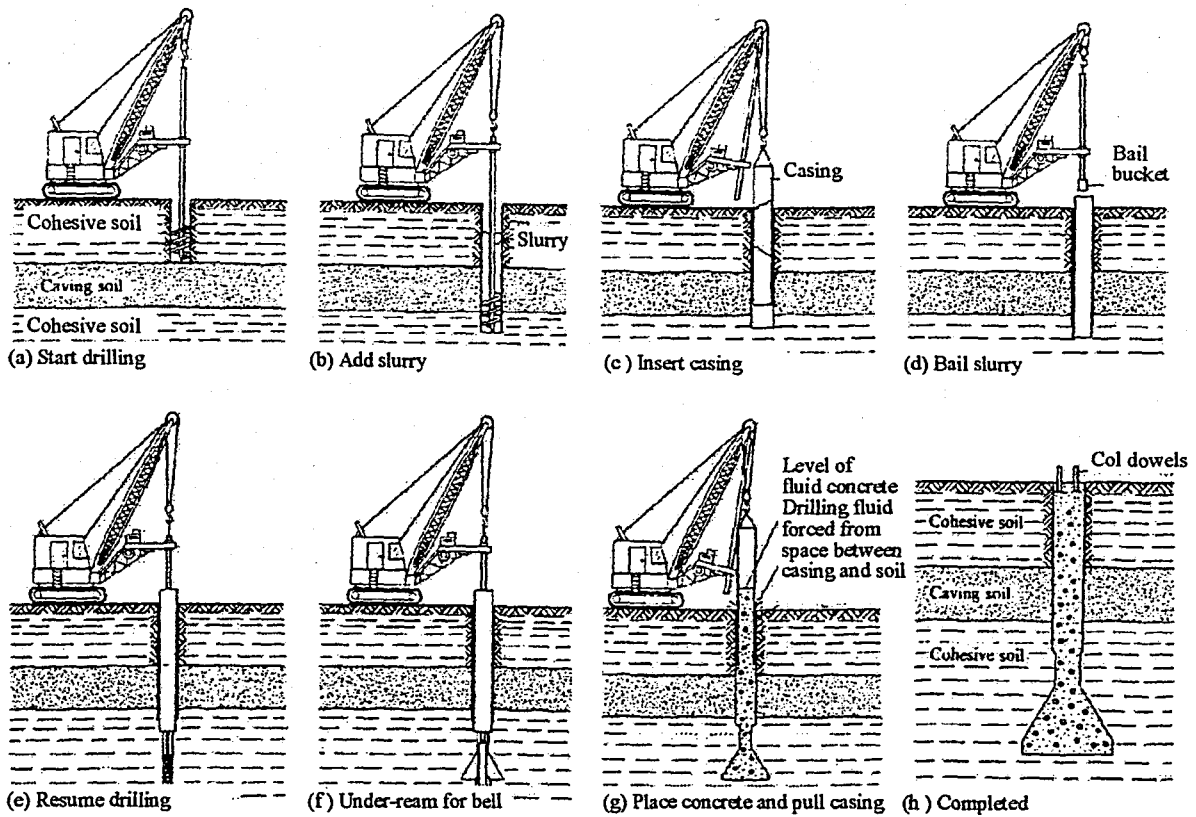


**FIGURE 2.12. : Casing in method of cast-in-situ construction [30]**

***Slurry Method :*** This method is applicable for any situation requiring casing. It is especially beneficial whenever the casing does not provide an adequate water seal for the shaft cavity against groundwater.

The important aspect in this method is that the available slurry head should withstand the pressure coming from the ground water table or the tendency of the soil to collapse. “Bentonite slurry” is the most commonly used one and consists of 4 to 6 per cent of bentonite by weight and water. However, the phase of the slurry should be capable of forming a filter cake on the shaft wall and carry the smaller excavated particles in excavation [30].

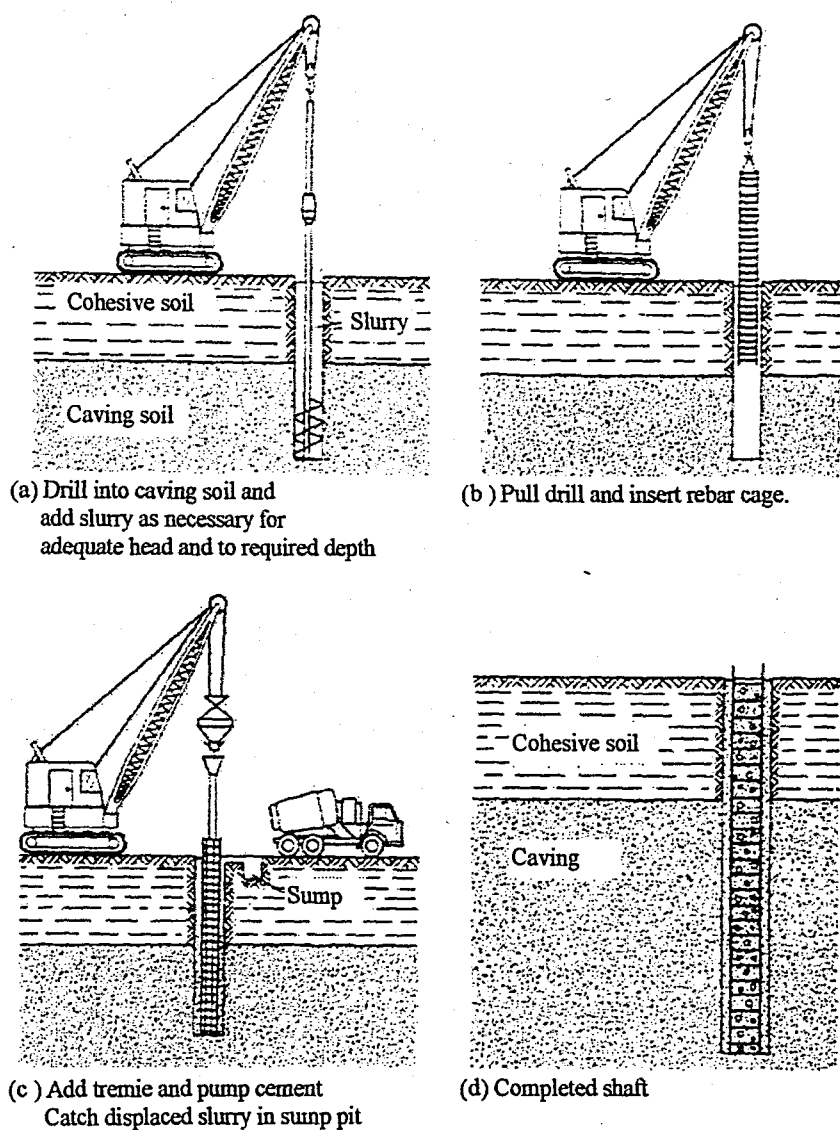


**FIGURE 2.13. : Slurry method of cast-in-situ construction [30]**

The application time of the slurry should be adjusted such that an excessively thick filter cake formation on the shaft wall is avoided since, otherwise, the displacement of a thick cake with concrete during shaft filling is difficult. Besides it is generally desirable to have the slurry pumped and the larger particles in suspension screened out with the “conditioned” slurry returned to the shaft just prior to concreting. Finally, of equal practical importance is the excavating procedure of clay through the slurry whereby pulling a large fragment could cause significant negative pore pressure to develop and gear a partial collapse of the shaft [30].

After the shaft is completed, the rebar cage is set in place and the tremie is installed, concrete is pumped ensuring that the tremie is well submerged in the concrete. Following this procedure provides that the concrete adequately displaces slurry from the rebar cage and forms a good bond [30].

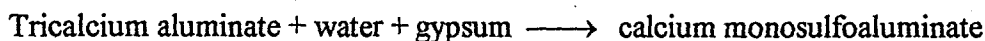
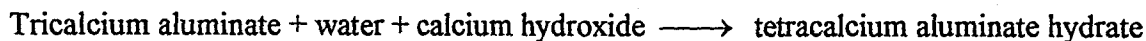
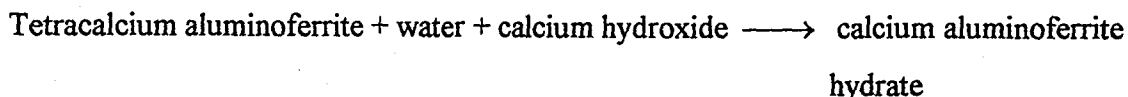
## 2.5. Stabilization Effect of Lime on Clayey Soils

First attempts to improve the engineering properties of cohesive soils in-situ with lime were made about 1960 by filling holes drilled in the soil with lime slurry. However, the use of lime as a stabilizing agent has remained limited mainly to semi-rigid road bases and subgrades in road construction as well as for the improvement of clayey bearing layers. Meanwhile this method is also employed also to the construction of embankments, soil exchange in sliding slopes, the backfill of retaining walls, soil improvement under foundation slabs and for lime piles.

The mechanical properties of clayey soils can be improved even by the addition of a small percentage by weight of lime. The shear strength of lime stabilized clayey based soils will acquire higher values than that of the undisturbed clay within one to two hours after contact with lime [49]. This rate of strength increase is valid even if the clay is highly sensitive and has lost a large portion of its initial shear strength due to remolding [49]. Hydrated lime, slaked lime and calcium hydroxide serve as natural stabilization agents for cohesive soils. Calcium hydroxide is no binder but will produce a binder mainly consisting of calcium silicate hydrates by slow chemical reactions principally with the silicates in the clay mineral of cohesive soils [49]. Because of its binding property and reactivity, it may be considered to be used for the stabilization of soils which are in contact with concrete structures. Its use would be specially beneficial in cases where skin friction such as cast-in-situ concrete piles or drilled piers is important for the bearing capacity.



Since cement is a mixture of many compounds, its exact representation by a chemical formula is difficult. However, four components; tricalcium silicate ( $C_3S$ ), dicalcium silicate ( $C_2S$ ), tricalcium aluminate ( $C_3A$ ), and tetracalcium aluminoferrite ( $C_4AF$ ) make up more than 90 per cent of the cement by weight [50]. All the compounds that constitute the clinker are anhydrous, but when water is added to portland cement, the basic compounds present are transformed to new compounds by chemical reactions as shown in Equations 2.37 [50].



Rapidly after mixing with water the dissolution reaction of the cement particles starts. Two calcium silicates, which constitute about 75 per cent of portland cement by weight, react with the water to produce two new compounds : tobermorite gel (not crystalline), and calcium hydroxide (crystalline). The excess lime is released as calcium hydroxide,  $Ca(OH)_2$ . Although both calcium silicates require the same amount of water,  $C_3S$  produces more than twice as much  $Ca(OH)_2$  as is formed by the hydration of  $C_2S$ . Thus, the  $Ca(OH)_2$  precipitates out as crystals from the supersaturated  $Ca(OH)_2$  solution produced by the rapid rate of hydrolysis of tricalcium silicate [51]. In completely hydrated portland cement paste, the calcium hydroxide accounts for 25 per cent of the weight and the tobermorite gel makes up about 50 per cent. The principal reaction products are ions like  $Ca^{+2}$ ,  $OH^-$ ,  $H_2SiO_4^{-2}$ ; which are mobile and may diffuse into the bulk of the solvent [50,51]. At this stage the ion concentrations in the bulk of the solvent are very low so that strong ion fluxes from the dissolution front away into the solvent can be monitored [52]. For a given temperature and pressure the ion concentrations can not take arbitrary high values. The ion concentrations are bounded by finite solubility products above which solid phases start to precipitate from the solution [52].

There are two associated precipitation reactions : (a) the precipitation of calcium hydro-silicate sometimes referred as “cement gel” and (b) the precipitation of calcium hydroxide or “*Portlandite*”. The growth of the cement gel is the basis for the whole cement binding process. Whereas the growth of *Portlandite* mainly happens in order to compensate for the accumulation of  $Ca^{+2}$  and  $OH^{-}$  ions in solution. Thus, the process of cement dissolution, ion transport, and cement gel/*Portlandite* precipitation is usually referred as “cement hydration”.

The resulting free lime amount in “Normal Portland Cement” is detected as and hardly ever exceeds a value of 1-2 per cent by weight [1]. However, such amount of free lime expelled from the fresh concrete mortar during the curing process of cast-in-situ concrete piles in boreholes is not capable to stabilize the surrounding soil medium efficiently. It may basically serve as a contributor for enhancing the shaft adhesion. Previous studies predicted the shaft adhesion factor to be as small as 0.30-0.35 per cent that is actually doubled in practical applications ranging between 0.55-0.75 [53]. This difference is likely to occur from the stabilizing effect of lime on the neighboring clay layer(s).

### 2.5.2. Alteration of Soil Parameters by Stabilization with Lime

Some beneficial effects of lime treatment on soil parameters being important for practical application can be observed in Figure 2.14.-a,b. The selection bases on the illustration that the general tendencies are visible and on the other hand inadmissibilities of generalizations are given. Basically, almost all properties of lime-treated soils depend on the properties of the natural soil, the per cent of lime added by weight, the curing time/method, environmental conditions, water availability, moisture content during compaction as well as the compaction efficiency [54]. Lime-soil mixtures when compacted beyond their optimum water contents attain after short curing time higher strengths than those compacted with moisture content below their optimum [54].

*Sabry and Parcher* (1979) claimed that this is possible due to the fact that lime diffusion is enabled to be more uniform in the former case [54]. However, it has been agreed that the strength of soils can be enhanced by further addition of water after compaction. *Ingles and Metcalf* (1972) noted that montmorillonitic clays give lower strengths with dolomitic lime than with high high-calcium or semi-hydraulic lime [55]. They reported further that kaolinitic clays on the other hand yield the highest strengths when mixed with semi-hydraulic limes and the lowest strengths are acquired with high calcium limes [55]. The followings summarize the changes recorded in the mechanical characteristics of clayey soils upon contact with lime.

*Compressive Strength* : The compressive strength  $q_u$  first raises with increasing dosage but tends to decline after acquiring a peak. The particles loose contact to each other within the gel which can actually be regarded as a lubricant. The point of saturation is recognized by the maximum value which shifts towards higher dosage with increasing curing time. However, the increase of strength is considerably low, if the samples are water-saturated after compaction. *Brandl* (1981) observed that the strength increase flattens after 1 to 2 years and becomes negligible even in active clays after 7 years [56]. Relying on long term ( from the 7<sup>th</sup> day on ) tests, he further mentioned that the time dependent increase of strength is approximately linear with the logarithm of time. This continuous slow gain in strength provides a considerable factor of safety for design based on 7-, 14- or 28 day strength [56].

*Tensile Strength* : *Brandl* (1967) performed direct one-dimensional tension tests with cylindrical samples and founded that a too small dosage of lime may result in a reduction of strength since the mixture flocculates [57]. Increased lime amount increases the tensile strength up to the point beyond which too high dosages lead to the production of an “inactive” substance. The time respective increase of the tensile strength  $\sigma_z$  show close resemblance to  $q_u$ . The ratio of compressive to tensile strength of lime stabilization oscillates around  $q_u/\sigma_z = 10$  [56,57].

*Deformation Behavior* : Studies performed on samples from special Proctor cylinders subjected to oedometer test at their natural water content or even under saturated conditions revealed that the change of the modulus  $E_s$  corresponds to similar regularities as the compressive strength.

However, the relative improvement of the deformation resistance after the addition of lime is much significant than the increase recorded for  $q_u$  [56]. Increases of the modulus may be as much as 20 to 40 times. Evaluated values from the modulus of elasticity  $E_{qu}$  from relating unconfined compression tests are different in nature since soils with a small amount of lime behave “brittle” i.e. without having adequate strength, their deformation quantity in the elastic state is very limited [56]. After the addition of lime, the specific deformations  $\varepsilon$  at failure are considerably lower without exception when compared with the natural untreated soil case [56]. They tend to diminish further with increasing time of reaction.

**Shearing Parameters :** The shear strength of lime stabilized or treated clayey soils increases significantly due to the rise of the friction angle and cohesion. The friction angle and especially the residual angle of shear rise already effectively after adding small amounts of lime ( about 2 per cent ) [56]. A higher dosage has negligible influence on the increase of shearing resistance. The peak value is reached within the first few days after treatment under consolidated drained and slow shear environment. Quick shear tests conducted on samples with natural water content in the triaxial apparatus proved that the friction angle increased considerably between the 1<sup>st</sup> and 270<sup>th</sup> day after the stabilization procedure [56].

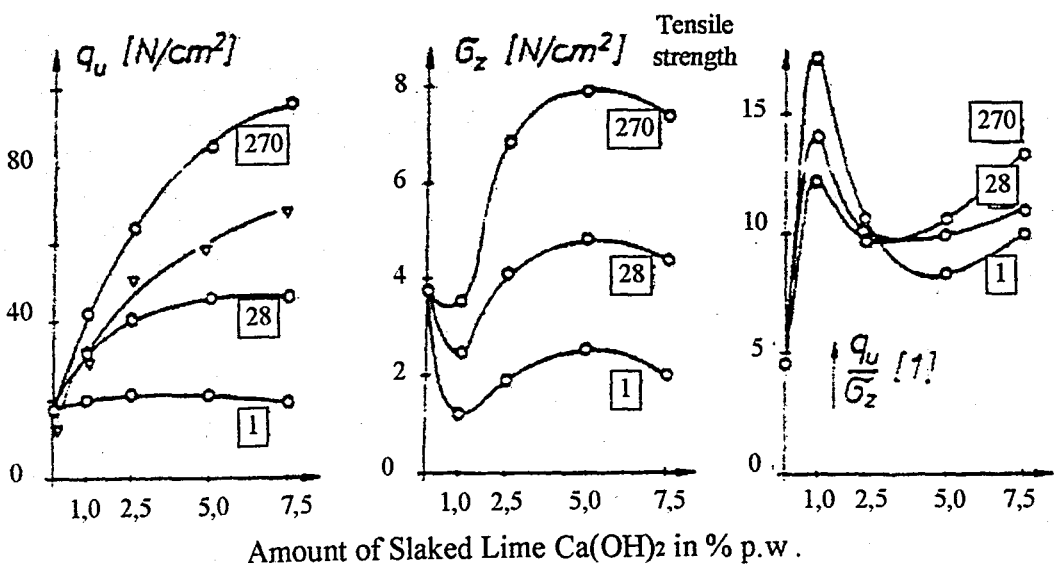


FIGURE 2.14.-a : Time respective effect of lime on parameters of clayey soils [56]

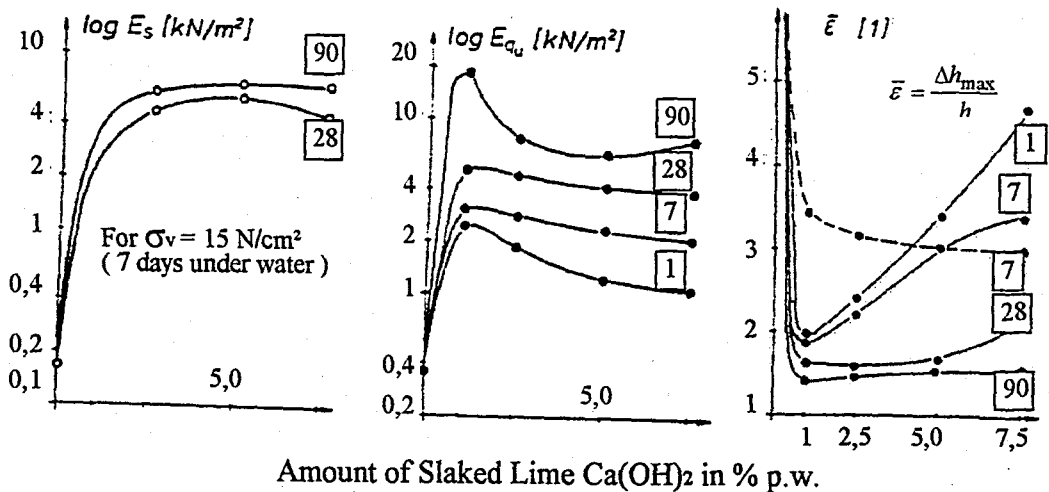


FIGURE 2.14.-b : Time respective effect of lime on parameters of clayey soils [56]

### 2.5.3. Theory and Mechanism of Lime-Soil Interaction

When clayey soils of high plasticity are treated with hydrated lime, or either ground quicklime or lime slurry, their plasticity index experiences an enormous decline [58]. All the same, as with cement, the mode of failure of the soil is changed from plastic to brittle after lime treatment and compaction at optimum moisture content [58]. A consequent improvement in shrinkage and drainage characteristics is also observed. The mixture being cured shows increased compressive strength and durability with time. A wide range of soils are suitable for treatment, although only some soils experience a remarkable increase in strength. The beneficial effects of lime can be declared through to the interaction between the lime added and the clay minerals present in the soil [58-60].

It is a well-known phenomena that clay minerals are structurally very tiny crystalline materials formed primarily from chemical weathering of certain rock forming minerals. The chemical combination of the minute, colloidal-sized clay crystals consists of hydrous aluminosilicates and other metallic ions [61]. Each of the distinct crystals resembles to miniature plates which consist of a number of crystal sheets that inherit repeated atomic structure. *Silica* and *alumina* are recognized as the principal sheets.

Beside their different bonding characteristics and their different metallic ions they accommodate in their crystal lattice, clay minerals simply differ from each other through the way in which these sheets are stacked together. Lime undoubtedly attacks all kinds of clay minerals while the amount of available silica determines the reaction intensity. In other words, three-layer clay minerals, whose lamellae expose silica faces on both sides, are more reactive than two-layer clay minerals whose lamellae expose silica at one face only [62]. A silica surface is not regarded as available if it is bound to a resembling surface by ions which are easily exchangeable. Accordingly illite, although still attacked is much less reactive than montmorillonite [62].

The reactions that take place when lime (calcium hydroxide) is introduced into a cohesive soil can be divided into two principal phases. Some reactions take place immediately while some of them occur during curing. The first phase being rather short, comprises the *ion exchange* and *flocculation* process whilst long term reactions establish the second phase of the stabilization process namely *cementation* and *carbonation*.

*PHASE (1)* [49,60-63] : Within a period of a couple of minutes up to some hours the texture of the soil is considerably changed. The transformation of the structure is a consequence of the *cation exchange* process. With the addition of lime, excess  $Ca^{++}$  ions are provided to the soil. A base exchange reaction occurs whereby strong dissociated bivalent calcium cations of lime present in the pore water replace weaker univalent alkali ions like sodium and hydrogen which are normally attracted to the negatively charged clay particles [63]. The number of electrical charges on the surface of the clay particles are thus altered. Cations like  $Na^+$ ,  $K^+$ ,  $Ca^{++}$ ,  $Mg^{++}$ ,  $Al^{+++}$  have an order of replaceability ascending generally from monovalent to multivalent [63]. As a consequence,  $Ca^{++}$  ions will replace dissimilar cations from the soil complex. Quicklime,  $CaO$ , would therefore immediately react with the water in the soil. This drying action is particularly beneficial in the treatment of moist clays. In the placement of lime columns and layers, the heat generation and expansion of the lime further enhance the consolidation effect [49]. Nevertheless, the cation exchange capacity depends very much on the pH value of the soil water as well as on the type of the clay mineral present in the soil [49]. Among the types of clay minerals montmorillonite has the highest and kaolinite has the lowest cation exchange capacity [63]. However, as many soil scientists do agree, natural soils are highly calcium saturated.

Recent work demonstrated that the natural saturation of montmorillonitic clays with calcium ranges between three third to three fourth. Therefore, the factor of cation exchange has not been regarded as a very significant effect of lime on clayey soils. During the cation exchange, particles containing clay minerals flocculate to larger-sized aggregates resulting in an apparent change in texture [63]. The plastic limit of the material is increased while the soils strength and stiffness are significantly enhanced. Flocculation is essentially inadequate to explain the improvement effect of lime on clayey soils since some soils (deposited in salt water-marine clays) may be found initially flocculated in nature. Moreover, naturally flocculated soils are instable and do not respond to the desired sense of lime treatment.

*PHASE (2)* [49,60-64].: The term "Pozzolan" is used to describe naturally occurring artificial siliceous or siliceous aluminous materials. Such materials possess actually little or no cementitious value. In the presence of moisture or a solvent like water, *pozzolanic reactions* occur between soil, lime, silica and alumina. These reactions are part of the second phase of the clay-lime reactions where lime acquires silica from the clay mineral lattice or from other pozzolans present in the soil to form compounds possessing cementitious properties. The soil type governs both the reactivity effectiveness and the type and amount of pozzolans produced. A high ground temperature and a high pH-value ( $\text{pH} > 12$ ) will accelerate the chemical reactions since the solubility of the silicates and the aluminates increases with increasing temperature and pH-values [49]. The base exchange and thus the reaction is remarkably low when the pH-value is less than seven. The pH-value will normally exceed 12 even when only a few per cent of lime have been contacted the soil [49]. Unfortunately, in the longer term the high basic pH medium may deteriorate the crystal lattice of clay as well as the formation of the cementitious products. Such produced cementing agents are generally regarded as the major source of strength increases noted in lime-soil mixtures. The shear strength of the stabilized soil gradually increases with time through pozzolanic reactions as the lime reacts with the silicates and aluminates in the clay. The reactions may last for over many months and years. The higher the surface area of the soil particles, the more effective is this process.

Nevertheless, lime is not suitable for improving the engineering properties of clean sands and gravels. Cementation is, however, limited by the amount of available silica. Increasing the quantity of lime added will increase strength only up to the point where all the silica of the clay is used up [64]. An excessive addition of lime can actually be counterproductive. Cementation takes place on the surface of clay lumps and causes a rapid initial strength gain. Further mass transport of the lime into the soil will bring about continued improvement in the longer term, measured in weeks or months. The process called *lime carbonation* is known as the reaction of lime with carbondioxide present in the soil voids or in the atmosphere [64]. Calcium carbonate regarded as relatively weak cementing agents are formed, depending on the type of lime used. These cementing agents are prone to deter pozzolanic reactions and diminish the amount of normal strength gain [63]. Nevertheless, since the long-term reactions of uncarbonated lime with soil itself would far exceed the contribution of calcium carbonate, carbonation is said to be a deleterious rather than a remedial phenomenon in soil stabilization.

Reactions prescribed in phase (1) lead to immediate improvement in soil plasticity, workability, uncured strength, and load deformation whereas the permanently developed strength is comparatively low. Plasticity and swell are reduced and workability is substantially improved as a result of the low plasticity and friable character developed by the lime-soil mixture [62]. Reactions explained in phase (2) and recognized through their relatively slow speed, lead to the formation of cementing products as well as to the accumulation of soil-lime reaction products. Pozzolanic reactions being the major shear strength contributor give rise to long-term increase in soil strength causing little or no change in water content, even many months after mixing and compaction [59,60].

*Saskatchewan* [65] has concluded to the following correlation among various factors in order to estimate the effectiveness of lime stabilization and measure the gain in shear strength at a particular time;

$$S_u = f(S_{uo}, A, A_w, W_0, c, t_a, t) \quad (2.38)$$

where  $S_u$  (kPa) is defined as the acquired undrained shear strength subsequently after compaction;  $A$ , being a mineralogical parameter, comprises influences like mineralogy, specific surface, grain size and cation exchange capacity.  $A_w$  implies an initial pore-water parameter;  $W_o$  (%) denotes the molding water content and  $c$  (%) stays for the concentration of the additive.  $t_a$  and  $t$  (days) refer to the time of mellowing and curing, respectively. The mellowing time is defined as the time span between the addition and compaction process, whereas the curing time reflects the time elapsed since compaction. It must also be notified that the texture of soil changes since the chemical attack on minerals results in alteration of parameters such as mineralogy and grain size distribution [59]. Index properties such as liquid and plastic limits, as stated earlier, are thus undoubtedly modified. These considerations obviously declare that only empirical approaches are feasible for the field of soil stabilization assessment.

*Locat et al.* [59] have claimed according to their laboratory observations that for a given particular soil specimen, the acquired long term strength is directly dependent upon both the molding water content and quicklime concentration. They concluded further that the increase in undrained shear strength  $S_u$  is directly proportional with increasing quicklime concentration and decreasing molding water content of the soil. That the initial governing reaction parameters are the grain size and the specific surface area has been announced by *Choquette* (1988) [66]. The evolution of pozzolanic reactions evidently declared the mineralogy of clay as the unique parameter that is positively related to strength development [59].

It has been agreed that lime concentration in solution diminishes during the pozzolanic reactions such that more lime must be dissolved so as to prevent the solution equilibrium. Hence, any increase in quicklime concentration is favorable for the strength development even though 0.1 per cent lime is adequate to saturate pore-water solution [59]. Furthermore, solid lime dispersion functions actually as a strong stabilization contributor. Tests reported by *Berube and Locat* (1987) accentuated that mixing lime with more energy such as under applied pressure yields in higher strength at equivalent lime concentration and time, being more evident for higher plasticity soils [67].

The schematic model describing the physicochemical process of lime stabilization proposed by *Ingles and Metcalf* (1972) is illustrated in Figure 2.15 [68]. It can be perceived from this model that reaction products diffuse into soil particles and create bridges or cover between or on soil particles. The produced cementitious agents provide increase in strength acting primarily on the cohesion factor of the shear strength parameters of the soil [59]. The model explicitly implies that a high water content soil may show a better performance than a low water content soil, because of the ease of movement of solutes through porous space.

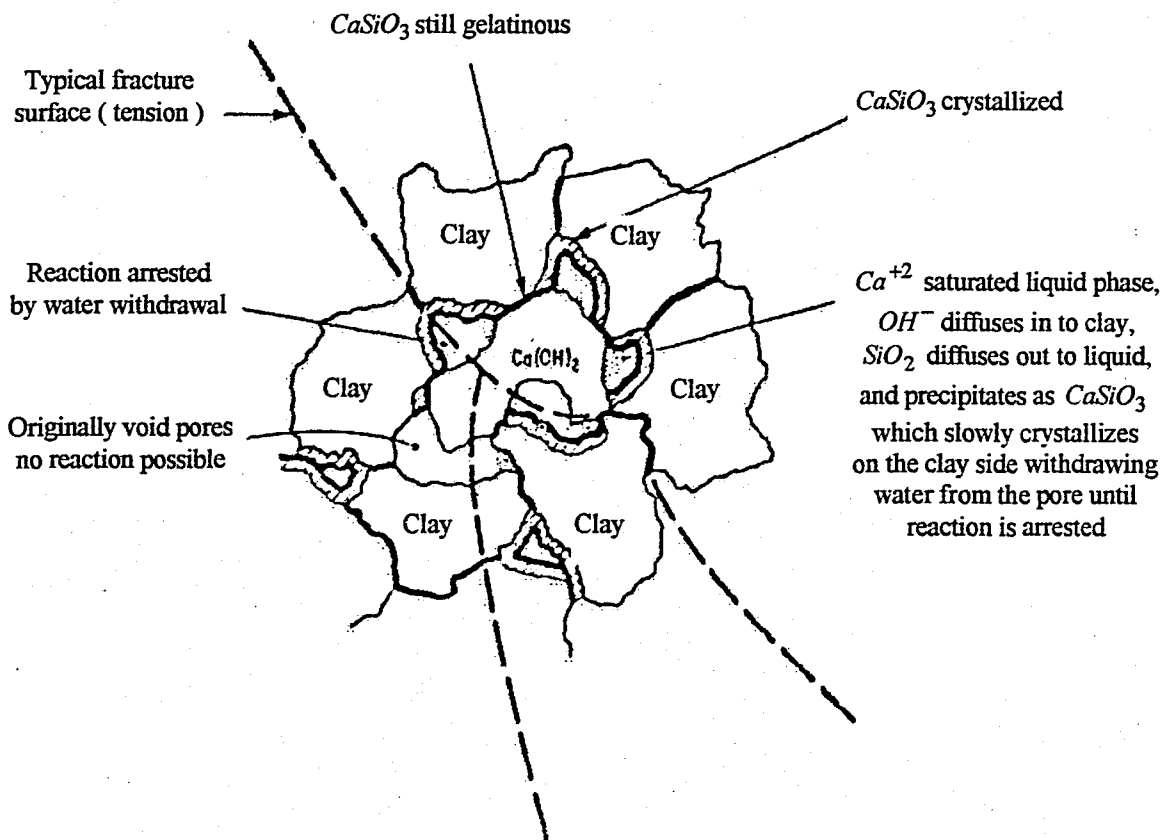


**FIGURE 2.15. : Illustration of mechanism of lime stabilization for clayey soil [68]**

#### 2.5.4. Effect of Curing Conditions on Strength Development

Curing is regarded as a major parameter affecting the strength of lime stabilized soil. Its effect on strength development is a function of time, temperature and relative humidity. Many researchers in the past have examined the effect of temperature curing on the compressive strength of lime treated cohesive soils. Every series of tests conducted on clayey soils yielded that the unconfined compressive strength increased with increasing length of curing time [62]. *Lagueros et al.* (1956) reported that higher temperatures accelerated curing, resulting in a higher strength and found also that 90 per cent of relative humidity gave the greatest ultimate strength gain when different curing conditions are compared [69]. That specimens cured at 35°C developed more than twice as much as the specimens cured at 25°C were among the findings of *Mateous* (1964) [70]. *Thompson* (1968) articulated that at temperatures less than 4°C the pozzolanic lime-soil reactions are retarded or even stopped [71]. Reactions commence again as long as free lime remains in the system and temperatures attain favorable conditions.

Referring to the schematic model illustrated in Figure 2.15 and utilizing their laboratory observations, *Locat et al.* have presented the mechanical model plotted in Figure 2.16 to describe the strength development with time for lime-stabilized clayey soils. A low water content soil that can be compacted and a high water content soil that cannot be compacted have been regarded as two soil-lime mixes. The model that *Perret* proposed in 1977 for silty soils is also involved. Mainly due to the successful compaction of the samples, low water content mixes exhibit a significant initial shear strength. In this model, *Locat et al.* have assumed that the reason for the strength increase is mainly provided through the particle bridging by the pozzolonic reaction products on condition that sufficient amount of reactants are available [59]. They claimed further that since the precipitates have finite dimensions, the greater the initial void ratio ( or water content ), the more time needed to create significant bridges or contacts between soil particles.

The time respective strength gain development can be separated into three phases, as illustrated in Figure 2.16 [59]. Despite the possibility of highly active chemical reactions and cements formed, Phase *I* represents the commencing period where bridging is yet not mechanically present. This is generally encountered by soils having a high water content value. Phase *II* is designated to the time span where bridging development is efficient during pozzolanic reactions which are mechanically felt as a harsh growth in strength gain. Phase *III* is distinguished by a decline or even a leveling in the rate of increase of shear strength that may be attributed to : (a) completion of pozzolanic reactions because of the exhaustion of available lime in the medium, (b) although reactions are still proceeding, it becomes more awkward for solutes to diffuse within the soil-cement matrix, (c) reaction products are not as effective on strength as they are in phase *II*. However, they are still in production because the soil has a more rigid state in this phase when compared with the previous one - phase *II*.

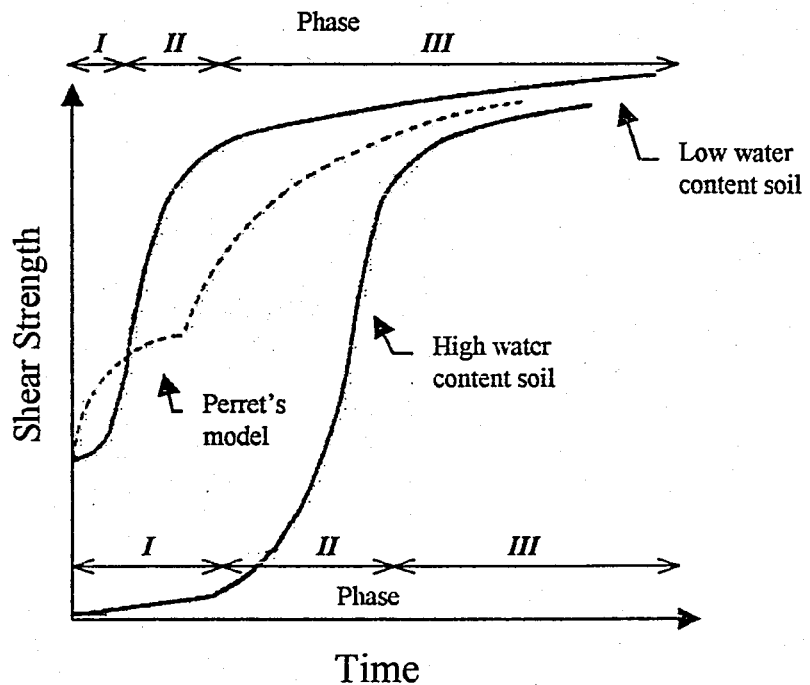


**FIGURE 2.16. : Mechanical conceptual model of shear strength development with time for high water content and low water content varying lime-stabilized soils ( p refers to the model of Perret ) [59]**

## 2.6. Mechanism of Mass Transport into Clayey Soils

The bearing capacity of cast-in-situ concrete piles and drilled piers depends very much on the shear strength of the surrounding soil medium. Beside the tip resistance of these load carrying structures, the skin resistance developed due to the relative movement of the soil and the pile shaft can be significantly increased by the application of lime slurries prepared in their bore-holes prior to casting the concrete.

However, the duration of this application is often limited up to a time span of 2~3 days since otherwise the shaft soil would considerably deteriorate in texture due to liquefaction [49]. Many field tests reported, however, that the advection-diffusion rate of calcium ions into uniform soft clays is very low. It has been observed by many researchers that only a few millimeters around the boreholes of lime slurries is affected even after several weeks [49]. Alternatively and more effective is the widecommen applied method in which the lime slurry is pressure injected into the soil to a depth of 4-5 meters and occasionally deeper to cover the active zone where a acquired mixture of 5 per cent is sufficient in most cases in order to achieve desired stabilization [40].

Thus, the lime slurry is pressed into the fissures and crackings of the clayey soil. From here onwards, calcium ions may further slowly diffuse into the surrounding soil. By doing so, the shear strength of the soil in the contact zone with the pile is improved due to lime-soil interaction as a consequence of lime migration. Such shear strength improvements achieved within the vicinity of the pile shaft allows conveniently to reduce the pile dimensions during the design phase. For verifying this proposal the migration mechanism of lime into clayey soils is of paramount importance.

### 2.6.1. Background of Mass Transport into Soil

Besides diffusion, there are two other transport mechanisms that are often considered; namely advection and dispersion [72]. Dominating mechanisms of mass transport with respect to the corresponding *Darcy* velocities confirmed that dispersion can be neglected since the *Darcy* velocity for mass transport through clayey soils is sufficiently small [72]. Under these conditions the mass flux can be regarded as the summation of the diffusive and advective components [72].

In the advection process, the solute is transported by flowing water in response to hydraulic gradient [73]. Governed by its seepage velocity the flow passes through the voids of the porous medium. Utilizing *Darcy's* law, the seepage velocity can be formulated as;

$$v_s = \frac{ki}{n} \quad (2.39)$$

where  $v_s$  denotes the seepage or average linear velocity of water (solvent);  $i$  represents the hydraulic gradient;  $k$  denotes the hydraulic conductivity whereas  $n$  accounts for the porosity of the porous medium.

If the initial solute concentration is  $C_o$ , the solution will trace then in time  $t_1$  a distance of  $d = vt_1$  as a plug flow due to advection [73]. However, in actual situations, the solute is monitored to spread out from the flow path. In porous mediums such as soils, the flow passes through the voids. The average velocity  $v$  will therefore be the seepage velocity,  $v_s$ , and is equal to  $v/n$ . Previous studies declared that in low permeability soils such as clays, effective porosity  $n_e$ , not the porosity  $n$ , governs travel time in a porous medium [73].

Effective porosity is recognized as the volume of void space that conducts most of the fluid flow divided by the total volume of the soil. Experiments by *Daniel et al.* (1991) indicate that the effective porosity ratio ( $n_e/n$ ) for kaolinite varied from 0.25 to 1 when hydraulic gradient,  $i$  was raised from 1 to 20 [73]. For another clay (Lufkin clay), the ratio varied from 0.02 to 0.16 for similar ranges of  $i$  [73].

It was traditionally assumed that the hydraulic conductivity dominated the rate of solute transport into earthen barriers [74]. However, recent field studies have indicated that diffusion is the controlling mechanism of solute transport in many fine-grained soils under low seepage velocity ( $v_s \rightarrow 0$ ) values [74]. As a result, the evaluation of the migration amount of chemicals through earthen barriers is becoming necessary.

Diffusion may be thought of as a transport process in which a chemical or chemical species migrates in response to a gradient in its concentration, although the actual driving force for diffusive transport is the gradient in chemical potential of the solute [75]. The process stops only when concentration gradients become essentially negligible. A hydraulic gradient, contrary to advection, is not required for transport via diffusion [73,75]. The fundamental equation that governs the diffusion process of a particular compound in an aqueous or free solution (i.e., no porous material) is *Fick's First Law* which may be written for one dimension as [74];

$$J = -D_o \frac{\partial c}{\partial x} \quad (2.40)$$

where  $J$  is the diffusive mass flux (i.e. mass transport per unit area per unit time),  $c$  the concentration of the solute of interest at a particular position  $x$  and time  $t$  in its liquid phase,  $x$  the mass transport direction, and  $D_o$  is the "free solution" diffusion coefficient of the chemical in a particular medium and is intended to represent the chemical aspects (i.e. effect of temperature, ionic radius, valence, etc.).  $\partial c / \partial x$  expresses the change in concentration with respect to the position [74]. The negative sign implies the movement direction ( i.e. from high to low concentration ) such that the gradient will be negative.

However, the prescribed equation cannot sufficiently account for the diffusion phenomena in soil. When compared with its ability to diffuse in either the liquid or gas phase, the diffusion of the element or compound in the solid phase will basically remain negligible. Mass transport rates show tremendous differences since the pathways present in soil for migration are more tortuous and the diffusive mass flux is less than in free solution as the presence of solid particles in soil occupy some of the cross-sectional area [74]. A schematic illustration of the effective length concept incorporates these effects and is given therefore in Figure 2.17.

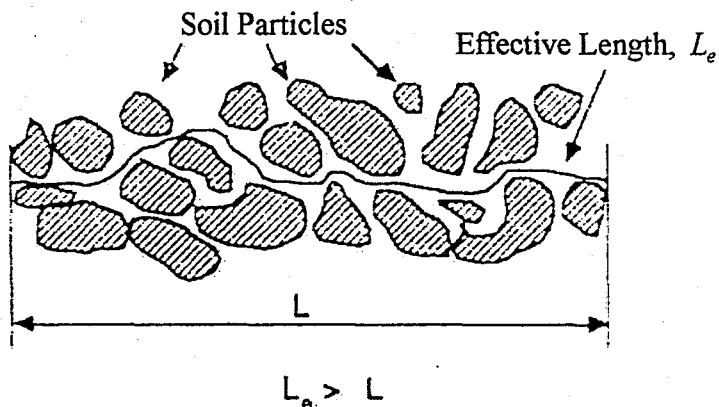


**FIGURE 2.17. Effective length concept in transport through porous medium [74]**

Beside several other environmental influences, the primary additional factors that tend to reduce the rate of diffusive transport of solutes into a saturated porous medium (e.g. soil) are a reduction of cross-sectional area, presence of tortuous pathways, fluidity, porosity and degree of saturation [74]. In order to take account for the impact of these factors on the diffusion process a modified form of *Fick's First Law* is used. The resulting formula that processes these additional effects has been formulated as;

$$J = -D_o \tau \alpha \gamma \theta \frac{\partial c}{\partial x} \quad (2.41)$$

where additionally to Equation 2.40,  $\tau$  is the dimensionless geometric tortuosity factor and is intended to represent the increased distance of transport and the effect of the soil upon the effective rate of diffusion.  $\alpha$  being the fluidity factor, accounts for the increased viscosity of the water adjacent to the clay mineral surfaces relative to that of the bulk water.  $\gamma$  expresses the exclusion of anions from the smaller pores of the soil.  $\theta$  is the volumetric water content and is expressed as;

$$\theta = n S_r \quad (2.42)$$

where  $n$  is the effective porosity of the porous medium representing the pore space through which diffusion is possible. The effective porosity term is required since the definition of the diffusive flux  $J$  is done with respect to the total cross-sectional area of the porous medium.  $S_r$  states the soil saturation degree.

*Shakelford and Daniel* [74] introduced the “apparent tortuosity factor”  $\tau_a$ , that comprises beside the actual tortuosity also the geometric tortuosity,  $\tau$ , as well as all other factors which may be inherent in its measurement, including solute-solute and solute-solvent interactions and expressed *Fick's* First Law for the diffusion of a chemical species into soil as;

$$J = -D_o \tau_a \theta \frac{\partial c}{\partial x} \quad (2.43)$$

The *Nernst* and the *Einstein-Stokes* equations indicate that  $D_o$  depends on numerous factors including the valence and ionic radius of the chemical species, the temperature and viscosity of the solution, the soil type, the pore size and pore size distribution [74]. By combining the chemical and soil components and expressing the effective diffusion coefficient as;

$$D_E = D_o \tau_a \quad (2.44)$$

*Shakelford and Daniel* [74] have revised the formulation of *Fick's* First Law to;

$$J = -D_E \theta \frac{\partial c}{\partial x} \quad (2.45)$$

Nevertheless, *Fick's* First Law is limited to describe the steady state diffusion flux of nonreactive solutes. For time dependent transport of a nonreactive solute in soil, *Fick's* second law is assumed to apply as;

$$\frac{\partial c}{\partial t} = -D_E \frac{\partial^2 c}{\partial x^2} \quad (2.46)$$

This equation is derived from *Fick's* first law and the equation of continuity, and governs the rate with respect to time at which solute can diffuse into porous materials. The solution of this equation can be obtained by means of error functions.

The transport of solutes that are subject to chemical reactions, can differ substantially from the transport of nonreactive solutes. To express the diffusion phenomenon of reactive solutes similar to the effect that lime has on clayey soils, Equation 2.46 is modified as [74];

$$\frac{\partial c}{\partial t} = -D_E \frac{\partial^2 c}{\partial x^2} - \frac{\partial q'}{\partial t} \quad (2.47)$$

where  $q'$  represents the sorbed concentration of the chemical species expressed in terms of the mass of sorbed species per unit volume of voids and is formulated as;

$$q' = \frac{\gamma_d}{\theta} q \quad (2.48)$$

where  $q$  is the sorbed concentration expressed as the mass of solute sorbed per mass of soil and  $\gamma_d$  is the dry density of the soil.

Several approaches have been used for the measurement of  $D_E$ . Effective diffusion coefficient can be measured in cells where compacted soil samples saturated with different solutions are used. The soil samples used are first presoaked to prevent mass transport via advection. The assembly exposed to a reservoir of leachate is later sectioned to determine the distribution of diffusing solutes at the end of the test [74]. The determination of effective diffusion coefficients can be made by analyzing the final solute profile in the soil or by measuring the rates of decrease of the solute concentration in the reservoir [74].

## 2.6.2. Diffusion of Lime into Clayey Soils

*Stocker* [76] has performed quantitative measurements of lime diffusion into unpulverized clay lumps in lime and cement stabilized mixtures of a heavy montmorillonitic clay soil and deduced that the physical properties of this soil could be modified even by the addition of 0.5 per cent lime [76]. He claimed further that 0.5 per cent diffused lime into lime or cement stabilized lumps was adequate to offset swelling on wetting from as-cured state, 2 per cent lime to expand as cured strength ten-fold, and 3 per cent lime to lower permeability significantly [76].

That very little montmorillonite was depleted even though impressive changes in physical properties had been produced was another remarkable conclusion from *Stoker* [76]. A total of 96 per cent of initial montmorillonite remained unreacted despite a ten-fold stronger soil had been produced.

The lime diffusion rate into soil is also a subject of great importance. *Stoker* [76] has observed that calcium uptake into lime stabilized clay cores and stated that about 7 per cent lime acquired in the first day in the outer 1mm of the lime stabilized cores [76]. It is also expressed that although lime in the first 1mm rapidly rose to 7 per cent, this lime had not been consumed by the usual clay/lime reactions until much later; alternatively if it was incorporated in early products, these had peculiarly high  $CaO : SiO_2$  and  $CaO : Al_2O_3$  ratios, and further reaction involved desorption of lime with no further uptakes. When the absorbed lime is consumed to react with clay it is not replaced even though diffusion still occurs through the outer layers to deeper parts [76]. At greater depth in a lump, *Stoker* [76] observed that the outer part of the lump itself is the lime source but the potential of this source is not high enough to affect this absorption and reaction of clay uses lime as fast as it is supplied.

After 1 day curing, 0.5 per cent lime which is enough to alter the physical properties of clayey soils has reached to 3 mm from outer parts of lumps and after the end of 3<sup>rd</sup> day, concentration at 3mm has reached to 1 per cent [76]. The diffusion of calcium into cores of lime stabilized clayey lumps is illustrated on Figure 2.18.

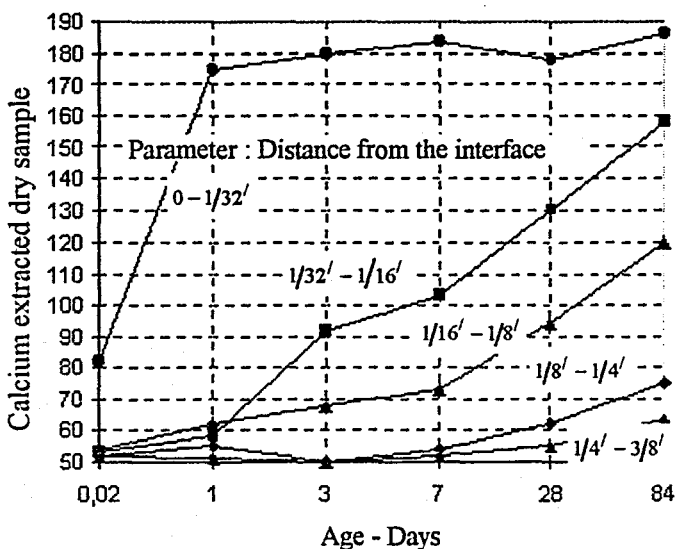


**FIGURE 2.18. : Diffusion of calcium into cores of lime stabilized [ 15 per cent ] clayey lumps [76]**

## 2.7. Review of Interface Testing Apparatus

The evolution of the shear zone structure is quite significant for the failure of clays subjected to applied shearing. Knowledge about the evolution of the shear zone structure in clays with respect to the applied shear and normal stresses in testing apparatus is essential to understand how clays fail and mobilize their drained peak and residual shear strengths. However, it is yet not possible to directly visualize and record the structure and generation of this zone with currently available procedures and equipment.

When compared with each other, interface testing apparatus have advantages as well as disadvantages. The specification of each testing apparatus is summarized in Table 2.1. However, an annular shear apparatus, is often not appropriate for the element tests of interface behavior. The normal stress on the interface is higher than the confining pressure since the elastic modulus of the structural material (concrete-steel) is higher than that of the soil. The dilatancy of the soil sample also affects considerably the normal stress on the interface [77]. Among the other three types of apparatus, the ring torsion type is recognized to be the most ideal one because of its endless interface. The endless interface avoids non-uniformity of normal and shear stresses to develop within a soil sample [77]. A ring torsion apparatus involves many technical difficulties. The apparatus operator must be highly skilled and extremely careful in preparing uniform soil samples with a uniform ring-shaped surface. Special care in finishing the surface of the metal ring uniformly and in seating the metal specimen on the soil surface evenly and in the correct position is required. The simple shear apparatus can be used with much less difficulty, mainly because of the simple shape of the soil-structure (steel-concrete) interface. Consistent results can be expected because of its simplicity. In simplicity and operational ease, a direct shear apparatus prevails against a simple shear apparatus. There is an uncertainty in the tangential displacement measured by this type of apparatus. Even though the outer shape of the soil is kept undeformed by the shear box, the middle part of the soil is known to deform under the shear stress [77]. The tangential displacement includes the displacement due to the deformation of the soil as well as the sliding displacement of the interface. In simple shear tests, the factors of tangential displacement can be measured separately.

Type	Example	Advantages	Disadvantages
<b>Direct shear</b>	<i>Potyondy (1961)</i> <i>Desai, Drumm &amp; Zaman (1985)</i>	<ul style="list-style-type: none"> <li>• Commonly available device</li> <li>• Simple system</li> <li>• Simple preparation</li> <li>• Simple procedure</li> </ul>	<ul style="list-style-type: none"> <li>• Displacement factors unable to be separated</li> <li>• Interface area reduced with increase in displacement</li> </ul>
<b>Annular stress</b>	<i>Brumund &amp; Leonards (1973)</i> <i>Kishida &amp; Kobayashi,</i> <i>Miyamoto (1975)</i>	<ul style="list-style-type: none"> <li>• Geometrically similar to skin friction of piles and friction of steel reinforcements</li> </ul>	<ul style="list-style-type: none"> <li>• Normal stress on interface unknown</li> <li>• Stress concentration at ends</li> </ul>
<b>Ring torsion</b>	<i>Yoshimi &amp; Kishida (1981)</i>	<ul style="list-style-type: none"> <li>• Endless ring interface</li> <li>• No stress concentration at ends</li> <li>• Constant interface area</li> <li>• Displacement factors observed by X-ray photography</li> </ul>	<ul style="list-style-type: none"> <li>• Complicated system and procedure</li> <li>• Difficult to prepare uniform soil mass in a ring shape</li> <li>• Difficult to finish surface roughness of metal ring uniformly</li> </ul>
<b>Simple shear</b>	<i>Kishida &amp; Uesugi (1986)</i>	<ul style="list-style-type: none"> <li>• Constant interface area</li> <li>• Simple preparation</li> <li>• Simple procedure</li> <li>• Displacement factors measured separately</li> </ul>	<ul style="list-style-type: none"> <li>• Stress concentration at ends</li> </ul>

**TABLE 2.1. : Comparison of interface testing apparatus [77]**

## 2.8. Principles of the Finite Element Method

*Discretization of the continuum* : The continuum is the physical body, structure, or solid being analyzed. Discretization may be simply described as the process in which the given body is subdivided into an equivalent system of finite elements as shown in Figure 2.19 [3]. The finite elements may be triangles, group of triangles, or quadrilaterals for a two-dimensional continuum. For three-dimensional analysis, the finite elements may be tetrahedra, rectangular prisms, or hexahedra. The intersections of the nodal lines separating the elements are called nodal points. The continuum can represent a physical body such as a pile-foundation system, where we are interested in displacement (of the nodes). The quantity such as the displacement is called the main, or primary unknown of the problem [3]. Required secondary quantities such as stresses are then computed from displacements. A problem can be formulated alternatively in terms of the stresses as primary unknowns or both displacements and stresses as primary unknowns for the stress-deformation problem. A basic characteristic of the finite element method is that the finite elements are analyzed and treated separately, one by one. Each element is assigned its physical or constitutive properties, and its property or stiffness equations are formulated [3]. Subsequently, the elements are assembled to obtain equations for the total assembly.

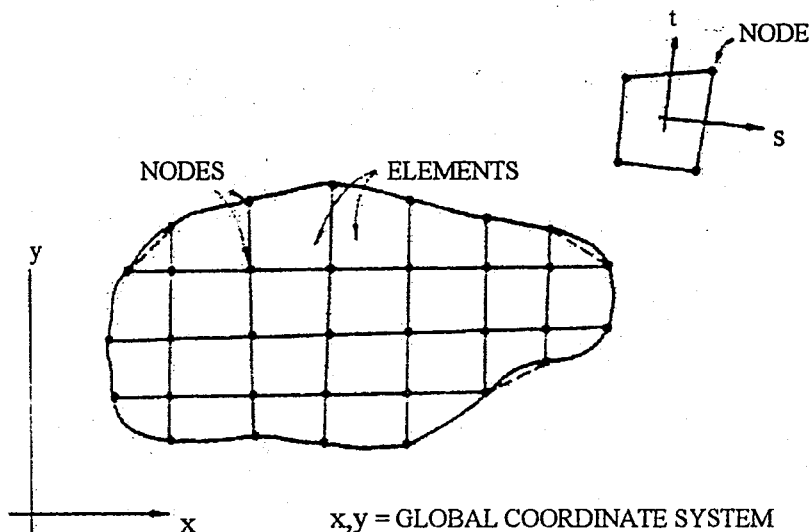


**FIGURE 2.19. : Subdivision into finite elements of arbitrary continuum [3]**

*Selection of the approximation functions* : The assumed displacement functions or models represent only approximately the actual or exact distribution of the displacements [3]. Obviously, it is generally not possible to select a displacement function that can represent the actual variation of displacement in the element. Hence, the basic approximation of the finite element method is introduced in this stage. There are three factors which influence the selection of a displacement model. First, the type and the degree of the displacement model must be chosen. Second, the particular displacement magnitudes that describe the model must be selected. These are usually the displacements of the nodal points, but they may also include derivatives of the displacements at some or all of the nodes. Third, the model should satisfy certain requirements which ensure that the numerical results approach the correct solution.

*Derivation of the element stiffness matrix using a variational principle* : The stiffness matrix consists of the coefficients of the equilibrium equations derived from the material and geometric properties of an element and obtained by use of the principle of minimum potential energy [3]. The stiffness relates the displacements at the nodal points (the nodal displacements) to the applied forces at the nodal points (the nodal forces). The distributed forces applied to the body are converted into equivalent concentrated forces at the nodes. The equilibrium relation between the stiffness matrix  $[k]$ , nodal force vector  $\{Q\}$ , and the nodal displacement vector  $\{q\}$  can be expressed as a set of linear algebraic equations,

$$[k]\{q\} = \{Q\} \quad (2.49)$$

The stiffness matrix for an element depends upon (1) the displacement model, (2) the geometry of the element, and (3) the local material properties [3]. For an elastic isotropic body the *Young* modulus  $E$  and the *Poisson* ratio  $\nu$  define the local material properties. Since material properties are assigned to a particular finite element, it is possible to obtain nonhomogeneity by assigning different material properties to different finite elements in the assemblage [3].

*Assembling the element properties to form global equations* : Equations in the form of “ $[k]\{q\} = \{Q\}$ ” are obtained for each element in the structure. This process includes the assembly of the overall stiffness matrix for the entire body from the individual element stiffness matrices as well as the overall force vector from the element nodal force vectors [3]. This is done essentially by adding together the matrix equations for each element one by one. The addition, which is called the direct stiffness method, is performed to satisfy the basic physical condition that the structure should remain continuous. Thus, the compatibility of displacements at nodal points across adjacent elements in the discretized assemblage is satisfied. The global equilibrium relations between the total stiffness matrix  $[K]$ , the total force vector  $\{R\}$ , and the nodal displacement vector for the entire body  $\{r\}$  can again be expressed as a set of simultaneous equations [3];

$$[K]\{r\} = \{R\} \quad (2.50)$$

These equations cannot be solved until the geometric boundary conditions are taken into account by appropriate modifications of the equations. A geometric boundary condition arises from the fact that displacements may be prescribed at the boundaries or edges of the body.

*Computation of primary and secondary quantities* : Using the displacement approach, nodal displacements are computed as primary quantities by solving equations in the form of “ $[K]\{r\} = \{R\}$ ”. Quantities like stresses and strains, known as the secondary quantities, are computed from the nodal displacements. In general, the stresses and strains are proportional to the derivatives of the displacements; and in the domain of each element meaningful values of the required quantities are calculated [3]. These “meaningful values” are usually taken as some average value of the stress or strain at the center of the element.

The displacement approach has been preferred in many geotechnical problems since the number and bandwidth of the final stiffness equations are remarkably smaller than those produced by other methods. The ease to establish approximation functions that satisfy compatibility requirements makes this approach even more friendly. This formulation is likely more sensitive to handle variations involved in problem parameters such as geometry, material properties and stress strain laws.

### 3. PRESENT STUDY

#### 3.1. Description and Scope of the Problem

Within the scope of this study the computer software *ANSYS 5.2*, performing finite element analysis, has been utilized to analyze the stress-strain response within the lime stabilized soil (clay)-structure (concrete) interface under static but time respective, non-cyclic loading conditions. The primary objective of this research could be further articulated as the compatibility determination of computer aided interface modeling.

Practically, the interface behavior can be most conveniently derived on the basis of direct shear tests simulating the junction between soil and structure. Typically, in the stronger soil masses, this behavior is highly nonlinear and involves significant coupling between the shear and dilational modes. However, most solutions of soil-structure interaction problems sought through numerical methods require certain simplifying assumptions in model geometry, material properties and behavior response. The simplified model examined herein has been proposed to achieve approximate, but still acceptable solutions for the complex soil-structure interaction phenomena.

A reasonable representation of the mechanical material properties and thus stress-strain characteristics of the soil has constituted the other main objective in this study. Recall that lime treated soil loses its plasticity, flocculates to larger sized soil aggregates and begins to possess brittle material characteristics which, in turn, has a nominal stress strain curve indicating that its ultimate strength coincides with its breaking point. *Brittleness* is a term denoting the tendency of the material to break or shatter when subjected to a stress exceeding its elastic limit. In other words, lime treated soil specimens fracture before any appreciable change in their cross sectional area and gauge length can take place. This behavior is in contrast to the gradual and continuous deformation of untreated natural soil under similar conditions. Although plastic deformations for brittle materials are negligible, an elasto perfectly plastic nonlinear stress-strain relationship has been assumed for both cases. These stress-strain relationships have been established with appropriate mechanical parameters and yield stresses.

Beside the assumption made for the material behavior, geometric nonlinearities are inevitably generated through the shearing mechanism which compels each individual finite element to deform beyond an infinitesimal amount. The models have been subjected to nonlinear analyses due to these facts. That is, such nonlinear properties have been employed in combination with an incremental analysis. The program used must permit the shearing load to be applied in small increments and must allow the deformations to develop in small increments so that the evolving pattern of stress and strain can be followed.

The representative model of the physical problem in concern, actually resembling the well-known direct shear box, has been basically intended to account for the interface of cast in-situ piles and drilled piers where the estimation of skin friction is of paramount importance for both bearing capacity and settlement calculations. It will primarily serve to explain how shear stress formation and thus skin friction is generated through applied relative displacements between two interacting mediums. Provided that the whole load transfer mechanism occurs within the softer soil medium, the model has been founded basically on the properties of the semi-finite soil domain and the interface whereby the concrete shaft has been involved only to supplement the pile-soil assembly. Instead of taking into account for the whole pile-soil system, the proposed models may only be considered for definite points along the pile shaft since the lateral earth pressure is beside other complex parameters a function of depth.

The problem of interfaces belongs to the general class of the contact and friction problems of mechanics encountered in various branches of engineering and physics. Thus, the contact between two dissimilar materials, in metals, composites, joints and interfaces involves similar physical and mathematical considerations. Similarly to the analysis of resistance to sliding of a rigid body in contact with soil, the theoretical approach for evaluation of unit skin resistance for cohesive soils consists of two main parts: *adhesion* and *friction* or *cohesion*. Adhesion, established during relative sliding under certain compressive pressure through the intimate contact of the microasperities distributed over the rough concrete surface and the soil particles, is normally small and often neglected. Unlike the naturally formed interfaces, the models proposed have been developed to describe and predict the behavior of perfectly mated interfaces. The influence of these microasperities (dilatency) has therefore been ignored such that the modeled shearing behavior has been founded merely on the internal shearing resistance of the soil grains.

In contrast to natural joints, the man-made interfaces usually involve a degree of bonding between two mediums as, for example, when a concrete foundation is cast into soil. In this case the cementation or bonding may be a significant contribution to the shear strength of the interface and will combine, usually in some complex way, with the other factors like surface roughness, friction and dilation to determine the complete shear behavior. This cementation process has been aimed to be emphasized due to the lime treatment process in which additional likewise cementitious agents are formed. Because of comparison purposes, no actual bonding or cementation across the interface has been assumed for the untreated natural soil case.

Some soil types, particularly clays, may exhibit special mechanisms such as strain softening, stress release, dilatation, and arching. However, successful procedures to represent such strain-softening behavior in numerical models has yet not been achieved and has therefore been ignored during the analyses. This has not been accomplished since such strain softening mechanism intimates unstable behavior in many instances and is therefore likely to cause nonunique results [3]. This is a physical fact, not a result of analytical inaccuracy. Indeed, to acquire unique solutions, the overall stiffness matrix of the assembly must be positive definite.

Furthermore, soils differ in behavior response under cyclic and dynamic loading, in which significant variations in the path of loading can occur from static loading, in which basically monotonic loading is exerted. Since neither repetitive cyclic nor dynamic loading have been approached in this study, deformation modes like debonding and rebonding beside other sophisticated reactions have not been prone to develop. For this reason only relative sliding with complete contact generated under certain compression stresses has been assumed in contrast with the fact that always some separation (dilation) is produced.

Nevertheless, the models are not capable to process the factors introduced by the construction and geological characteristics of the site. Influences affecting the actual skin resistance in the site like the initial ground-stress condition, method of placement of the pile as well as the pile shape (particularly when tapered) and length have not been involved in the analyses. Imminent water migration from the surrounding clay strata, water derived from the fresh cement paste, addition of water to simplify the advancing process of the pile are some examples encountered in the site causing the interface to become watery and eventually lead to degradation of its smooth texture.

Experiences reported also that disturbance is significantly pronounced if delay in subsequent concreting is permissible. The texture of the interface is then even further deteriorated resulting in significant shear strength losses. Comprehensive contributions to the ultimate shear strength alike the beforehand mentioned ones are barely convertible into existing finite element code. Hence, due to unavoidable limitations in numerical simulations, the study has been mainly restricted to distinguish the difference between the response behavior of the lime stabilized and the natural soil under identical shearing conditions.

Initially, the untreated soil response against applied shearing has been investigated. The beneficial effects of lime exposed from the fresh cement paste which is further accentuated through the diffusion-advection process of applied lime slurries have been conducted in the second part of this study. After all, the simulation of the diffusion-advection mechanism has been excluded from the models because of the uncertainties involved in the process. Hence, the width of the lime treated zone is presumed on the basis of previous studies, experiences and laboratory observations. Even so it has been assumed that the strength parameters diminished in magnitude with increasing distance from the concrete surface as a consequence of the prescribed infiltration mechanisms.

Parametric studies have been mainly concentrated on the factors dominating the interface behavior namely the interface aspect ratio defined as  $t/B$  (width/length), the ratio of *Young* modulus in the interface  $E_i$  to that of the surrounding soil medium  $E_s$ , the *Poisson* ratio  $\nu$  and the multiple improvements recorded in the yield stresses of the soil when treated with lime. Although it has no impact on the physical response of the behavior phenomena, the convergence tolerance employed in the iterative algorithm could alternatively have also been varied to reveal its effect on the results.

### 3.2. Fundamental Assumptions Regarding the Physical Problem

As implied earlier, the reason for developing the model with close similarity to the direct shear box is due to its practicality and flexibility characteristics. Triaxial tests are certainly more versatile than direct shear tests but are also much more difficult to express in numerical terms. Drainage control, pore pressure measurements, judgment of principle stresses and failure plane as well as the determination of deformation amount at failure are among its advantages over the direct shear device. For the special case of soil-structure interface studies, the triaxial apparatus appears to be less effective than the direct shear device. In the direct shear test, the failure plane is predetermined as the interface between soil and structure. The effectiveness of adapting the direct shear test method for this study is further pronounced especially due to its suitability for layered soil sample investigation. Serving primarily for the determination of soil strength parameters, the direct shear box is not appropriate for measuring the deformations of soils tested. The stress distribution pattern developed under continuous relative sliding is indicative for the portion of skin friction released.

The models simulating the problem with varying interface thicknesses have been subjected to relative displacements under normal stress magnitudes of 50, 100, and 150 kPa, respectively. Relying on the tacit assumption that stresses increase linearly with depth, such stress values roughly correspond to lateral earth pressures that a 10 m long pile experiences at depths of equal intervals. The estimation of the normal stress values has been founded on the postulation that the ground water table is leveled below the pile tip.

Even small values of relative slip provided between the pile and soil are sufficient for a pile to expose a significant portion of its ultimate skin resistance. The amount of generated slip is determined through the accumulated differences in shaft strain from axial load and the soil strain caused by the load transferred to it via skin resistance [30]. The correlation made between the required displacements that a pile undergoes to mobilize skin resistance and the dimensions of the prototype examined herein yielded a lateral displacement value in the order of % 0.1 ~ % 0.2 to be reasonable. As far as the constant interface width in the models has been assumed to be equal to 100 mm and piles mobilize a significant portion of their skin resistance once they have experienced 1~2 mm settlement, these values correspond to a relative sliding value of 0.1 ~ 0.2 mm for the models examined herein.

Regarding the pile-soil assembly in the site, the representative model of the physical problem in concern consists of three main segments namely the concrete pile shaft, the perfectly mated smooth interface zone and the semi-finite soil domain. The simulation quality of the interface behavior is highly influenced by the geological and environmental characteristics of the participating mediums, material (soil) behavior, applied pile installation procedure and the thickness or gap size of the interface zone. Inclusions of a finite thickness for the interface can be realistic since there is often a thin layer of soil which participates in the interaction behavior. Previous studies conducted both in the laboratory and in the field revealed that the interacting zone or, in other words, the interface itself hardly ever exceeds some millimeters even when permitted to be affected from lime slurries for some days. Depending on the pressure applied, higher interacting thickness values have been reported for cases where lime is injected into the soil. The presence of the interface zone has therefore been approached by the "thin-layer" concept. Still, if the thickness exceeds the width of the surrounding elements in a large extent the interface elements behave essentially as solid elements. Numerical difficulties characterized as poor aspect ratios are encountered by too small thicknesses. Thus, the question of proper choice of thickness prevails for consistent simulation and has been intended to be resolved by performing parametric studies in which the results from different thicknesses have been compared with each other. Despite it has been not concerned herein, the choice of thickness can become particularly important for dynamic analysis where the mass and damping effects need to be considered additionally.

As mentioned before the saturation process of the soil encircling the pile shaft with lime slurries should not exceed a time span of 2~3 days. The texture of the smooth interface zone would otherwise inevitably be deteriorated, whereof a stabilized soil structure is barely obtainable. A significant loss in the residual shear strength is often observed in prolonged treatments. Lime migration is fundamentally provided by means of the coupled diffusion-advection mechanisms through the cracks and fissures that are exposed during the augering process of the shaft soil. The propagation rate throughout the interface diminishes continuously and eventually flattens since cracks and fissures are undoubtedly occupied with cementitious agents formed earlier. Depending extremely upon the initial soil stress level, this retarding phenomena actually determines the width of the zone treated with lime and consequently the interface thickness.

Finally, accounting mainly for the duration of lime treatment, the interface thickness has been varied between 2 and 8mm with intervals of 2mm to visualize its effects on the results. Lower values have led to numerical ill conditioning. The constant contact width with the concrete surface has been set to be equal to 100 mm such that the aspect ratio of interface has been provided to vary between 1/50 and 1/12.5. For the lime treated case, the interface zone has been subdivided further into 4 equally thick layers in order to reasonably demonstrate the diminishing intensity of the infiltration mechanisms. A higher number of subdivision has not been preferred simply to avoid both generation of poor shaped elements and an unnecessary increase in the number of elements involved in the analyses. Thickness values for the upper semi-finite soil domain and the pile shaft have been arbitrarily chosen as 25 and 5 mm, respectively.

A representative not to scale drawn schematic illustration of the physical problem is depicted in Figure 3.1 whereby a detailed description of the incorporated material properties and the build-up procedure of the corresponding finite element models has been outlined in the succeeding sections.

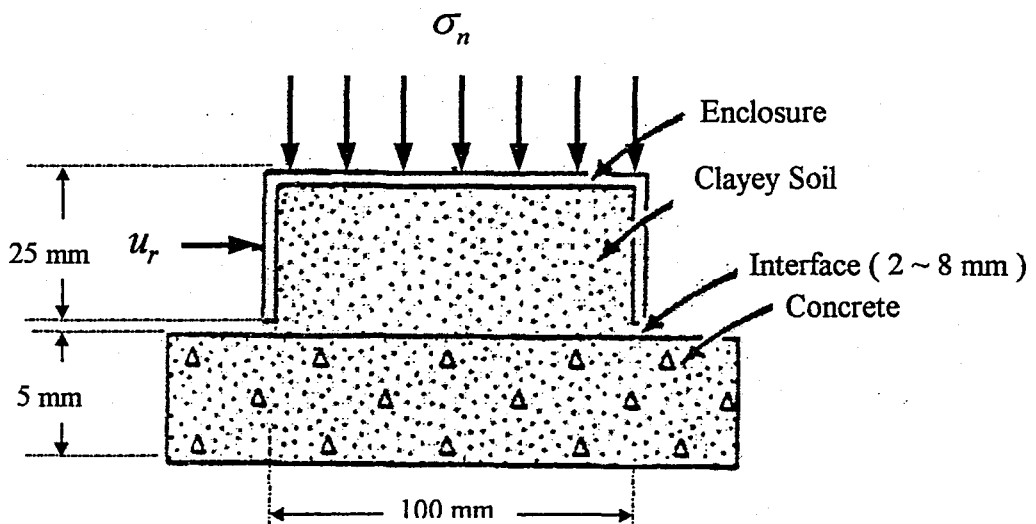


FIGURE 3.1 : Schematic illustration of the physical problem [12]

### 3.3. Material Properties

Another major section to setup a numerical treatment of a physical problem is the description of the constitutive relationship between its physical quantities such as stress-strain and time. The achievement of successful numerical approaches to geotechnical problems is only possible with the adoption of suitable constitutive relations.

There are many material-orientated factors that can affect the stiffness of an assemblage during an analysis. Nonlinear stress-strain relationships of plastic, multilinear elastic, elasto-plastic as well as hyperelastic materials will cause an assemblage's stiffness to change at different load levels. Creep, viscoplasticity, and viscoelasticity introduce nonlinearities which can be time-, rate-, temperature-, and stress-related. Swelling will provide strains that can be a function of temperature, time and stress.

Since it is well-known that soil behaves highly nonlinear, the relations between stress and strain are much more complicated than the simple linearly elastic ones. Some form of nonlinear behavior must be applied in order to approach a realistic representation of geotechnical problems. Constitutive behavior of geological media such as soils and rocks has been separated into three main groups to represent a given stress-strain curve : (1) Plasticity theories (2) Nonlinear elasticity theories (3) Curve-fitting methods. The plasticity theory being the basis for bearing capacity and assuming the *Mohr-Coulomb* law as the yield criterion theory has been utilized throughout this study to express the constitutive behavior of soil. The *Coulomb* law actually establishes the basis for many models representing interfaces. It assumes that no slip between two bodies will occur unless a critical tangential yield stress is reached whereas the relative motion is constrained to be along the contact surface. The yield stresses have been defined by assuming an elasto perfectly plastic material behavior for the soil. Application of this proposal to incremental analysis demands developing incremental relations between stress and strain.

Mechanical properties of soil govern its behavior under applied forces and loads. The response of soil to applied forces depends on the type of bonding and the structural arrangement of its grains. Bonding and structural arrangement of clayey soils may be greatly modified through the addition of natural binders like either quicklime from applied pressure injected lime or lime slurries and, although being highly less effective, through hydrated lime that is gradually expelled from the fresh cement paste. As a consequence of lime-clay interaction, the structural arrangement becomes remarkably stable due to the formation of cementitious agents over the individual clay minerals.

Since the proposal introduced for this study is valid for clayey based soils, bentonite, recognized through its high activity characteristics and high response to the stabilizing effect of lime, has been respected as the clay type. However, clay is in the field hardly present in its pure state. Therefore, as to be realistic and simulate similar characteristics of clayey soils commonly encountered in the field, it should actually always be considered that bentonite inherits, beside other additives, varying amounts of sand. Yet, the numeric values of the assigned mechanical parameters belong to pure bentonite.

The grain size distribution, the typical mineralogy and index properties as well as other fundamental geotechnical properties of the soil have not been considered in this study since the numerical simulations have been merely based on the improvements recorded in the mechanical soil characteristics (*Young* modulus, *Poisson* ratio, yield stresses). In other words, regardless whether considered in its drained or undrained condition, the contribution of all these individual influences do actually pinpoint the altered values of these mechanical properties. Such properties are therefore already incorporated and thus not mentioned elaborately. The expected improvements in soil properties are because of the beneficial effects of the enabled lime-clay interaction.

Like soils, the properties and composition of lime generally differ from location to location. Similar to the approach made with bentonite, both the sieve analysis and the exact amount of weight percentages of  $Ca(OH)_2$  and  $CaO$  inherited in the lime have been disregarded. Such characteristic properties of lime as listed in Table 3.1 could have actually be manifested through the utilization of the neutralization process via acid titration but did not coincide with the focus of this study. Instead, concentration on the multiple improvements recorded in the numerical values of the ruling mechanical parameters has been made.

## (a) Quicklime

Constituent (per cent)	High Calcium	Dolomitic
<i>CaO</i>	92.25 ~ 98.00	55.70 ~ 57.50
<i>MgO</i>	0.30 ~ 2.50	37.60 ~ 40.80
<i>CO<sub>2</sub></i>	0.40 ~ 1.50	0.40 ~ 1.50
<i>SiO<sub>2</sub></i>	0.20 ~ 1.50	0.10 ~ 1.50
<i>Fe<sub>2</sub>O<sub>3</sub></i>	0.10 ~ 0.40	0.05 ~ 0.40
<i>Al<sub>2</sub>O<sub>3</sub></i>	0.10 ~ 0.50	0.05 ~ 0.50
Specific Gravity	3.2 ~ 3.4	3.2 ~ 3.4

## (b) Hydrates

High Calcium		Monohyd. Dolomitic	Dihy. Dolomitic
Principle Constituent	<i>Ca(OH)<sub>2</sub></i>	<i>Ca(OH)<sub>2</sub> + MgO</i>	<i>Ca(OH)<sub>2</sub> + Mg(OH)<sub>2</sub></i>
Specific Gravity	2.3 ~ 2.4	2.7 ~ 2.9	2.4 ~ 2.6

TABLE 3.1. : Properties of commercially available limes

According to the complex factors of influence, the characteristics of soil-lime mixtures are extremely scattered and time dependent. Therefore, an accurate prediction of the alteration of soil characteristics caused by binding agents or electrolytes (ions) has yet not been possible. That concerns mainly the assessment of the strength-deformation characteristics. Though one may draw up for similar soils certain connections between the various reactions and soil parameters chemical-physical properties respectively, the correlation coefficient is usually too small for practical purposes. In general, qualitative indications can be expected only approximately from the single values which especially interests the strength-strain behavior. Nevertheless, direct soil mechanical tests continue to be obligatory for the accurate determination of efficiency of lime reactivity.

In many instances, beginning from the 7<sup>th</sup> day after treatment with the stabilizer a linear increase of the strength with the logarithm of time has been found, so that extrapolations have been made possible. The employment of the strength parameters that lime treated specimens acquire after 28 day of curing time have been supported with this fact. A similar change of the soil coefficients by treating with lime or a statistically secured correlation to compatibility, deformation and strength properties of the lime treated mixtures can generally be found only with soils of the entire same genesis.

Besides the environmental factors and depending upon the activity of soil as well as on the percentage weight of lime used, tests carried out up to date showed that lime stabilization of soil increased the value of *Young* modulus by some 15 times after 3 weeks from treatment and even up to 40 times after 16 months acquired curing period. Additionally, as mentioned before the increase rate in *Young* modulus increases considerably with increases in curing temperature. Finally, mostly due to liquefaction and degradation of the smooth interface zone the lower limit has been chosen as the multiplication factor to assess the values of the *Young* modulus for the lime treated soil case.

The *Poisson* ratio  $\nu$  that is initially equal to approximately 0.40 ~ 0.50 for undisturbed pure clays, actually varies between 0.33 ~ 0.35 for natural clayey based soils and diminishes further to the range of 0.23 ~ 0.25 upon contact with lime. The drop between the last mentioned two values is indicative for a more brittle material produced.

Differing in trend, for the lime treated case both the *Young* modulus and the *Poisson* ratio have been assumed to vary linearly throughout the interface zone. That is, while becoming distant from the pile shaft, the *Young* modulus descends whereas the *Poisson* ratio ascends to their corresponding unaltered values. Since the mechanical properties of the concrete shaft have no impact on the response behavior, constant values of 2.5E10 (Pa) to its *Young* modulus and 0.20 to its *Poisson* ratio have been assigned. The assigned values in Table 3.2 are intended to represent the material properties within the elastic limit expressed in Figure 3.2.

<i>Mechanical Property</i>	Untreated Natural Soil		Lime Treated Soil	
	* <i>E</i> (Pa)	$\nu$	* <i>E</i> (Pa)	$\nu$
1. <i>Interface Layer</i>	50e5	0.33	750e5	0.25
2. <i>Interface Layer</i>	50e5	0.33	580e5	0.27
3. <i>Interface Layer</i>	50e5	0.33	410e5	0.29
4. <i>Interface Layer</i>	50e5	0.33	240e5	0.31
<i>Semi - Finite Soil Domain</i>	70e5	0.33	70e5	0.33

**TABLE 3.2. : Assigned values for the *Young* modulus and *Poisson* ratio**

\* The *ANSYS* software is not capable to recognize the unit system adopted for a definite analysis. Since it is also not supplied with a unit system converter, it is imperative that the units of data entries are consistent with each other. The *Young* modulus values have therefore been converted into the SI unit system for consistency purposes.

Since the texture of the interface zone is always disturbed or somewhat weakened, slightly less *Young* modulus values have been assigned to the soil layers it accommodates. This provision has not been necessary for the lime treated case where the acquired strength distribution of soil is governed by the infiltration mechanisms, the duration of treatment and the amount of lime supplied.

Relying on the corresponding laboratory test results obtained by *Metehan C. T.*, the yield stresses supplementary to the prescribed elastic parameters have been implemented on behalf of the elasto perfectly plastic response assumption. *Metehan C. T.* reported in his laboratory studies that pure bentonite samples acquired an average yield stress of 180 kPa upon treatment with 7 per cent by weight of lime under varying confining pressures of 50 to 150 kPa. Likewise, his test results casted an average yield stress value of 60 kPa for natural bentonite tested under similar conditions. An averaging three-fold increase in yield stresses upon treatment with 7 per cent of weight by lime has been found reasonable when compared with test results obtained for other clay types. His results have therefore been arrayed as yield stresses into the model database as shown in Figure 3.2.

Furthermore, it has been derived from his study that untreated pure bentonite specimens failed approximately somewhat before a strain value of 0.01. This coincides with the adopted strain values at failure. Contrary, without having adequate strength, the deformation quantity in the elastic state of the lime treated specimens is very limited. After the addition of lime, the specific deformations  $\epsilon$  at failure are considerably lower without exception when compared with the natural untreated soil case. Depending on the amount of lime employed, the strain values at failure of lime treated clay specimens oscillates around 0.0025 which equals roughly to a quarter of the corresponding strain value of the natural soil case. This can also be recognized through the correlation made between the settled *Young* modulus values and their corresponding yield stress values. These strain values tend to decline even further with increasing reaction time and temperature [56].

<b>Lime Treated Case</b>			
<i>Yield Stresses (kPa)</i>			
<b>Overburden Pressure (kPa)</b>	<b>50</b>	<b>100</b>	<b>150</b>
<i>1. Interface Layer</i>	150	180	210
<i>2. Interface Layer</i>	130	160	180
<i>3. Interface Layer</i>	110	130	150
<i>4. Interface Layer</i>	90	100	110
<i>Semi - Finite Soil Domain</i>	70	70	70

<b>Untreated Natural Soil Case</b>			
<i>Yield Stresses (kPa)</i>			
<b>Overburden Pressure (kPa)</b>	<b>50</b>	<b>100</b>	<b>150</b>
<i>1. Interface Layer</i>	50	60	70
<i>2. Interface Layer</i>	50	60	70
<i>3. Interface Layer</i>	50	60	70
<i>4. Interface Layer</i>	50	60	70
<i>Semi - Finite Soil Domain</i>	70	70	70

**TABLE 3.3. : Adopted yield stresses derived from laboratory direct shear tests conducted on pure bentonite specimens [ after *Metehan C. T.* ].**

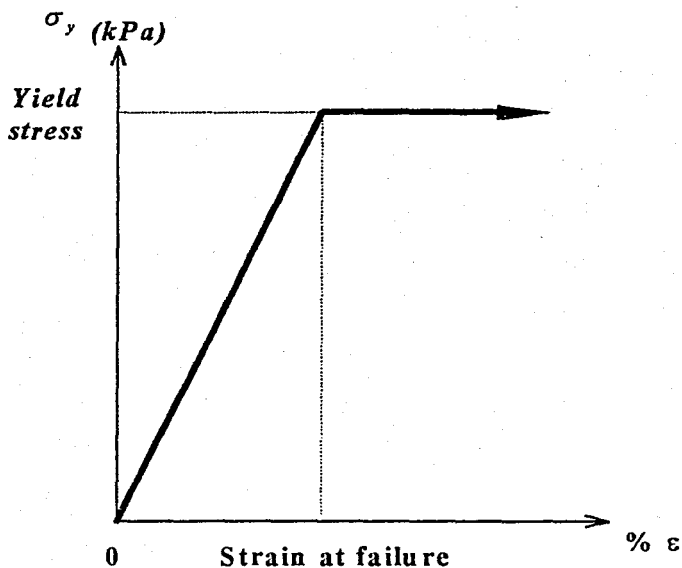


**FIGURE 3.2. : Adopted elasto-perfectly plastic stress- strain relationship**

### 3.4. Application of the Finite Element Method to the Physical Problem

The ultimate purpose of the finite element analysis has been to re-create mathematically the behavior of the engineering problem. In other words, it has been intended to propose a corresponding mathematical model of the prototype introduced earlier in Figure 3.1. In the broadest sense, the final models erected comprise all the nodes, elements, material properties and behavior, boundary conditions and other features required for the logical representation of the physical system.

Static but time respective analyses have been employed to determine the stresses within the interface exposed through external loads that actually do not induce any inertia or damping effects since steady loading and response conditions have been assumed. Structural orientated loads such as *nodal displacements* (relative displacements), *surface loads* (pressures) and *degree of freedom constraints* (DOF, boundary conditions) have been implicated in the analyses.

The following procedure has been followed for the analyses :

- Building the models
- Application of loads and obtaining the solution
- Reviewing the results.

*Building the Models* : The database comprising the element type and its options, elasto-plastic material properties (*Young* modulus, *Poisson* ratio, yield stresses), the model geometry and the resulting finite element mesh has been explicitly created with the commands and features available in preprocessor *PREP7* module of *ANSYS*.

Nevertheless, the choice of the appropriate element type is often crucial for effective finite element analysis. The category (structural, thermal, magnetic, etc.) the element belongs to, the degrees of freedom at its nodes, the features it supports (plasticity, large deformation, creep, etc.) should account for its intended usage. Each element type serves a different purpose and is identified by a group label followed by a number combination. The label identifies the category name of the element whilst the number combination expresses the number of nodes and number of degrees of freedom available at each node.

Similar to the status of elements within a finite element model, the nodes are the fundamental parts of an element. Elements are connected to the nodes in the sequence and orientation as shown in Figure 3.3. This connectivity has been provided along with the *automatic meshing* feature of *ANSYS*. The degree of freedom set (displacements, rotations, etc.) of each element constitute the primary nodal unknowns to be determined by the analysis. Derived results such as stresses and strains have been computed from these degree of freedom results. The element type attributed to the nodes have explicitly defined their degrees of freedom .

The element type designated with *Plane42* has been chosen for the finite element mesh generation. *Plane42* is a two dimensional structural solid element and is applicable to the modeling of two dimensional solid mediums. The geometry, node locations and the coordinate system for this element are shown in Figure 3.3. The element is defined by four nodes having two degrees of freedom at each node; translation in the nodal  $x$  and  $y$  directions. Plasticity, creep, swelling, stress stiffening, large deflection and large strain are among the capabilities of this element from which the last two mentioned ones have been correlated. However, prior the determination of the stress-strain response of the problem the nature of the finite element analysis has been acknowledged. There are basically three types of finite element analysis for two dimensional planar computations : plane strain, plane stress and axisymmetric stress analysis. As far as the *Plane42* element supports each of them its plane strain capability, which is consistent with the problem, has been adjusted throughout the analyses.

As mentioned before, the simplified model assembly has been intended to cast the two-dimensional shear stress distribution. Still, regions where stresses or strains have been of interest (the interface itself), have been provided with a reasonable integration point density. Lower-order elements, when compared with higher-order elements provide essentially the same number of integration points per element. They have therefore been conveniently preferred for this purpose such that the number of nodal unknowns has not unnecessarily been increased. Mesh density has become especially important in hinged regions, because large deflection requires that an individual element cannot deform (bend) more than 30 degrees for an accurate solution. Additionally, the mesh density has been set sufficiently high to allow for stress resolving and to account for the highest mode shape.

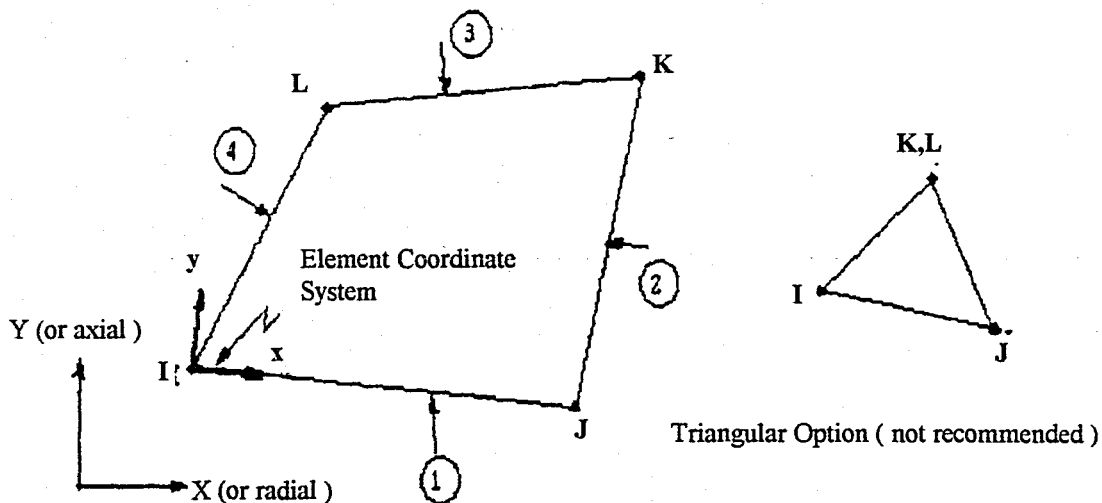


**FIGURE 3.3 : Plane-42, two dimensional structural solid element**

Defining the geometric boundaries of the models, controlling the size and shape of the individual elements have been fulfilled by using the *solid modeling* feature of *ANSYS* which requests a relatively small number of data items. The automatic generation of all the nodes and elements has been achieved by means of the *automatic meshing* feature of *ANSYS*. However before this has been accomplished, the assignment of appropriate element attributes such as the element type and the material properties set (*Young* modulus, *Poisson* ratio and yield stresses) have been completed for each distinct part of the model. Finally, the resultant meshed finite element model with assigned material properties has been obtained as depicted in Figure 3.4.

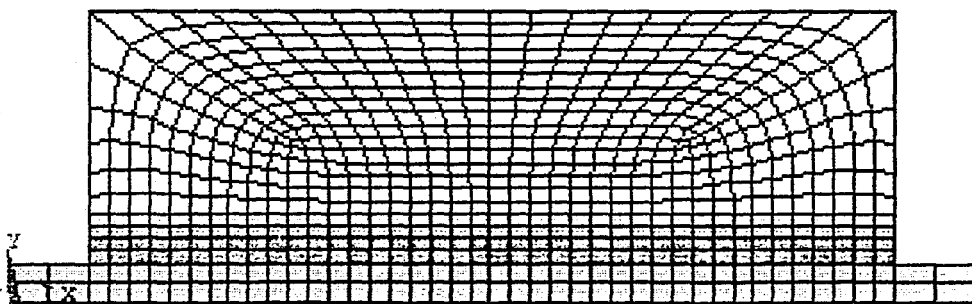


**FIGURE 3.4 : Resultant meshed finite element model with assigned appropriate element attributes and material properties**

*Application of loads and obtaining the solution* : The primary objective of a finite element analysis is to examine the response of a model to certain predefined loading conditions. Specification of the proper loading conditions and sequence has therefore been regarded as a key step in the analyses. Application of loads and degree of freedom constraints (DOF) has been accomplished within the *solution* module of *ANSYS*.

Nonetheless, a system is said to be conservative, if all energy put into a system by external loads is recovered without any loss whenever the applied loads are removed. If some of the inherited energy is dissipated through plastic deformation or internal friction, the system is said to be non-conservative. The analysis of a conservative system is path independent implying that loads can be applied in any sequence and in any number of increments without causing an impact on the end results. In contrast, an analysis of a nonconservative system is path dependent where the actual load-response history of the system must be closely followed if accurate results are desired. Path dependent problems usually require that loads be applied gradually (i.e., using many substeps) to the final load value.

Other kind of nonlinear behavior might also emerge along with plasticity. In particular, large deflection and large strain geometric nonlinearities will often be accompanied with plastic material response. Both geometric and material nonlinearities encountered are thus nonconservative, path-dependent phenomena. In other words, the sequence in which loads causing irrecoverable strain responses are applied affects the final solution. Thus, because such nonlinear responses are imminent in the analyses, the desired loads have been applied as a series of small incremental load- or time-steps. A specific *load step* defines a definite load configuration for which a solution is obtained. *Substeps* are, however, explicitly defined instants within a load step for which solutions have been calculated. Substeps are also known to be *time steps* - the difference in time between two successive solution steps. In fact, for static but time respective analysis, the "time" concept is used simply as a counter to identify the sequence of load steps and substeps. Contrary to a linear solution, a nonlinear solution often requires multiple load increments and always requests equilibrium iterations at each substep. By explicitly defining the load step in which loads are assumed to increase linearly over a time span, it has been intended that the model will chase the load-response path as closely as possible.

Most loads can be either applied on the solid model (keypoints, nodes, lines or areas) or even on the finite element model (nodes and elements). Surface loads such as pressures can be specified on lines and areas or on nodes and element faces. Regardless of how the loads have been specified, the solver of the program expects all loads to be in terms of the finite element model. Therefore whenever loads have been applied on the solid model, the program automatically has converted them to the nodes and elements before it has initialized the solution.

Nodes laying on the borders of the upper semi-finite soil domain located above the interface zone have been *coupled* in such a fashion that the rigid enclosure of Figure 3.1 is modeled as shown in Figure 3.5. That is, the vertical degree of freedom values of the upper border as well as the horizontal degree of freedom values of its both side borders have been linked, i.e. they have been forced to make the same amount of displacement that has been either computed or predefined. This resembles to the confined specimens sheared in the laboratory under applied vertical load. As illustrated in the Figure 3.5 the side and bottom nodes representing the concrete shaft of the pile have been completely constrained in both x and y direction. The DOF constraints have been defined simply by assigning the related displacement value to be equal to “zero”. Similar to the DOF constraint symbols, the coupling effect is symbolized by smaller support icons.

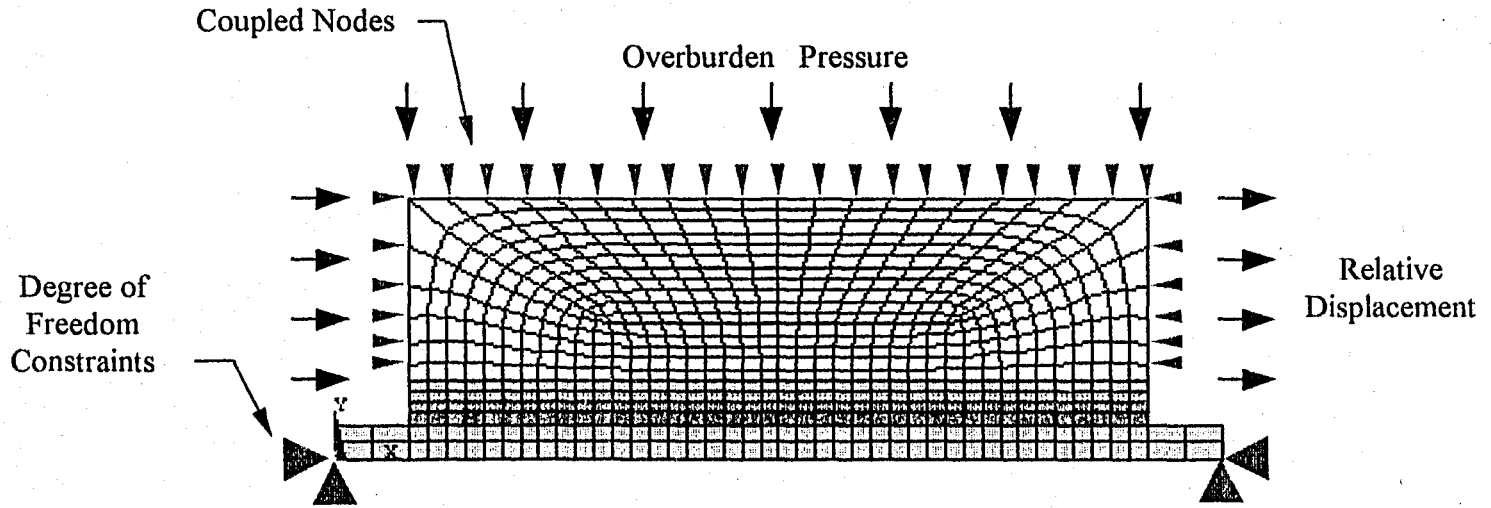


**FIGURE 3.5. : Overburden pressure, DOF constraints, coupled node sets and relative displacements applied on pre-meshed model**

The compressive overburden pressure representing the lateral earth pressure that a pile is subjected to has been immediately applied onto the enclosure of the upper soil medium once the solution is initialized. The pressure has been held at its constant initial value during the analyses as shown in the load step diagram depicted in Figure 3.6. Contrary, the amount of relative displacements has been gradually increased to simulate the shearing mechanism. Although the transversing horizontal displacement rate in actual direct shear tests is actually about 0.03 mm/s, such a rate would unnecessarily increase run times tremendously. Instead, the planned amount of relative displacement for each run has been approached with a single load step which is further subdivided into 10 equal substeps. Solutions have been calculated for each substep in order to visualize the change in shear stress as well as the stress distribution pattern evolved throughout the interface.

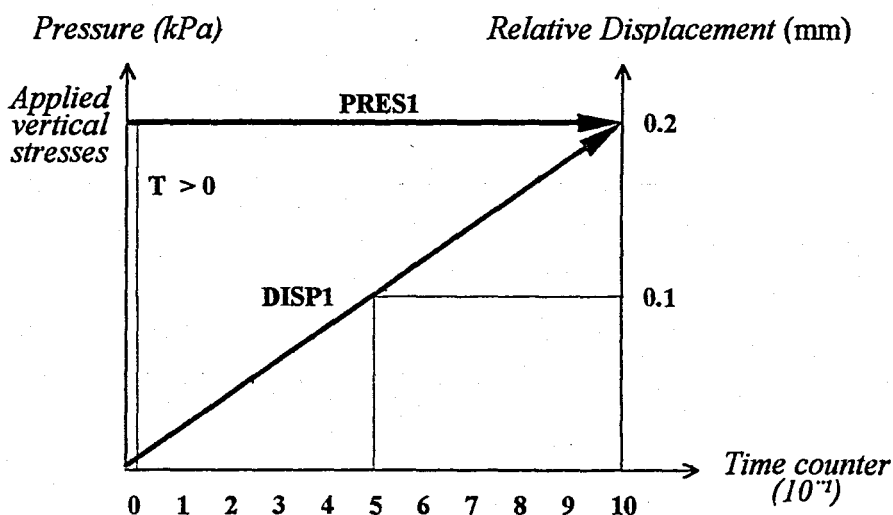


**FIGURE 3.6. : Diagram of applied load step history**

Using the *array parameter method*, the succeeding lines have been incorporated to define the loading condition approach of Figure 3.6; i.e. the input data for the load step history explained in the previous paragraph. The basis of the method is to define load-time arrays which supply the program with the desired loading conditions for every time increment as the do-loop proceeds. All loads, except the predefined degree of freedom constraints (DOF), have been created by the do-loop macro imitating the load-time history graph plotted in Figure 3.6.

These input data lines are part of the total model data and comprises : the definition of the array parameters, application location (on lines or nodes) and magnitudes of the loads (overburden pressure and relative displacements) as well as the do-loop solution of the problem. Each loading condition has been defined separately but following basically the same procedure. The subdivisions of the input data regarding the loading sequence and their related explanation are given below;

```
*DIM,PRES1,TABLE,2,1
```

```
*DIM,DISP1,TABLE,11,1
```

```
PRES1(1,1) = 50000,50000
```

```
PRES1(1,0) = 0,1
```

```
PRES1(0,1) = 1
```

```
DISP1(1,1) = 0,2E-5,4E-5,.....,20E-5
```

```
DISP1(1,0) = 0,0.1,0.2,.....,1
```

```
DISP1(0,1) = 1
```

```
TM_START = 1E-5
```

```
TM_END = 1
```

```
TM_INCR=0.1
```

```
*DO, TM, TM_START, TM_END, TM_INCR
```

```
TIME, TM
```

```
SFL, #, PRES, PRES1(TM)
```

```
NSEL, S,,, #, #, 1
```

```
D, ALL, UX, DISP1(TM)
```

```
SOLVE
```

```
*ENDDO
```

First, labels and dimensions have been attributed to the array parameters.

The predefined arrays have been filled with the load history data as for the case shown for 50 kPa overburden pressure. Pressure and displacement values are then coupled with corresponding time values. Every couple indicates a point on the load-time history graph plotted before in Figure 3.6.

The do-loop including the starting time (must be positive definite), ending time and time increments has been created in this section. *TM* indicates the counter value. The *SFL* and *NSEL* commands practice the time-dependent surface and nodal displacement loads onto the desired line and nodes, respectively.

The last two commands trigger the solution phase and the do-loop which governs the loading procedure.

Eventually, the proposed finite element models have been analyzed with respect to the above mentioned procedure and in the light of the formerly made simplifying assumptions on dimensions and geometry of the proposed prototype as well as material properties and response behavior of the soil. The simultaneous equations, which express the physical problem in mathematical terms, have been automatically generated and subsequently solved by the program during the solution phase of the analyses.

*Reviewing the results* : Postprocessing is the phase of the analyses in which the results have been reviewed. *Post1*, the general postprocessor has been used for reviewing the results of the entire model for every substep. A typical but not to scale drawn representative deformed shape of an analyzed model has been obtained as plotted in Figure 3.7.

As mentioned earlier, results data calculated during the solution phase by the program can be grouped into two categories : (1) Primary data consisting on displacements has composed the degree-of-freedom solution calculated at each node. (2) Stresses and strains have constituted the derived data, those results that have been derived from the primary data. The latter result set has been examined in order to establish conclusions for the scope of this study.

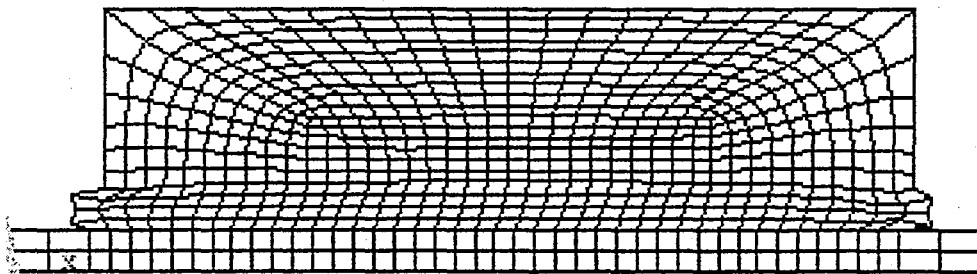


**FIGURE 3.7 : Deformed shape of a typical analyzed model**

### 3.5. Employed Technique for Nonlinear Analysis

It is widely known that almost every type of problem handled in geotechnical engineering exhibits nonlinear behavior. This is due to the fact that soil possessing highly nonlinear characteristics is the governing material in all geotechnical problems. Moreover, many factors can influence a material's stress-strain properties, including load history (as encountered in elasto-plastic response), environmental conditions (such as temperature, in-situ stresses, presence of fluids in the pores), history of loading as well as the presence of joints and discontinuities.

Geometric nonlinearity being the other kind of nonlinearity encountered is caused by significant changes in the geometry of the loaded body. Since the individual finite elements are forced to experience large deformations due to applied relative displacements, they are subjected to significant changes in geometric configuration leading to cause the assembly to respond nonlinearly. Incremental and iterative are the two main techniques used for nonlinear analyses. A combination of these two techniques is also possible.

A nonlinear assembly's behavior like the stress-deformation problem can not be represented directly with a set of linear simultaneous equations. The nonlinear behavior has been approximated as piecewise linear such that the program could utilize the linear laws for each piece. Thus, a series of successive linear approximations with corrections have been made to solve this nonlinearly responding physical problem.

The *ANSYS* software uses the incremental loading and equilibrium iterations approach to obtain nonlinear solutions. The load applied to the assembly is broken into a series of load increments in this process. These load increments can then be applied either over several load steps or over several substeps within a load step. At the completion of each incremental solution, the program adjusts the stiffness matrix to reflect the nonlinear changes in structural stiffness, before proceeding to the next load increment. The main drawback of a pure incremental approach is that it inevitably accumulates error with each load increment, causing the final results to be out of equilibrium, as shown in Figure 3.8.-a.

This difficulty has been intended to overcome by the *ANSYS* software through the application of *Newton-Raphson* equilibrium iterations, which enables the program to adjust the solutions to equilibrium convergence (within some predefined default tolerance limit) at the end of each load increment. Convergence tolerances for equilibrium iterations can be based on loads, deflections or even both. However, force-based convergence provides an absolute measure of convergence, whereas displacement-based convergence provides only a relative measure of apparent convergence and should therefore not be used alone. For this reason the default force-based convergence criteria has been enabled. *ANSYS* is also capable to base convergence checking on various physical values such as forces, moments, displacements, or rotations, or any combination of these.

Before each solution, the *Newton-Raphson* method has evaluated the out-of-balance load vector, which equals to the difference between the restoring forces (the loads corresponding to the element stresses) and the applied forces. The program has then performed a linear solution, using the out-of-balance loads, and has checked for convergence. If the predefined convergence criteria has not been satisfied, the out-of-balance vector has been re-evaluated, the stiffness matrix has been updated, and a new solution has been obtained. This iterative procedure has continued until the problem converged.

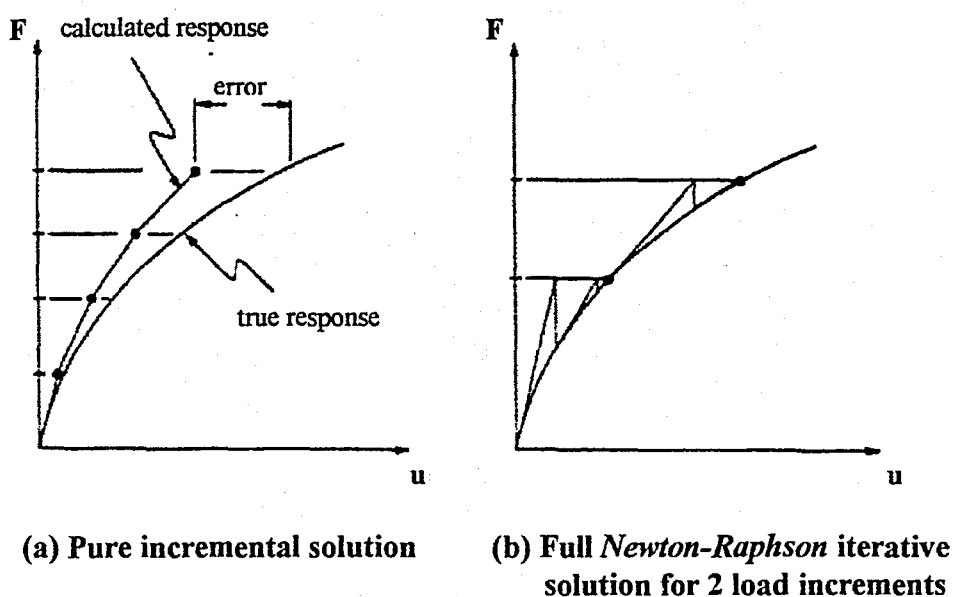


**FIGURE 3.8. :** Comparison between the pure incremental approach and the *Newton-Raphson* approach

Figure 3.9 predicts in which displacement convergence checking when used alone, could give a false indication of successful convergence. The small  $\Delta u$  calculated after the second iteration could be misinterpreted as a converged solution, even though the solution is still far from a true solution. To avoid such errors is possible by applying force-dependent checking.

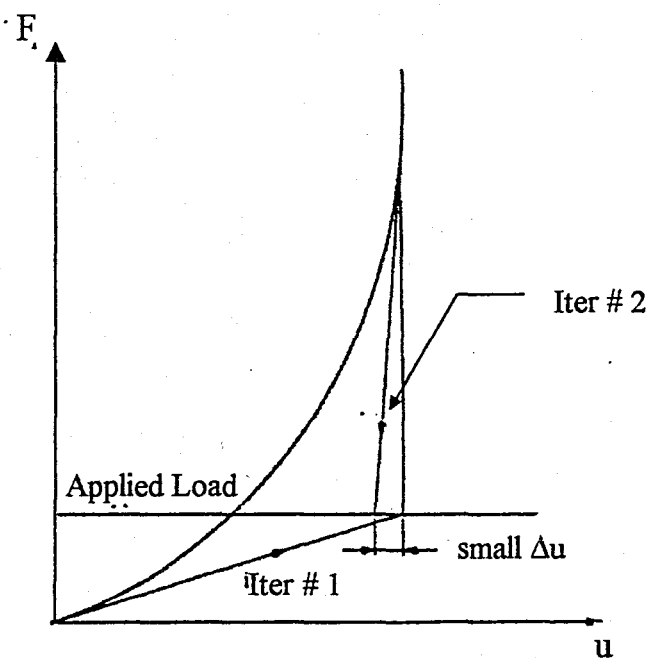


**FIGURE 3.9. : Errors are imminent when relied only on displacement convergence checking**

## 4. RESULTS AND DISCUSSION

Finite element analyses have been performed on models that have been proposed and explicitly explained in previous sections in order to distinguish the change in shear stresses and recognize the awaited improvements in corresponding shear strength parameters  $c$  and  $\phi$  at the interface of lime treated soil and concrete. Relying on the fact that a soil layer with finite thickness is always present within the interacting pile-soil assembly, the study has been founded on the "thin-layer" concept introduced earlier by other researchers.

As implied in previous sections, this research has been restricted to examine, in accordance with the proposed models, the influence of varied mechanical (*Young* modulus, *Poisson* ratio and yield stresses) and geometric (interface thickness) parameters onto the interface response behavior. The mechanical parameters ( $E, \nu$ ) have been employed in order to incorporate the altered failure mode as well as the stabilization effects of lime on clayey soil. In other words, these parameters have been accepted to enable for distinction between the two conditions analyzed, namely the lime treated and the untreated natural soil case. The difference between the results obtained for these cases will be indicative of the effectiveness of the introduced proposal. The utilization of the geometric parameter ( $t$ ) has been intended to assess the influence of treatment duration. Resting on the tacit assumption that the application length of lime slurries determines the width of the interacting zone, the employed thicknesses or interface gap sizes have simply referred to the relative duration of treatment. That is, the thicker the employed interface gap size, the longer the imitated treatment duration. By this means it has been aimed to judge whether a prolonged treatment would yield an additional benefit beside its drawback on the residual shear strength.

The analyses have been performed to simulate the response behavior of modeled natural and 7 per cent lime treated pure bentonite specimens under shearing. The shearing mechanism has been provided by subjecting the semi-finite soil domain (rigid enclosure) to relative displacements under pre-applied constant overburden pressure. Each of the proposed models has been analyzed under 50, 100 and 150 kPa vertical compression, which accounts approximately for the lateral earth pressure that a 10 m long pile shaft is subjected to at equal intervals.

Results have been grouped into four for the same interface thicknesses 2, 4, 6 and 8 mm. Such a classification provides not only a better interpretation but also casts the effect of treatment duration. Every group has been subdivided further into two accounting namely for the untreated and the lime treated soil case. By this means, it has been intended to provide a better illustration of the improving effects of lime onto the shear stresses and its corresponding shear strength parameters. Thus, the effects of lime treatment as well as the influence of treatment duration onto the response behavior and acquired ultimate shear stresses have been outlined in Figure 4.1 through Figure 4.4. Provided that the analyses have been two dimensional (XY) planar computations, each individual graph obtained has been plotted as relative horizontal displacements versus corresponding average shear stresses ( $S_{XY}$ ) exposed within the interface zone.

The difference between the magnitudes of the ultimate shear stresses and accompanied shear strength parameters of the lime-treated and the untreated soil case will be indicative of the beneficial lime stabilization effects. Accordingly, the maximum shear stresses obtained from the stabilized specimens have been approximately twice as much as those obtained from the untreated ones. Such a remarkable acquired gain in sustainable shear stresses implies to enhance both the cohesion and the internal friction angle of the bearing shaft soil. This in turn, undoubtedly advocates for improvements in shaft friction coefficient  $f_s$  between any particular clayey soil strata and the pile shaft.

A more comprehensive graph derived from Figure 4.1 through Figure 4.4 and depicted in Figure 4.5 has yielded the evolved failure envelopes for both the lime treated and the natural case. These failure envelopes have been obtained by simply combining the points that indicate the ultimate shear stresses of the graphs plotted in Figure 4.1 through Figure 4.4 for different levels of exercised overburden pressure. Indeed, the comparison between these figures has confirmed that both shear strength parameters ( $c, \phi$ ) have been improved upon application of the method. A consequence of this kind verifies the proposal and permits piles to resist more axial load per unit shaft area whereby a reduction in their dimensions would not endanger the stability of the supported superstructure.

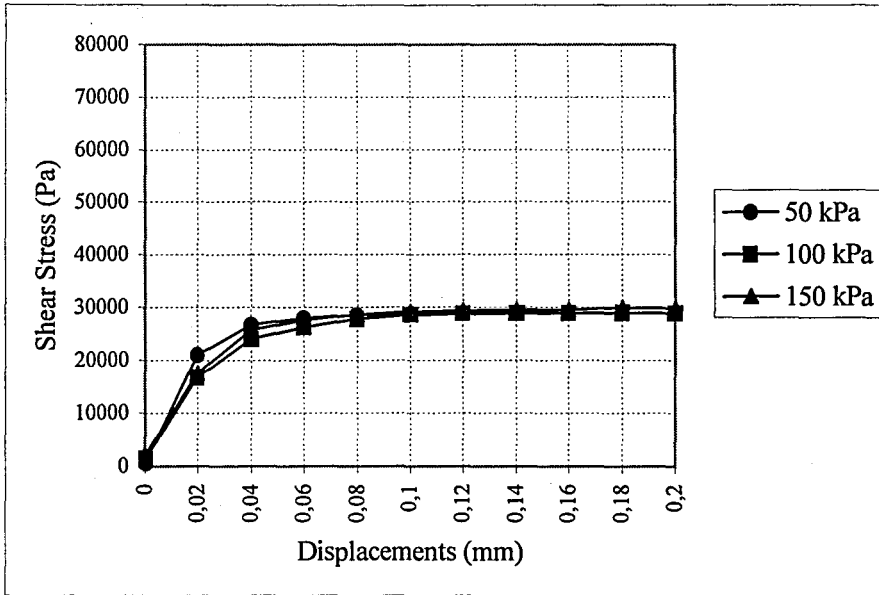
Additionally, the nature of the curves representing shearing versus deformation in Figure 4.1 through Figure 4.4 is actually determined by the structural arrangement of the cohesive soil grains. It is inferable from those figures that lime treated bentonite specimens reached their failure state (scattered) remarkably before their corresponding natural ones since they flocculate to larger-sized aggregates and acquire brittle material characteristics. This kind of response behavior is consistent with the assigned material properties and has been therefore within our expectations. Contrary, a more gradual and continuous deformation rate has been developed for the modeled natural specimens. Since the interface soil represents in its untreated natural condition a remolded or dispersed structure, the few contacts generated in this case demonstrate a resistance to shear which increases with deformation until a constant shearing resistance is established at a particular shear rate. These response behaviors state that the ultimate shear resistance can be manifested at smaller relative displacement values such that the amount of total pile settlement can be reduced.

The effect of varied interface thickness (treatment duration) onto the acquired ultimate shear stresses has also been investigated. However, neither a definite contribution to the maximum shear stresses nor a remarkable influence onto the response behavior arising from the duration of treatment has been recorded. Maximum shear stresses remained somewhat intact as changes in interface thickness have been made for the lime treated case shown in Figure 4.6.-b. Likewise, analyses resulted in a much more unstable response for the untreated natural soil case as plotted in Figure 4.6.-a. Although these results are restricted to the models proposed, the corresponding laboratory tests showed close similarity. The ultimate shear stresses obtained in the laboratory showed also no remarkable increase whereby the residual shear stresses experienced a major decline suggesting that prolonged treatments act actually counterproductive. Such visualized strain softening behavior is only expressive by the assignment of negative stiffness values which intimates unstable behavior in many instances and is therefore likely to cause nonunique results. Unlike the laboratory tests, numerical simulations could not recognize the drawback resulting from lengthened treatments. Moreover, it has been agreed that the width and nature (condition) of the soil layer participating in the interaction phenomena ascertain the magnitude of tolerable stress levels.

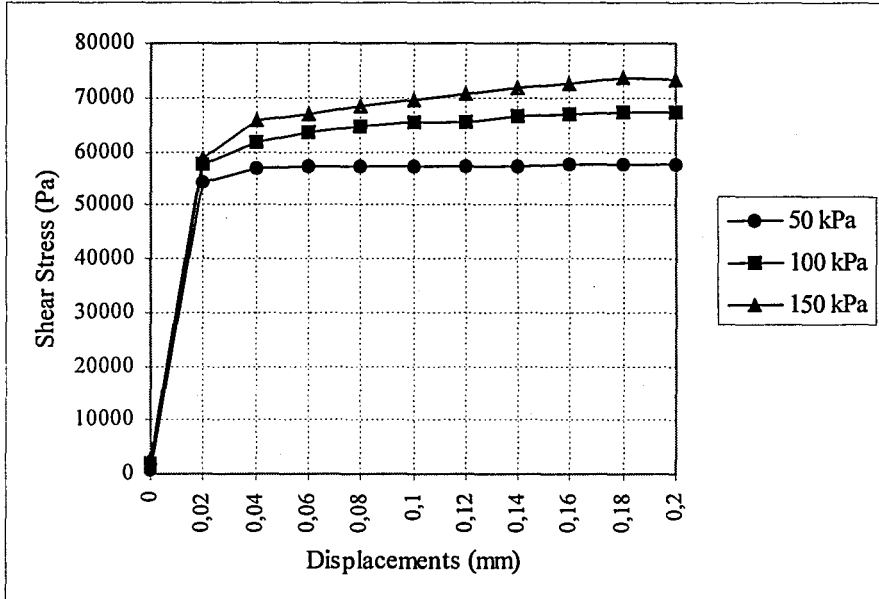
The evolved  $S_{XY}$  shear stress distribution patterns for typical models analyzed under 150 kPa overburden pressure for both cases with 4 and 8 mm interface thicknesses have been plotted in Figure A.1 through Figure A.4. Each of these images has been designated with a time counter that links it to a predefined substep within the load history diagram. Such a sequential presentation has been conceived to make the shear stress evolution visible. These figures further state that the necessary skin resistance of piles or drilled piers is exposed from the sheared interface zone. It is also perceptible from these images that the intensity of the shear stresses diminishes from the interface outwards. Nevertheless, failure is inevitably to occur in this highly stressed zone once the ultimate shear stress level has been exceeded.

From the numerical point of view, the number of cumulative iterations increased with decreasing interface thicknesses suggesting that numerical ill conditioning is imminent for too small thicknesses. Indeed, severe convergence difficulties have been encountered for cases analyzed with thicknesses below the 2 mm level. All recovery promoting features such as the *bisection* and the *arc length* method available within *ANSYS* for nonlinear analyses have been enabled without success in order to guide the program to a successful converged solution.

A convergence failure problem arises when the problem experiences a negative main diagonal, calculates for a specific aspect ratio (ratio of thickness to width of the interface) exceedingly large displacements, or fails to satisfy the pre-defined convergence criteria (has been set as default) within the specified maximum number of equilibrium iterations. A physical instability (i.e., having zero or negative stiffness) in the assembly or as a result of some numerical problem in the finite element model may also lead to a convergence failure. Although the models have been modeled physically stable and the convergence criteria has been eased, the relative displacements applied to models to interface thicknesses below the 2 mm level still caused divergency whereof a valid numerical solution could not be obtained.

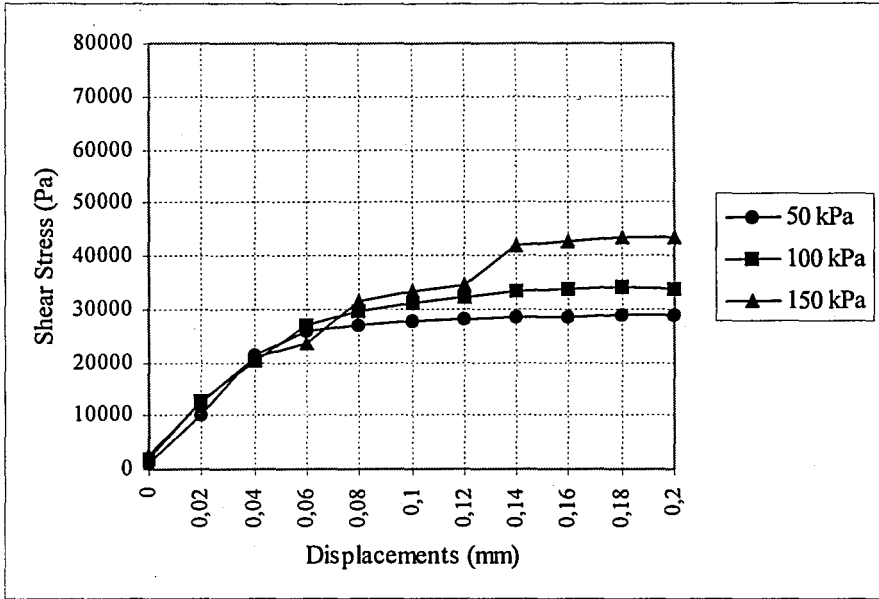


(a) Without lime treatment

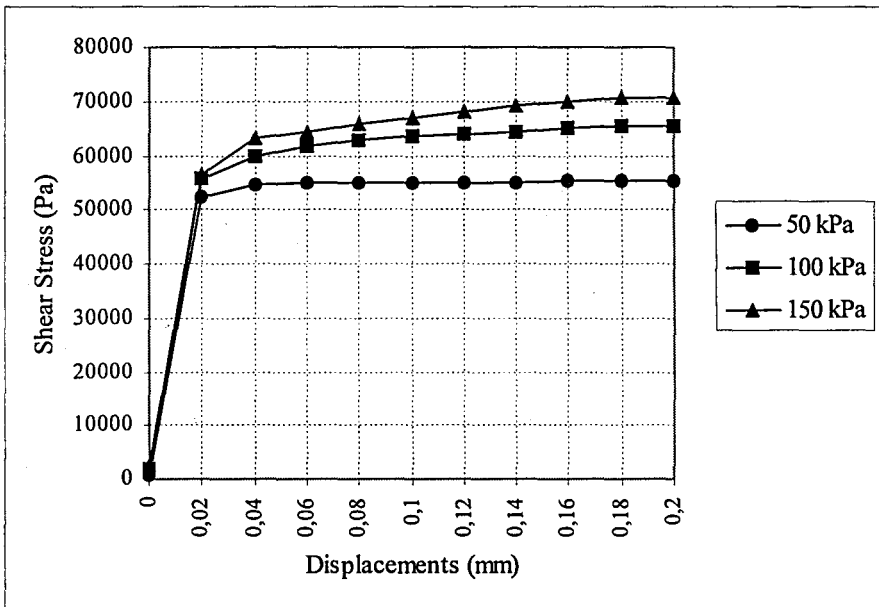


(b) Treated with 7 % lime

**FIGURE 4.1. : Average shear strength vs displacement behavior of pure bentonite samples with 2 mm interface thickness (a) Without lime treatment (b) Treated with 7 % lime**

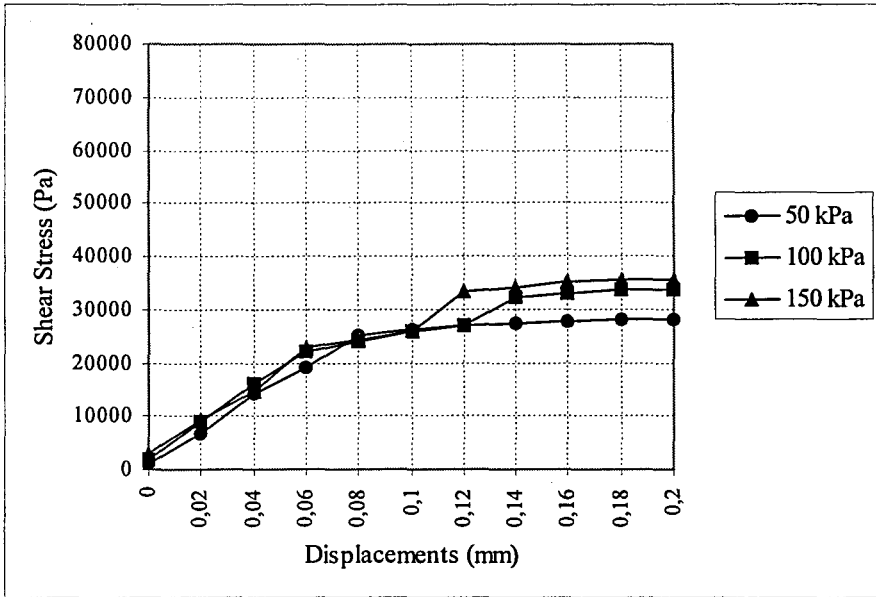


(a) Without lime treatment

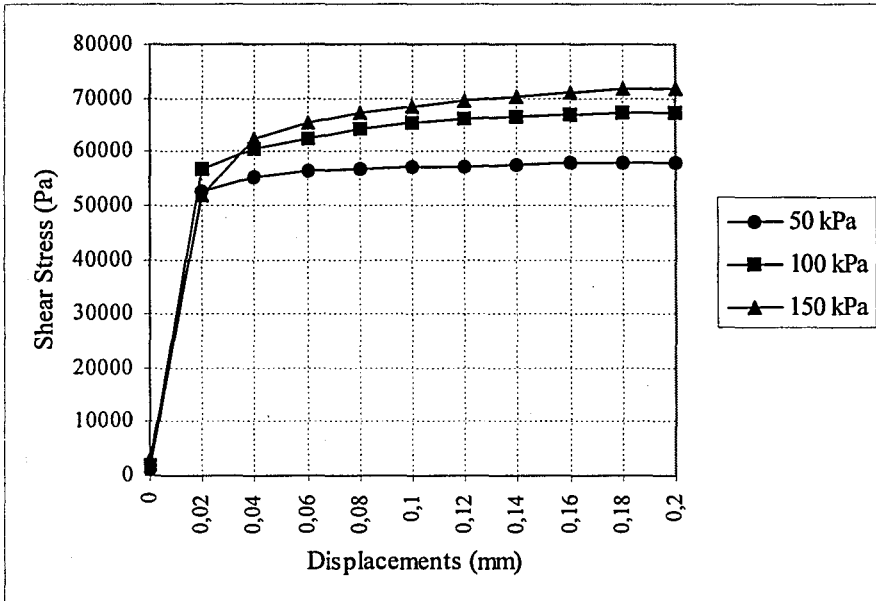


(b) Treated with 7 % lime

**FIGURE 4.2. : Average shear strength vs displacement behavior of pure bentonite samples with 4 mm interface thickness (a) Without lime treatment (b) Treated with 7 % lime**

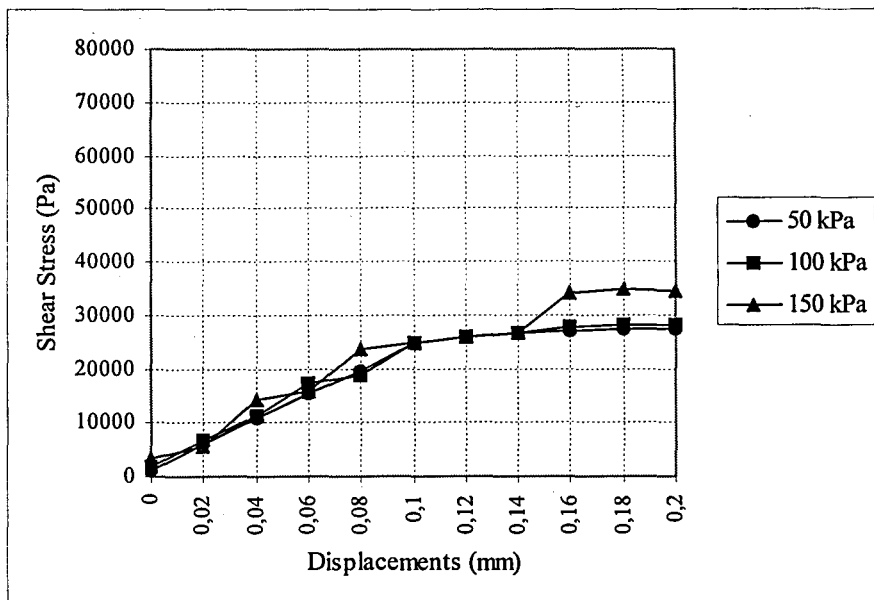


(a) Without lime treatment

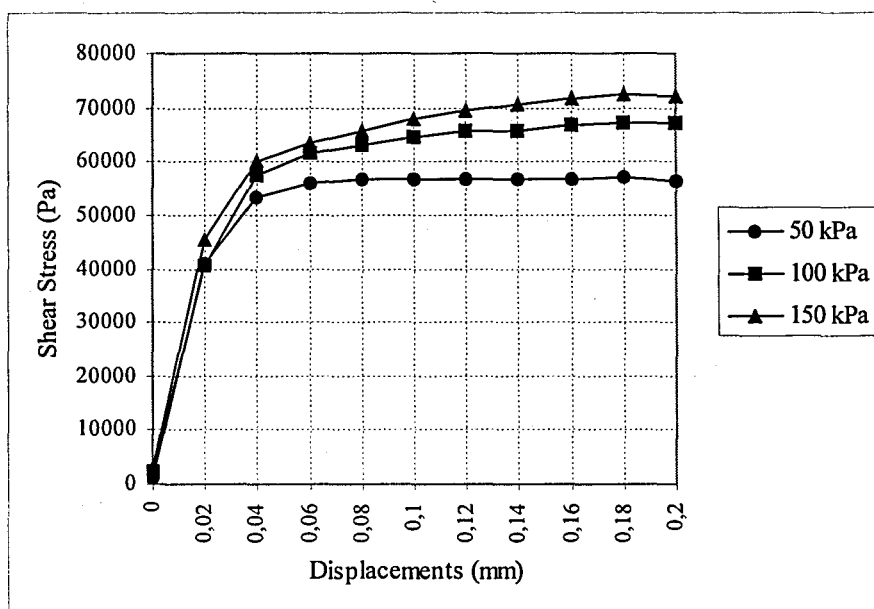


(b) Treated with 7 % lime

**FIGURE 4.3. : Average shear strength vs displacement behavior of pure bentonite samples with 6 mm interface thickness (a) Without lime treatment (b) Treated with 7 % lime**

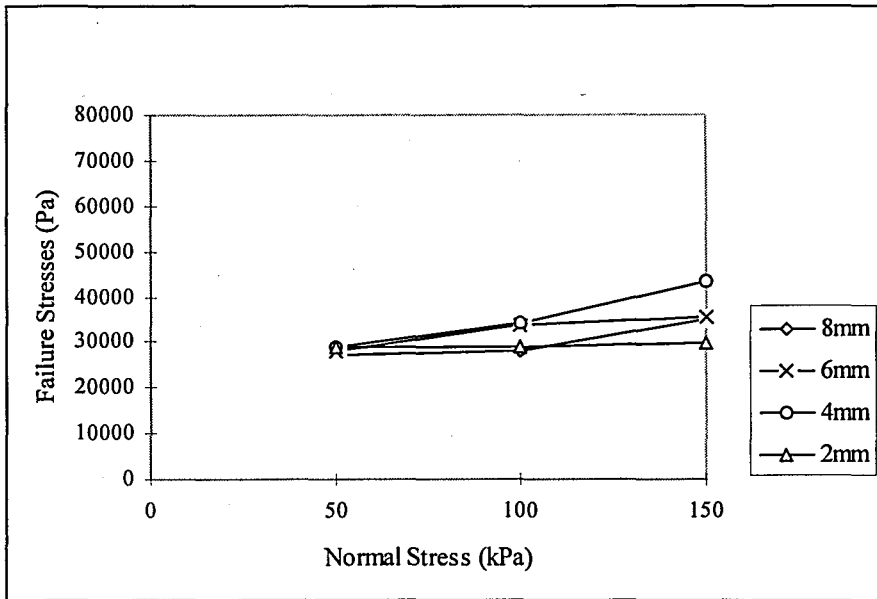


(a) Without lime treatment

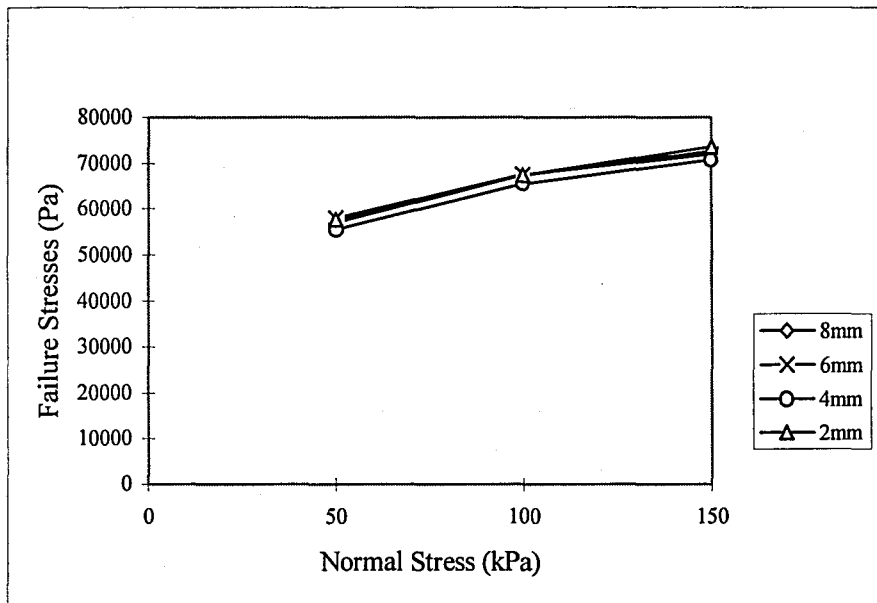


(b) Treated with 7 % lime

**FIGURE 4.4. : Average shear strength vs displacement behavior of pure bentonite samples with 8 mm interface thickness (a) Without lime treatment (b) Treated with 7 % lime**

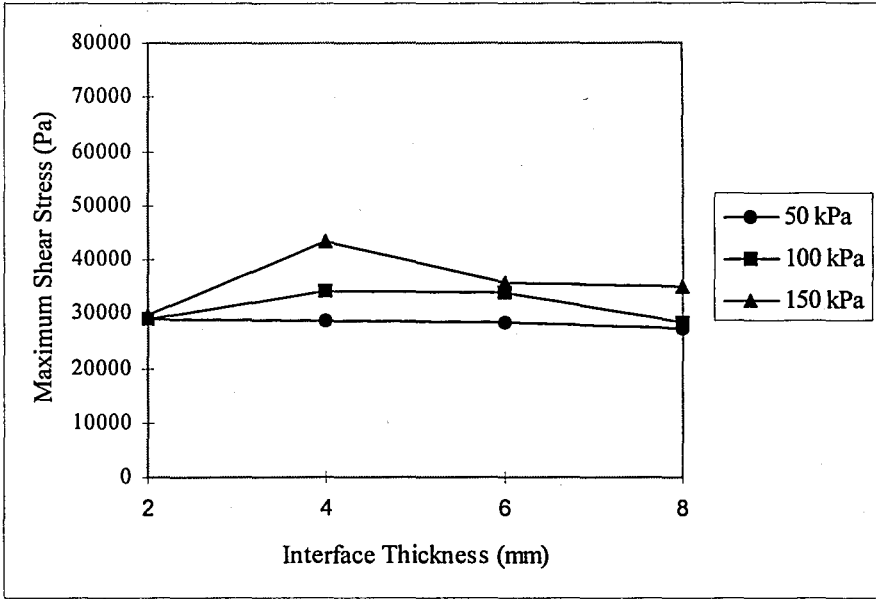


(a) Without lime treatment

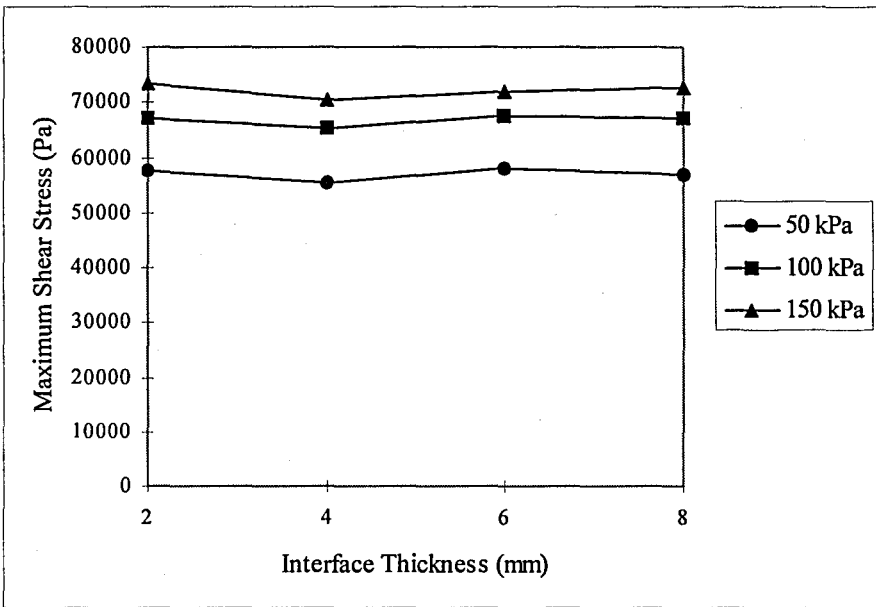


(b) Treated with 7 % lime

FIGURE 4.5. : Interface respective failure envelopes for pure bentonite specimens  
 (a) Without lime treatment    (b) Treated with 7 % lime



(a) Without lime treatment



(b) Treated with 7 % lime

FIGURE 4.6. : Effect of interface thickness onto maximum acquired shear stresses  
(a) Without lime treatment (b) Treated with 7 % lime

## 5. CONCLUSIONS

Using the finite element method, the influence of lime stabilization and varied treatment duration onto the shear strength at the soil-concrete interface has been investigated. Furthermore, the compatibility of computer aided interface modeling as well as the performance of the thin layer concept has been examined. The conclusions summarized below are restricted to the proposed analysis method, developed models and obtained results. The findings and conclusions have been found in consistency with both laboratory tests conducted formerly by *Metehan C.T.* and contemporary field applications.

First, the performance of the thin layer concept as well as the compatibility of computer aided interface modeling has been concluded as follows;

1. Inclusions of a finite thickness for the interface is realistic since there is very often a thin layer of soil which participates in the complex soil-structure interaction phenomena. Implementation of such a solid medium serves primarily as a continuum between the two interacting mediums. The actual response of the interface behavior is therefore still influenced by the characteristics of its surrounding environment but depends mainly upon its own properties. Since the formulation of the thin layer is essentially the same as for other solid elements, its characteristic properties can be easily defined and implemented into existing finite element code. That is, the thin layer concept permits for the assignment of appropriate mechanical material properties in order to pinpoint its desired status (firm, weak, etc.) and behavior characteristics (brittle, plastic, etc.). The determination of the effectiveness of a particular application (i.e., stabilization promoting) on the interface soil can therefore be achieved. In view of the ease and success in the application of the simple thin element, it may not be necessary to develop more complex approaches unless they are required by particular problems where complicated mechanisms coincide. However, the influence of some special mechanism that soils do experience (strain softening, dilatency, arching, etc.) are hardly convertible into numerical terms and constitute the main drawback of computer aided interface simulations.

2. The quality of proper interface modeling depends, beside reasonable implementations of material properties and behavior characteristics also on its aspect ratio. The correct aspect ratio is actually determined by the intensity of the involved individual mechanisms (dilatancy, strain softening or as for the case examined herein the infiltration depth of stabilizing agents, etc.) and requests therefore parametric handling. By handling the aspect ratio, the contributions of all these mechanisms have been discarded except the ones that govern the amount of lime infiltration, namely the diffusion-advection mechanisms. Accounting for different infiltration depths, results obtained for different thicknesses revealed that the improved shearing characteristics are independent of the applied treatment duration. This judgment is, however, valid for the ultimate shear strength since the decline in residual shearing characteristics (strain softening) is not obtainable from numerical simulations. This conclusion implies in other words that prolonged lime treatment has provided no additional gain in the ultimate shear strength. One can further infer that prolonged treatments could be even counterproductive by recalling that the interface is prone to degrade and likely to lose significant shear strength. Contemporary laboratory tests have verified this fact by monitoring the decline in residual shear strength once the treatment duration surpasses a time span of 1-2 hours.

The following conclusions can be drawn for the application of this method on cast in-situ concrete piles or drilled piers;

1. Sustainable shear stresses and thus shear strength parameters of the soil-structure interface increase remarkably with lime stabilization. Such improvements recorded in the properties of the bearing shaft soil accounts for higher unit skin friction and advocates therefore reductions in pile dimensions (length and diameter). The desired skin resistance can still be supplied whereby a great amount of cost saving is undoubtedly achieved.

2. Because of the increase in shear strength parameters at the interface of clayey-soil and concrete upon treatment with lime, slip deformations at failure are also expected to increase. Nevertheless, as agreed previously by many investigators, the relative displacement necessary for a pile to mobilize full skin resistance hardly ever exceeds 10 mm regardless of the bearing soil, pile type and dimensions.

One may conclude therefore that the decrease in slip deformations may not endanger the applicability of this proposal.

3. Cast-in-situ concrete piles or drilled piers have been considered for verifying this proposal. Nevertheless, other types of bored piles such as pre-cast concrete piles would not jeopardize the applicability of the method. The reason for this is that the infiltration of lime into soil provides not only a better bonding with concrete but also improves the properties of the shaft soil. They might be even considered more attractive due to their overall lower costs (especially labor costs).

4. Finally, for convenience, a linear diffusion rate throughout the interface zone has been assumed. However, the proposed application bases on the diffusion-advection mechanism of lime from the pre-saturated bore-hole into the neighboring shaft soil. Although correlation has been mentioned from literature regarding the width of the lime affected interface zone, the point of infiltration intensity needs further research. Validation and standardization of the proposal should be supported with a wide range of field trials.

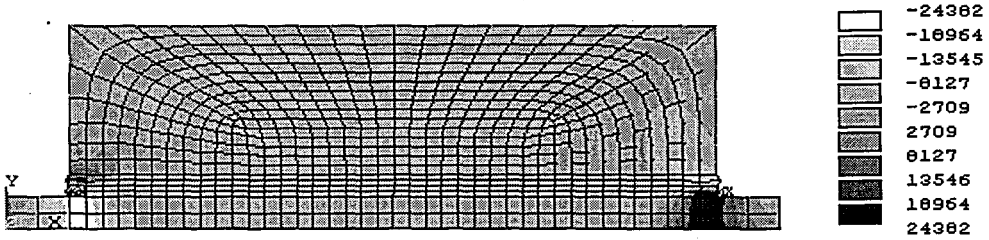
## APPENDIX

The images of Figure A.1 show the time respective evolution of shear stress patterns (Pa) for the untreated case with 4 mm interface thickness and 150 kPa overburden pressure.

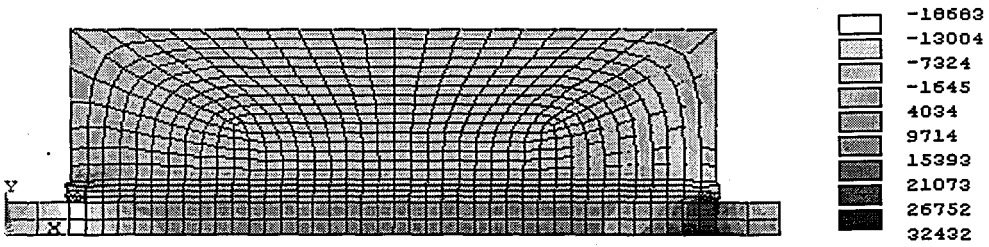
The images of Figure A.2 show the time respective evolution of shear stress patterns (Pa) for the lime treated case with 4 mm interface thickness and 150 kPa overburden pressure.

The images of Figure A.3 show the time respective evolution of shear stress patterns (Pa) for the untreated case with 8 mm interface thickness and 150 kPa overburden pressure.

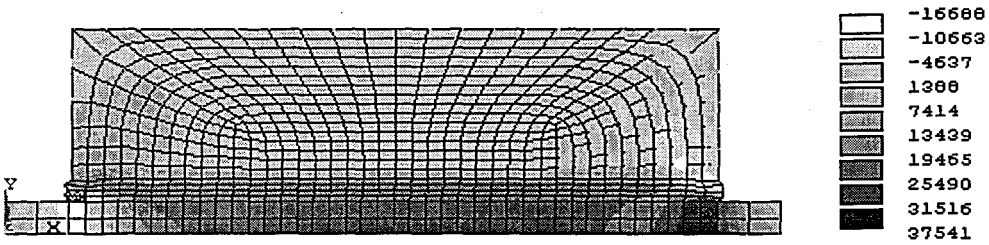
The images of Figure A.4 show the time respective evolution of shear stress patterns (Pa) for the lime treated case with 8 mm interface thickness and 150 kPa overburden pressure.



(a) Evolved shear stress pattern for time counter = 0

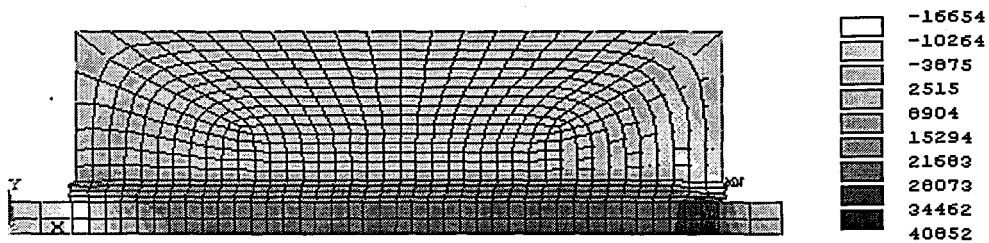


(b) Evolved shear stress pattern for time counter = 0.2

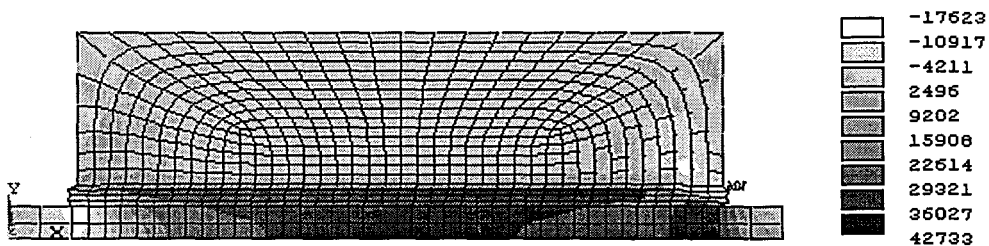


(c) Evolved shear stress pattern for time counter = 0.4

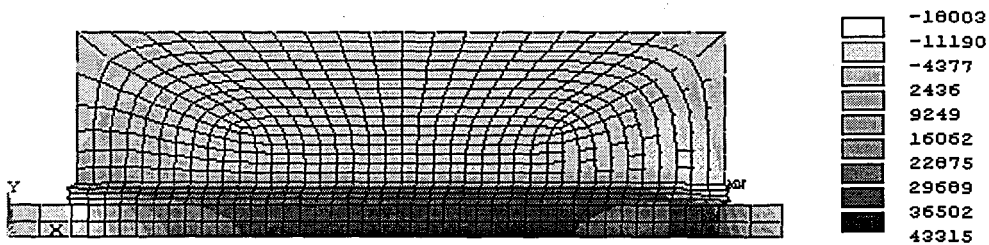
**FIGURE A.1. : Time respective evolution of shear stress patterns (Pa) for the untreated case with 4 mm interface thickness and 150 kPa overburden pressure**



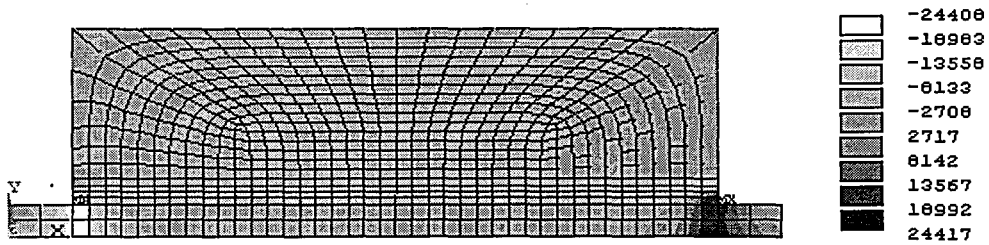
**(d) Evolved shear stress pattern for time counter = 0.6**



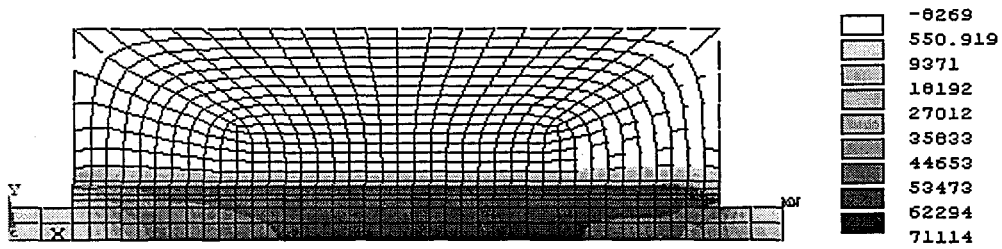
**(e) Evolved shear stress pattern for time counter = 0.8**



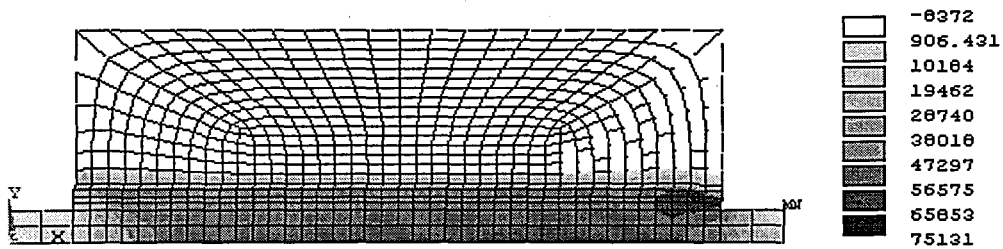
**(f) Evolved shear stress pattern for time counter = 1.0**



(a) Evolved shear stress pattern for time counter = 0

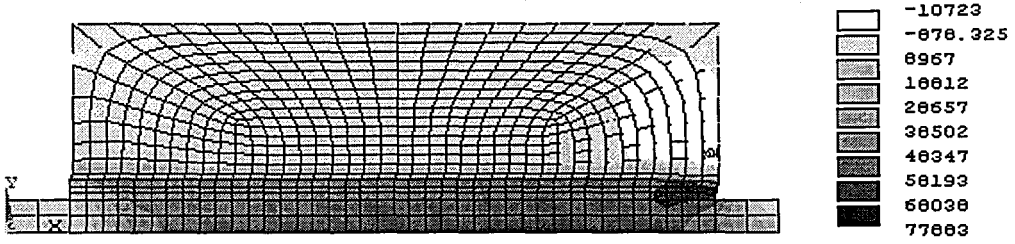


(b) Evolved shear stress pattern for time counter = 0.2

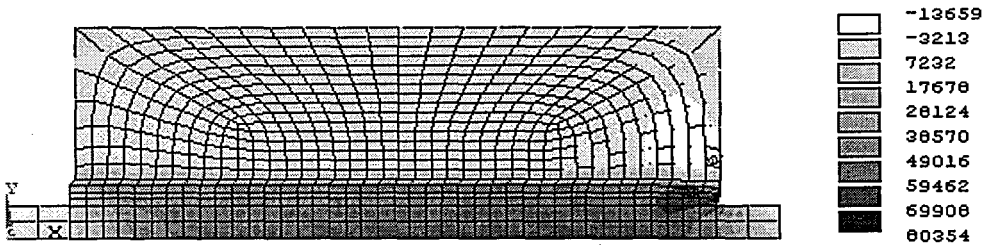


(c) Evolved shear stress pattern for time counter = 0.4

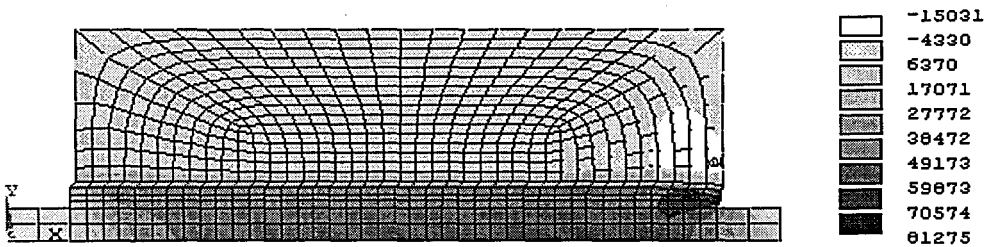
**FIGURE A.2. : Time respective evolution of shear stress patterns (Pa) for the lime treated case with 4 mm interface thickness and 150 kPa overburden pressure**



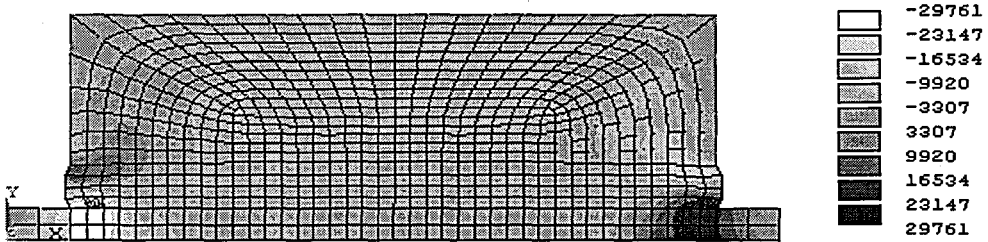
(d) Evolved shear stress pattern for time counter = 0.6



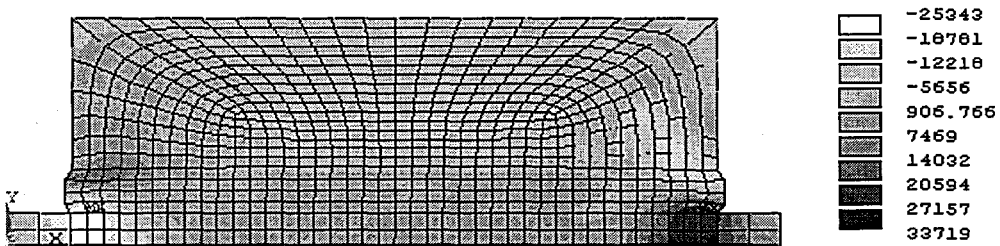
(e) Evolved shear stress pattern for time counter = 0.8



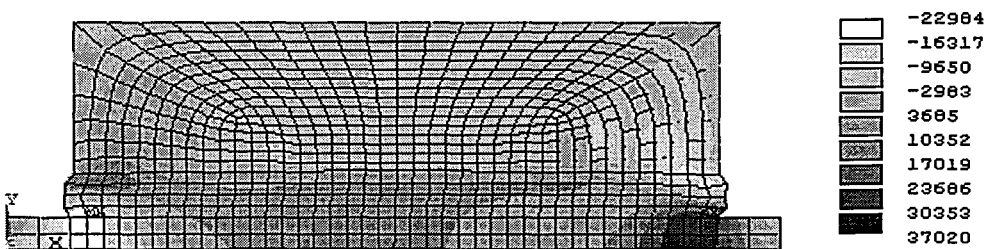
(f) Evolved shear stress pattern for time counter = 1.0



(a) Evolved shear stress pattern for time counter = 0

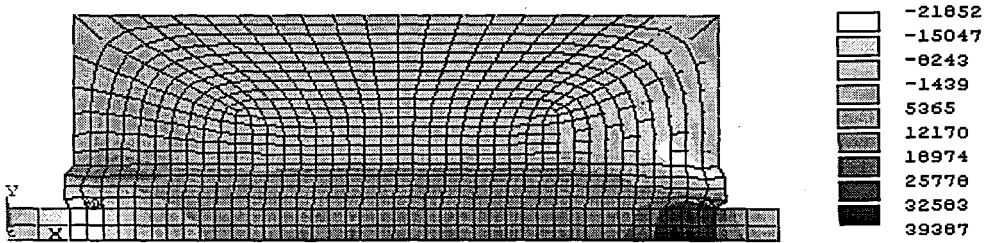


(b) Evolved shear stress pattern for time counter = 0.2

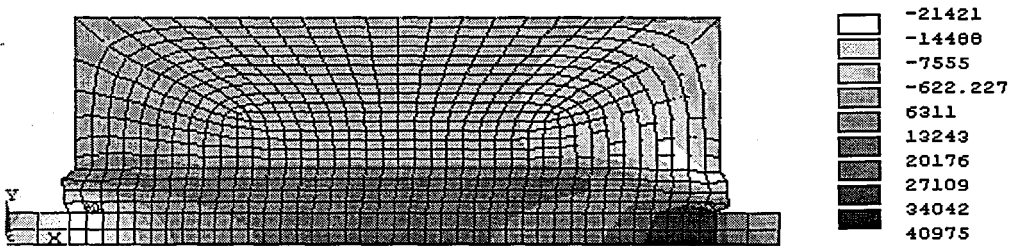


(c) Evolved shear stress pattern for time counter = 0.4

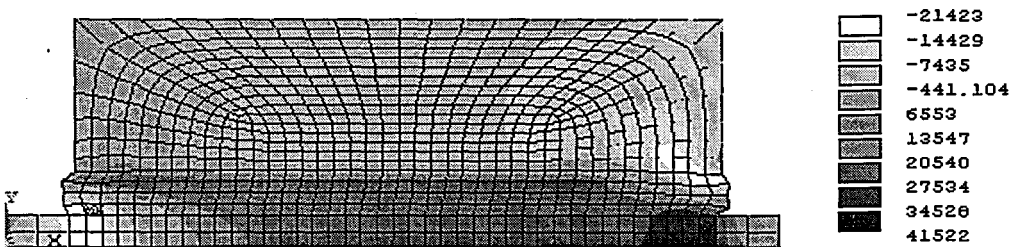
**FIGURE A.3. : Time respective evolution of shear stress patterns (Pa) for the untreated case with 8 mm interface thickness and 150 kPa overburden pressure**



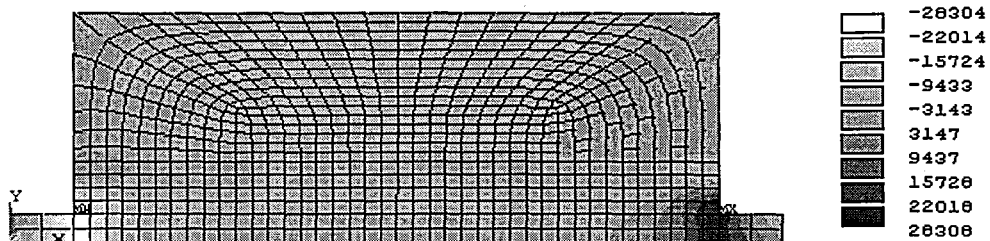
(d) Evolved shear stress pattern for time counter = 0.6



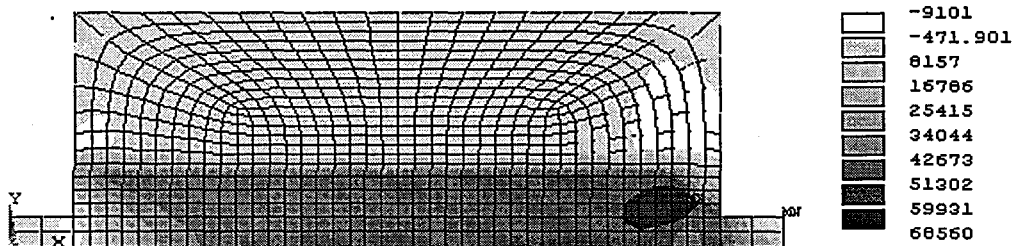
(e) Evolved shear stress pattern for time counter = 0.8



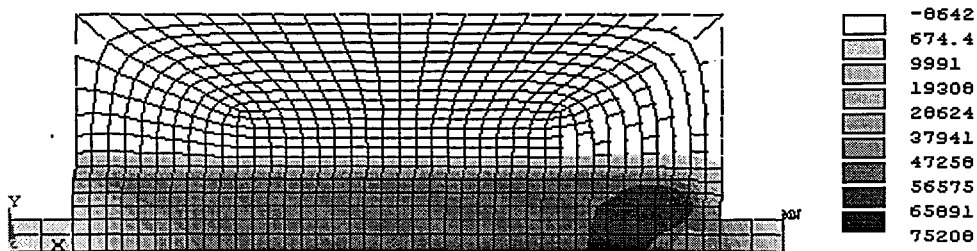
(f) Evolved shear stress pattern for time counter = 1.0



(a) Evolved shear stress pattern for time counter = 0

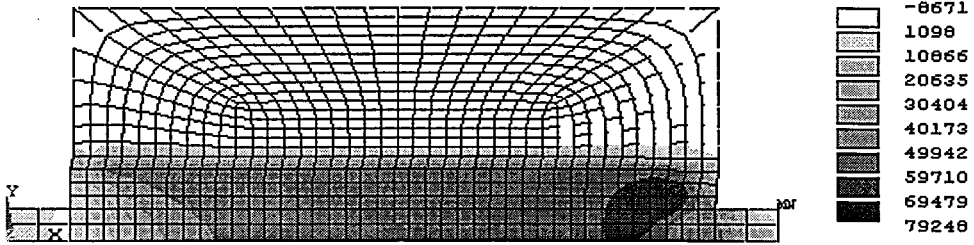


(b) Evolved shear stress pattern for time counter = 0.2

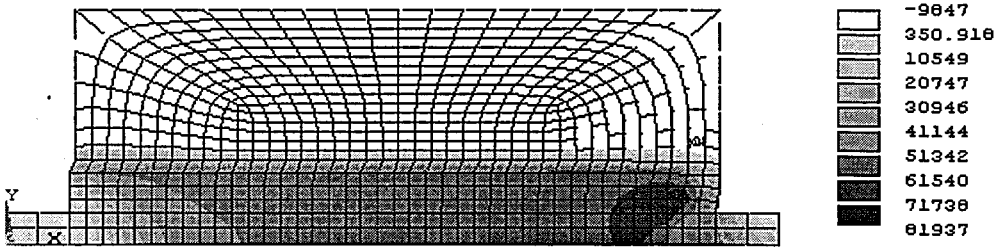


(c) Evolved shear stress pattern for time counter = 0.4

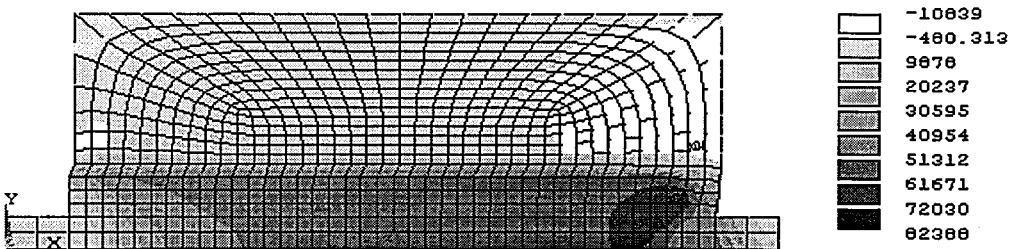
**FIGURE A.4. : Time respective evolution of shear stress patterns (Pa) for the lime treated case with 8 mm interface thickness and 150 kPa overburden pressure**



(d) Evolved shear stress distribution pattern for time counter = 0.6



(e) Evolved shear stress distribution pattern for time counter = 0.8



(f) Evolved shear stress distribution pattern for time counter = 1.0

## REFERENCES

1. Lea, F. M., *The Chemistry of Cement and Concrete* (2<sup>nd</sup> Edition), Edward Arnold Ltd., London, 1956.
2. Desai, C. S., "Static and Cyclic Response of Interfaces for Analysis and Design of Soil-Structure Interaction Problems," in Sayed M. Sayed (Ed.), *Geotechnical Modeling and Applications*, pp. 147-168, Gulf Publishing Company, Book Division, Houston, London, Paris, Tokyo.
3. Desai, C. S. and Christian, John T. (Ed.), *Numerical Methods in Geotechnical Engineering*, Mac-Graw-Hill, New-York, 1977.
4. Carter, J. P. and Ooi, L. H., Swoboda (Ed.), "Application of a joint model to concrete-sandstone interfaces," *Numerical Methods in Geomechanics*, Innsbruck, 1988.
5. Boulon, M., Hoteit, N., and Marchina, P., Swoboda (Ed.), "A complete constitutive law for soil structure interfaces," *Numerical Methods in Geomechanics*, Innsbruck, 1988, Balkema-Rotterdam, 1988.
6. Huck, P. J., and Saxena, S. K., "Response of Soil-Concrete Interface at High Pressure," *Earth-Tech Research Corporation*, Washington D.C., Illinios Institute of Technology, Chicago, USA.
7. Jastrzebski, D., *Nature and Properties of Engineering Materials*, John Wiley & Sons, Inc., USA.
8. Bowden, F. P., and Tabor, D., *The Friction and Lubrication of Solids, Parts I and II*, Clarendon Press, Oxford, (1950,1964).
9. Navayogarah, N., Desai, C. S., Fellow, and Kiouisis, P. D., "Hierarchical Single-Surface Model for Static and Cyclic Behaviour of Interfaces," ASCE, *Journal of Engineering Mechanics*, Vol. 118, No. 5, 1992.
10. Sharma, K. G., Desai, C. S., Fellow, "Analysis and Implementation of Thin-Layer for Interfaces and Joints," ASCE, *Journal of Engineering Mechanics*, Vol. 118, No.12, 1992.

11. Ronald F. S., *Principles of Soil Mechanics*, Addison Wesley Pub. Company, Massachusetts Palo Alto, London.
12. Desai, C. S., Zaman, M. M., Lightner, J. G., and Siriwardane, H. J., "Thinlayer element for interfaces and joints," *International Journal for Numerical and Analytical Methods in Geomechanics*, Vol. 8, pp. 19-43, 1984.
13. Goodman, R. E., Taylor, R. L., and Brekke, T. L., "A model for the mechanics of jointed rock," ASCE, *Journal of Soil Mechanics and Foundation Division*, Vol. 94, (SM 3), 1968.
14. Ghaboussi, J., Wilson, E. L. and Isenberg, J., "Finite elements for rock joints and interfaces," ASCE, *Journal of Soil Mechanics and Foundation Division*, Vol. 99, (SM 10), pp. 833-848, 1973.
15. Zienkiewicz, O. C., et. al., "Analysis of Nonlinear Problems in Rock Mechanics with Particular Reference to Jointed Rock Systems," *Proceedings of the 2<sup>nd</sup> Congress of the International Society for Rock Mechanics*, Belgrade, Yugoslavia, 1970.
16. Beer, G., "An isoparametric joint/interface element for finite element analysis," *International Journal of Numerical Methods in Engineering*, Vol. 21, pp. 585-600, 1985.
17. Frank, R. et al., "Numerical analysis of contacts in geomechanics," 4<sup>th</sup> ICONMIG, Edmonton, 1982.
18. Zaman, M. M., "Evolution of thin-layer element and modelling of interface behaviour in soil-structure interaction," 5<sup>th</sup> ICONMIG, Nagoya, 1985.
19. Isenberg, J. and Vaughan, D. K., "Nonlinear effects in soil-structure interaction," in Desai, C. S. and Saxena, S. K. (Eds), *Proceedings of Symposium on Implementation of Computer Procedures and Stress-Strain Laws in Geotechnical Engineering*, Chicago, Illinois, Vol. 1, pp. 29-44, 1981.
20. Pande, G. N. and Sharma, K. G., "On joint / interface elements and associated problems of numerical ill-conditioning," Short Comm., *International Journal of Numerical Analysis Methods in Geomechanics*, Vol. 3, pp. 293-300, 1979.

21. Katona, M. G., et al, "CANDE- a modern approach for the structural design and analysis of buried culverts," *Federal Highway Administration*, Report No. FltWA-RD. 77-J, Washington D.C., 1976.
22. Katona, M. G., "A simple contact-friction interface element with applications to buried culvert," in Desai, C. S. and Saxena, S. K. (Eds), *Proceedings of Symposium on Implementation of Computer Procedures and Stress-Strain Laws in Geotechnical Engineering*, Chicago, Illinois, Vol. 1, pp. 45-63, 1981.
23. Herrmann, L. R., "Finite element analysis of contact problems," ASCE, *Journal of Engineering Mechanics Division*, Vol. 104, (EM 5), pp. 1043-1057.
24. Desai, C. S., "Dynamic Soil-Structure Interaction with Constitutive Modelling for Soils and Interfaces," *Finite Element Problems for Nonlinear Problems Europe-US Symposium*, Trondheim, Norway, 1985.
25. Desai, C. S., "Behaviour of interfaces between structural and geologic media," *Proceedings of International Conference on Recent Advances in Geotechnical Earthquake Engineering and Soil Dynamics*, St. Louis, Mo., 1981.
26. Lightner, J. G., and Desai, C. S., "Improved numerical procedures for soil-structure interaction including simulation of construction sequences," Report No. VPI-E-79.32, Dept. of Civil Eng., Va. Tech., Blacksburg, Va., 1979.
27. Zaman, M. M., "Influence of interface behaviour in dynamic soil-structure interaction problems," Ph.D. Dissertation, Dept. of Civil Eng. and Eng. Mech., Univ. of Arizona, Tucson, AZ, 1982.
28. Clough, G. W., and Duncan, J. M., "Finite element analyses of retaining wall behavior," ASCE, *Journal of Soil Mechanics and Foundation Division*, Vol. 97, (SM12), 1971.
29. Desai, C. S., "Finite element method for analysis and design of piles," *Misc. Paper S-76-21*, U.S. Army Engr. Waterways Expt. Stn., Vicksburg, Mississippi, Oct., 1976.
30. Bowles, J. E., P. E., S. E., *Foundation Analysis and Design* (4<sup>th</sup> Edition), Singapore, McGraw Hill, 1988.

31. Orrje, O., and Broms, B., "Effects of Pile Driving on Soil Parameters," ASCE, *Journal of Soil Mechanics and Foundation Division*, Vol. 93, SM 5, Sept., part 1, pp. 59-74, 1967.
32. Flaate, K., and Selnes, P., "Side Friction of Piles in Clay," 9<sup>th</sup> ICSMFE, Vol. 1, pp. 517-522, 1977.
33. Flaate, K., "Effects of Pile Driving in Clays," *CGJ*, Vol. 9, No. 1, Feb., pp. 81-88.
34. Anderson, W. F., Young, K. Y. and Sulaiman, J. I., "Shaft Adhesion on Bored Cast-in-situ Piles," *Proceedings of the Eleventh International Conference on Soil Mechanics and Foundation Engineering*, San Francisco, 12-16 August 1985, Vol. 3, pp. 1333-1336, Boston, 1985.
35. Skempton, A. W., "Cast in-Situ Bored Piles in London Clay," *Selected Papers on Soil Mechanics by Skempton A.W.*, pp. 85-105, Thomas Telford Ltd., London, 1984.
36. Vesic, A. S., *Design of Pile Foundations*, Transportation Research Board, No. 42, Washington D. C., 1977.
37. O'Neill, M. V. and Reese, L. R., "Behavior of Bored Piles in Beaumont Clay," ASCE, *Journal of Soil Mechanics and Foundation Division*, Vol. 98, SM 2, pp. 195-213.
38. Chandler, R. J. and Martins, J. P., "An Experimental Study of Skin Friction around Piles in Clay," *Geotechnique*, Vol. 32, 4, pp. 479-495, 1977.
39. Meyerhof, G. G., "Scale Effects of Ultimate Pile Capacity," ASCE, *Journal of Soil Mechanics and Foundation Division*, Vol. 109, GT 6, pp. 797-806, 1983.
40. Braja, M. D., *Principles of Foundation Engineering* (2<sup>nd</sup> Edition), PWS-KENT Publishing Company, Boston, 1990.
41. Coyle, H. M. and Reese, L. C., "Load Transfer of Axially Loaded Piles in Clay," ASCE, *Journal of Soil Mechanics and Foundation Division*, Vol. 92, pp. 1-26., SM 2, March.
42. Vesic, A. S., "Tests on Instrumented Piles, Ogeechee River Site," ASCE, *Journal of Soil Mechanics and Foundation Division*, Vol. 96, No. SM 2, Proc. Paper No. 7170, pp. 561-584, March 1970.

43. Sulaiman, I. H. and Coyle, H. M., "Predicted Behaviour of Axially Loaded Piles in Sand," *3<sup>rd</sup> Ann. Offshore Tech. Conf.*, Houston, Paper No. 1482, 10 pp., 1971.
44. Touma, F. T. and Reese, L. C., "Behavior of Bored Piles in Sand," ASCE, *Journal of Geotechnical. Division*, Vol. 100, No. GT 7, Proc. Paper No. 10651, pp. 749-761, July 1974.
45. Tomlinson, M. J., "The Adhesion of Piles Driven in Clay Soils," Proc. ASCE, *4<sup>th</sup> International Conference in Soil Mechanics and Foundation Engineering.*, Vol. 2, London, pp. 66-71, 1957.
46. Skempton, A. W., "Cast in-Situ Bored Piles in London Clay," *Geotechnique*, Vol. IX, pp. 153-173, December 1959.
47. Vasic, A. S., "Bearing Capacity of Shallow Foundations," in Winterkorn, H. and Fang, H. Y., (Eds.), *Handbook of Foundation Engineering*, Van Nostrand, New York, pp. 121-147, 1974.
48. Schultze, E., "Experimental Method and Evaluation of Some Loading Tests on Piles," *Symposium on Bearing Capacity of Piles*, pp. 60-88, Roorkee, India, 1964.
49. Broms, B., *Stabilization of Soil with Lime Columns*, Design Handbook, (3<sup>rd</sup> Edition), Lime Columns AB.
50. Frederick, S. M., *Standart Handbook for Civil Engineers* (3<sup>rd</sup> Edition), Mc-Graw-Hill, NewYork, 1990.
51. Taylor, W. H., *Modern Chemistry of Cements, Chemistry and Industry*, 1981.
52. Lea, F. M., *The Chemistry of Cement and Concrete* (3<sup>rd</sup> Edition), Edward Arnold Ltd., London, 1976.
53. Skempton, A. W., "Cast in-Situ Bored Piles in London Clay," in Skempton, *Selected Papers on Soil Mechanics by A.W. Skempton*, pp. 85-105, Thomas Telford Ltd.. London, 1984.
54. Sabry M. A. and Parcher J.V., "Engineering Properties of Soil-Lime Mixes," Proc. ASCE, *Journal of Transportation Engineering*, Vol. 107, TE1, pp. 25-35, 1979.
55. Ingles O. G. and Metcalf J. B., *Soil Stabilization*, Butterworths, Sydney, 1972.

56. Brandl, H., "Alteration of soil Parameters by Stabilization with Lime," *Proceedings of 10<sup>th</sup> International Conference in Soil Mechanics and Foundation Engineering*, Stockholm, Vol. 3, pp. 587-594, 1981.
57. Brandl, H., "Der Einfluss des Frostes auf kalk- und zementstabilisierte feinkörnige Böden," *Mitteilungen des Institutes für Grundbau und Bodenmechanik*, Heft 8, Technische Hochschule Wien, Austria, 1967.
58. Lund, O. L., and Ramsay, W. J., "Experimental Lime Stabilization in Nebraska," *Highway Research Board Bull*, Vol. 231, pp. 24-59, 1959.
59. Locat, J., Berube, M. A. and Choquette, M., "Laboratory Investigations on the Lime Stabilization of Sensitive Clays : Shear Strength Development," *Canadian Geotechnical Journal*, Vol. 27, pp. 294-394, 1990.
60. Jan, M. A., and Walker, R. D., "Effect of Lime, Moisture, and Compaction on Clay Soil," *Highway Research Record*, No. 29, pp. 1-12, 1963.
61. Holtz, R. D. and Kovacs, W. D., *An Introduction to Geotechnical Engineering*, Prentice Hall, London, 1981.
62. Bell F. G., "Lime Stabilization of Clay Soils," *Bulletin of the International Association of Engineering Geology*, Paris, 1989.
63. Diamond, S., and E. B. Kinter, "Mechanism of soil-lime stabilization : an imperative review," *Highway Research Board*, Washington, USA, 1964.
64. Eades, J. L. and Grim, R., "Reactions of Hydrated Lime with Pure Clay Minerals in Soil Stabilization," *Highway Research Board Bull*, Vol. 262, pp. 51-63, 1960.
65. Saskatchewan, R., Presented in Part at the Fortieth Canadian Geotechnical Conference, 1987, in Locat, J., Berube, M. A. and Choquette, M., "Laboratory Investigations on the Lime Stabilization of Sensitive Clays : Shear Strength Development", *Canadian Geotechnical Journal*, Vol. 27, pp. 294-394, 1990.
66. Chaquette, M., "La Stabilization a la Chaux des Sols Argileux du Quebec," Ph.D. Dissertation, University Laval, 1988.

67. Berube, M. A. and Locat, J., "Stabilization a la Chaux des Argiles Sensibles: Role de la Nature du Sol," *Ministre des Transports du Quebec*, Final Report GGL-87-03, 1987.
68. Ingles, O. G. and Metcalf, D. B., "Lime Stabilization," *Soil Stabilization*, Melbourne, pp. 127-167, 1972.
69. Laguros, J. G., Davidson, D. T., Handy, R. L., and Chu, T. Y., "Evaluation of lime stabilization of loess," Proc., ASTM, Vol. 56, pp. 1301-1319, 1956.
70. Mateous, M., "Soil-lime research at Iowa State University," Proc., ASCE, *Journal of Soil Mechanics and Foundation Division*, Vol. 90, SM2, pp. 127-153, 1964.
71. Thompson M. R. and Harty J. R., "Lime Reactivity of tropical and subtropical soils," Highway Research Record No. 442, *Highway Research Board*, Washington DC, pp. 105-112, 1973.
72. Rowe, R. K., "The Role of Diffusion and the Modelling of its Impacts on Groundwater Quality," Geotechnical Research Center, Department of Civil Engineering, University of Western Ontario, London, Ontario, Canada N6A 5B9.
73. Olgun, C. G., "Numerical Modeling of Contaminated Transport by Advection Dispersion in two Dimensions", Bebek-Istanbul, December 1996.
74. Shackelford, C. D. and D. E. Daniel, "Diffusion in Saturated Soil. I: Background," ASCE, *Journal of Geotechnical Engineering*, Vol. 117, pp. 467-484, March 1991.
75. Shackelford, C. D. and D. E. Daniel, *Geotechnical Practice for Waste Disposal*, Chapman & Hall, pp. 33-65., London, 1993.
76. Stocker, P. T., "Diffusion and Diffuse Cementation in Lime and Cement Stabilised Clayey Soils-Chemical Aspects," *Australian Road Research*, Vol. 5, No. 9, pp. 6-47, November 1975.
77. Kishida, H. and Uesugi, M., "Tests of Interface between sand and steel in the simple shear apparatus," *Geotechnique* 37, No.1, pp. 45-52, 1987.